Politecnico di Torino

Corso di Laurea Magistrale in
Ingegneria Energetica e Nucleare

Solar Concentration and Membrane Distillation coupling: System Model and Case Studies

Supervisor:
prof. Eliodoro Chiavazzo
Co-supervisor:
prof. Alberto Tiraferri

Author:
Francesco Artuso

Torino, 6 Dicembre 2018

Contents

Abstract

The issue of freshwater access has grown dramatically over the years due prominently to population increase, climate change, pollution. The simultaneous presence of freshwater scarcity, salt water reserves and high insolation in several locations in the world suggests the use of solar energy to drive desalination process. Since those locations are often situated in remote and underdeveloped regions, it is crucial to utilize stand-alone, simple and inexpensive technologies. A membrane distillation process coupled with a solar concentrator can meet these requisites.

In this thesis work, it is proposed the model of a solar desalination system that includes a solar parabolic-dish concentrator (Trinum by INNOVA), a back-up conventional boiler, a sensible heat storage, and a membrane distillation lab unit (by AQUASTILL), to simulate the operation in three different geographical locations: Turin (ITA), Palermo (ITA) and Abu Dhabi (UAE).

Simulink software was used to construct a dynamical system model, taking advantage of the software ability to run dynamic simulation and to handle results conveniently, while PVGIS database website provided the input climatic data. The membrane distillation lab unit model was validated comparing computational results with data from experiments conducted on a prototypical device at DIATI department (Politecnico di Torino). The simulated period spanned over a year to compute the most relevant quantities involved in the system operations, used to assess the system freshwater annual production of the system and the solar to total energy fed factor, which represents the renewable share of the energy involved in the freshwater production over one year.

The results show promising performances: in all the three case studies, the solar share is larger than 70%, with the Abu Dhabi case study reaching the maximum of 93%. It is possible to take further steps to advance the work, for example considering commercial size membrane distillation devices and performing economic feasibility analysis.

Introduction

Water is the essential component of life on Earth. Greek philosopher Thales chose it as *archè*, origin, of the world and all the most important ancient civilizations flourished on the banks of great rivers such as the Nile, the Tigris and Euphrates, the Yangtze and Huang He, the Ganges. Unfortunately, of the approximately $1.4{\cdot}10^9$ km^3 of water that exists on the Earth, the 97.5% is saltwater contained in the Oceans and seas of Earth, and the 80% circa of the remaining freshwater portion is trapped in solid state in the polar ice caps and in the glaciers. The available freshwater so it's limited to the 0.5% of the total amount.[1]

In Nature freshwater is made available by the Water Cycle, a close-loop mechanism fuelled by the radiation energy of the Sun: at the sea, this energy evaporates the water, then the steam travels the world forming clouds carried by wind currents, then precipitations occur and the water returns in liquid state to the ground, in which creates groundwaters that in turn make river springs and the rivers travel to the seas, hence closing the loop. Following this cycle, is possible to conclude that freshwater is not evenly distributed on the ground surface of the planet, therefore not all the human population inhabiting it has access to this resource in a reliable and sufficient way.

The World Health Organization states that the minimum pro capita quantity of water needed for survival is about 15-20 litres per day, that covers the fundamental operations as drinking, cooking, personal hygiene and laundry. Obviously, this quantity has to increase in order to satisfy public infrastructure needs such as hospitals and schools, and to sustain an increased quality of life, reaching a maximum of 400 litres in developed countries, in which a large amount is misspent and can be reduced adopting responsible behaviours. [1]

The present conditions of odd distribution, scarcity and misspending are aggravated by the forecasts of demographical increase and the moral imperative of the life quality improvement for the population in underdeveloped parts of the world, making availability of freshwater a great global issue. One of the solution to this more and more pressing problem can be Seawater Desalination, a process in which salt and freshwater are separated from each other using different technologies and energy sources to operate them. With desalination is possible to obtain freshwater that can be used both for primary, agricultural and industrial needs given the fact that energetic facilities are present. It is worth noting that at the moment the desalination processes require a considerably amount of energy in the form of heat or electric power.

Energy supply is one of the important issues that mankind is called to face. The actual primary mean of energy production is the exploitation of fossil fuels to generate heat, that can be used directly or to produce electric power with thermodynamic cycles. These energy sources have several drawbacks: they are not evenly distributed on Earth and not renewable, considerable efforts are used to extract them, and both extraction and consumption are main contributors to environment pollution.

The greatest concern associated with fossil fuels is their effect on the CO_2 concentration in the atmosphere, being it one of the products of the combustion reaction. The solar radiation that hits the planet has a wavelength spectrum that allows it to go through the atmosphere layer and land on the surface; part of the radiation is reflected by the Earth surface with a larger wavelength and some gases, among them CO_2 , present in the atmosphere can reflect it back to the Earth surface. This phenomenon is known as "Greenhouse Effect" and causes the world temperature to increase, causing climate changes that threaten life as we know it on Earth, such as draughts, increase in the sea level, extreme weather events.

Due to extraction, transport and plants need of fossil fuels, their cost can be a real problem for underdeveloped countries, creating in these countries the so-called energy poverty, that prevents their development in term of infrastructure, production and in general life quality.

However, fossil fuels are not the only energy sources: the technological advancements allow to handle natural forces, as sun, wind or tide energy, that are almost free, renewable, clean and better distributed, to produce heat and power. Their peculiar characteristics shift the usual paradigm of energy production and consumption in a way that can benefit also the freshwater production by desalination.

Coupling the various desalination technologies and their need with the production from renewable energy sources (RES), is it possible to overcome the most important challenge of desalination, the considerable utilization of energy, making this technology a viable path to deal with the issue of freshwater scarcity in a cost-efficient way.

Among the other RES, solar energy is a good candidate to build desalination plants powered by renewable energy. Technology can harness this solar energy to produce both electric power and heat that can feed the diverse possible methods of desalination; photovoltaic panels can directly convert solar radiation into power used to drive Reverse Osmosis desalination for instance, Concentrated solar energy can provide heat directly to a Multi stage desalination or use the same heat to produce power, solar collectors harvest heat from radiation that can be used, for instance, in a membrane distillation process.

The prominent factor that make the solar energy-desalination coupling promising is the simultaneous presence, on a vast world area, of the phenomena of water scarcity, presence of

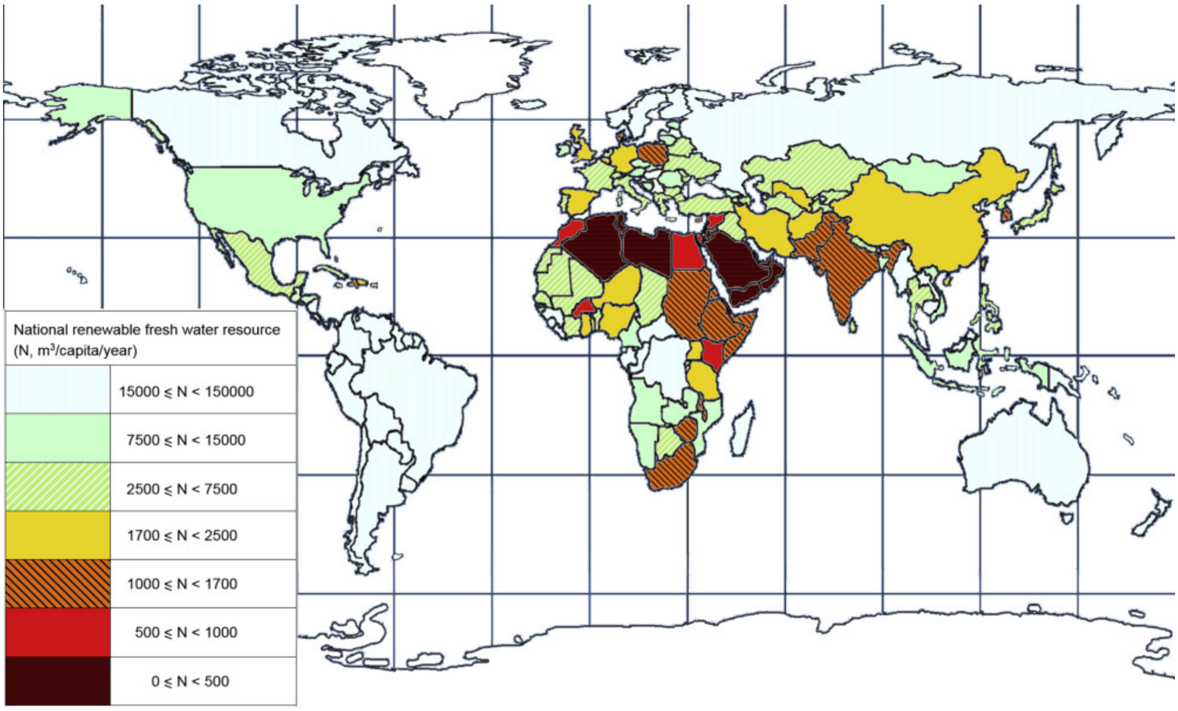

Figure 1: Water scarcity according to [2] processing of [5] data. Darker colours highlight the countries in which the annual pro capita water availability is scarcer.

saltwater, and abundance of solar irradiation. This coincidence can be noted by observing the world maps that report the water scarcity using a measure of m^3/ capita/ year of water (Figure 1), the saltwater reserves present in the world (Figure 2), and the annual solar irradiation using kWh/ m^2 (Figure 3).

These maps are taken from Pugsley et al. [2] that also combine these data in order to obtain a world map representing the areas in which solar desalination can be a good option to tackle the water scarcity issue without using conventional fossil resources (Figure 4).

The map shows a vast world area on which solar desalination can be applied. Also, it is worth noting that the areas involved are often in remote locations and/or in underdeveloped Countries. These facts suggest that the technologies to be considered to set solar desalination in these locations shall have as characteristics the capability to be not expensive, to be of simple design and maintenance and to be used in stand-alone configuration.

Membrane Distillation technology is a good candidate to fulfill the characteristics listed above, but currently it is still in a phase of research and development and operating commercial plants do not exist. Further researches are carried out, and this Master's Degree work can be regarded as a little contribution to this topic.

Here, we numerically investigate a system coupling the Solar parabolic-dish concentrator Trinum by Innova (IT) [3] and the membrane distillation lab unit by Aquastill (NL) [4]. To allow continuous operation of the MD unit, a sensible heat thermal storage is provided, with also a back-up conventional boiler to maintain adequate operating conditions for the MD unit.

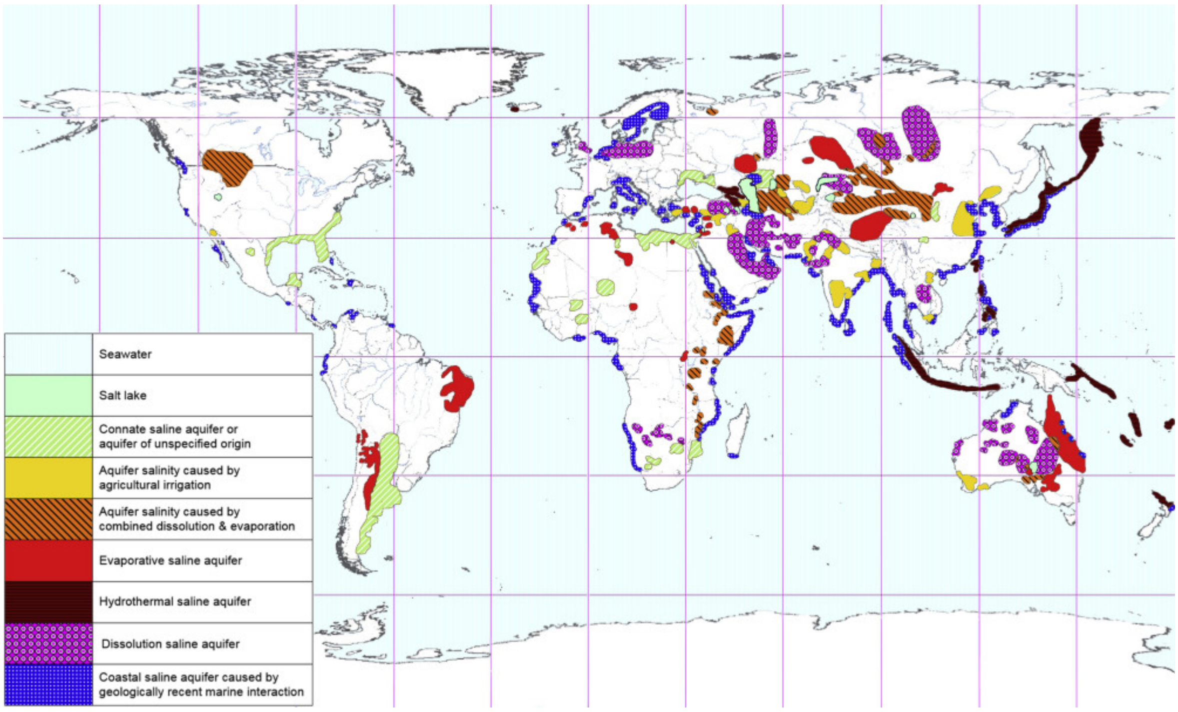

Figure 2: Saltwater reserves according to [2] processing of [6] and [7] data. Large parts of the world possess saltwater reserves that can be tapped to produce freshwater; the different patterns and colours represent various types of saltwater origin.

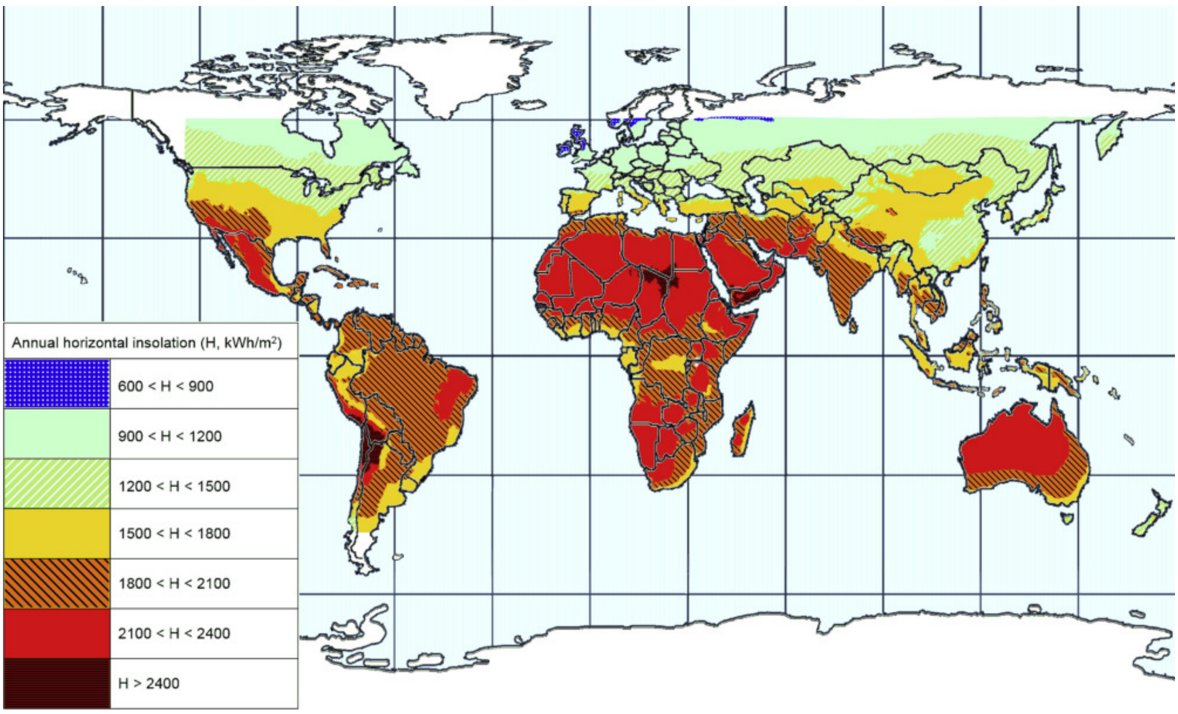

Figure 3: Annual insolation according to [2] processing of [8] data. Tropical and equatorial latitudes can take advantage in the high insolation values to collect solar energy to be used in desalination.

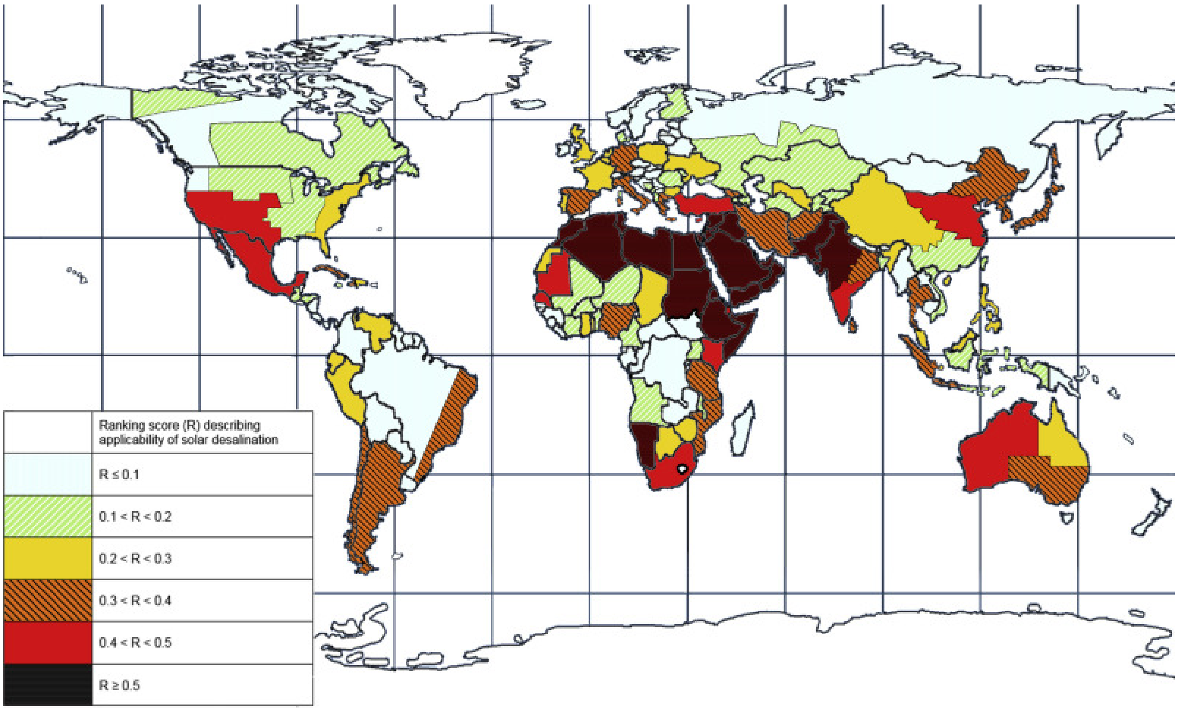

Figure 4: Ranking score of solar desalination applicability according to [2]. Combining the previous maps, a solar desalination applicability ranking is computed; in the Figure darker colours indicate where solar desalination can be applied with most benefits.

The MD unit model is validated using empirical data taken from experimental activities on the real device, performed by Francesco Ricceri, a Research Assistant at DIATI department of Politecnico di Torino.

The entire model is finally used to evaluate system performances in different locations.

Chapter 1 provides a general overview of solar technologies and desalination processes. Among solar technologies a focus on Concentrated Solar devices is put and Trinum concentrator is described. For desalination a short excursus is given on processes, and a more complete insight is devoted to Membrane Distillation, with physical description of the phenomena occurring at the membrane. Also, Aquastill unit outline is depicted. Lastly, a general glance at the different thermal storage technologies is provided, with description of the sensible heat storage allSTOR implemented in the model.

Chapter 2 illustrates assumptions and structure of the MatLab SimuLink model of the system of interest, with presentation of the real data used to implement it.

Chapter 3 is devoted to the MD unit model validation through comparison of model outputs and experimental data.

Chapter 4 includes the description of the different case studies and their simulation results, with an evaluation of the energy performance of the modelled system in the various situations.

Chapter 1

Technologies review

Chapter 1 is devoted to the technologies considered in the simulation model object of the thesis work.

The two main typologies are solar thermal energy production and seawater desalination; in particular, concentrated solar thermal energy production is the chosen energy input to drive a membrane distillation saltwater desalination process. Solar energy is an intermittent energy source on both a daily as well as seasonal basis. Energy storage is needed to store the thermal energy surplus produced during high irradiance periods, and use it during low irradiance periods, thus mitigating fluctuations and allowing a continuous functioning of the MD unit.

Before focusing on the technologies specifically used in this work, a short review of the several solar energy and desalination technologies can be useful to have a general glance on the context in which the work is set. First, solar energy production will be treated in its two main applications, thermal energy and electric power, with the description of the different technologies and a focus on solar concentration.

Then the different typologies of saltwater desalination will be outlined, with attention devoted to membrane distillation and its physical mechanisms and technological application.

At last, a brief overview on the various thermal energy storage methods will be provided, and a discussion on the sensible heat storage used for the model.

1.1 Solar energy

Thermonuclear fusion reactions happen nto the core of the Sun, spreading radiative energy into space that hits the Earth.

This energy is quantified in nearly 4 million exajoules (EJ=10^{18} J) per year, a quantity that has the potential to satisfy the current world energy demand even if only the 50 thousand EJ that are claimed to be easily collectible were retrieved [9]. The abundance alone would make this energy source a convenient one for mankind; furthermore, the actual awareness of the climate change issue and of its principal driver, the greenhouse effect by CO_2 emissions, candidates the solar energy as an environment-friendly source, since very low emissions are related to its energy production.

Actually, it is possible to collect the radiative energy of the Sun in three main forms: electric power, directly with photovoltaics cells or using the heat in a thermodynamic cycle, thermal energy, using solar thermal collectors or solar concentrators, and chemical energy, stored into synthetic solar fuels. These technologies will be reviewed in this section, with a more precise focus on concentrated solar energy, as the simulation model object of the work features a representation of a parabolic dish concentrator.

1.1.1 Photovoltaics systems (PV)

Photovoltaics systems are capable to convert the sun radiative energy directly into electric power. Typically, a PV system is composed by solar panels, power storage devices such as batteries and inverters enabling the connection to the electric grid, by conversion of DC current from PV to AC current for the grid.

A PV panel is composed by solar cells connected among them in series or in parallel, in which the direct conversion happens. The cells are manufactured from semiconducting materials, the most popular of them is Silicon, but also Indium, Tellurium and others are used, while the electrodes and connection are usually made of Silver.

The solar cell is composed of a wafer in which a p-type semiconductor is coupled with an n-type semiconductor, creating a difference of potential due to vacancies and extra electrons respectively. The two semiconductor sides are connected by an electric conductor in which, when electrons of the cell are promoted to the conduction band thanks to solar radiation and are subjected to the before mentioned difference of potential, electric current flows (Figure 1.1).

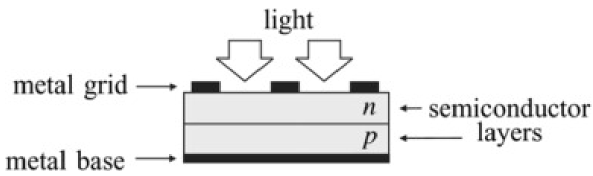

Figure 1.1: PV cell scheme. Two differently doped silicon semiconductor wafers are coupled; on the solar irradiated surface a metal grid connector is build, while on the back side a metal connector plate is present (Source [10]).

A typical panel is composed of interconnected PV cells, drowned in a polymeric layer, encased in aluminium frame for sturdiness and ease of installation. On the rear of the panel is fixed a box with diodes in it, from which the electric connectors depart (Figure 1.2).

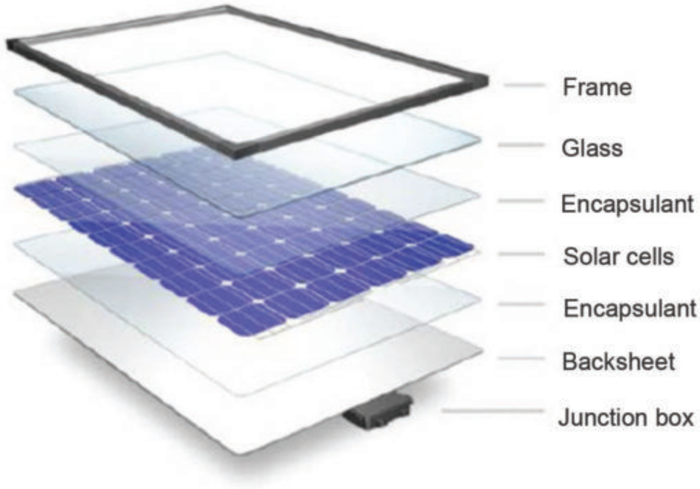

Figure 1.2: PV module structure. Solar cells are connected and encapsulated in polymer sheet; the cells sheet is encased in frame with glass cover and a junction box contains electric connection and diodes (Source [11]).

1.1.2 Solar thermal collectors

Solar thermal collectors can be viewed as a peculiar form of heat exchanger, in which flows a working fluid that is heated up by the solar radiation energy. The absorption of the solar energy is enhanced using special coating painting on the receiver plate, while insulation is prescribed to reduce thermal losses toward the environment in which the collectors are installed.

Typically, this technology is used to produce heat for the purpose of domestic heating and hot water in small to medium size systems. Two main designs are adopted to produce solar thermal collectors: flat plate collector and evacuated tubes collector [12].

Flat plate collectors (FPC)

In FPC a receiving flat plate is put together with a serpentine filled with fluid that takes away the thermal energy absorbed from the sun. To avoid excessive heat dispersion the assembly is encased in a frame that is insulated in the back and side surfaces, while the top is glazed by transparent material (Figure 1.3). This material is often glass, that presents a high transmittance of the radiation in the visible-light and UV spectrum, while having a good reflection of the infrared radiation that is emitted by the hot plate.

This technology performs best in warm environment, since the effect on efficiency of the thermal losses is lower. The working fluid can be air or water, the second one has a better heat capacity but in colder environments has to be mixed with an antifreeze agent, such as glycol [12].

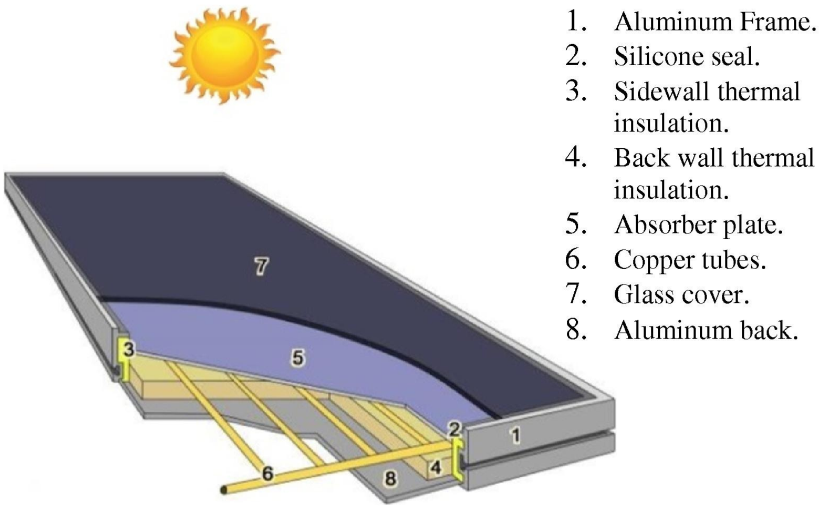

Figure 1.3: Construction schematics of a Flat Plate Collector. The plate receiver is coupled with copper piping to collect solar thermal energy; Insulation is provided in order to mitigate the heat losses to environment; glass covering allows visible radiation in, and prevents infrared radiation escape (Source [13]).

Evacuated tubes collectors (ETC)

To overcome the problem derived from thermal losses ETC technology was developed. It consists of heat pipes insulated in transparent vacuum tubes. The heat pipes are coated with selective painting that allows a large collection of solar radiation. The fluid inside the heat pipes, usually methanol, is heated up and evaporated by radiation, then naturally moves to the condensing zone, in which it exchange its sensible and latent heat with a second fluid. Once again condensed, the fluid flows to the evaporating zone thanks to gravity and the circle starts again.

The insulation provided by the vacuum permits a higher exit temperature from the collector and a higher efficiency. ETC can in this way be installed even in colder climates and used in cloudy days without a great drop on efficiency. Obviously, the more refined productive process, mainly due to vacuum creation and conservation, makes this kind of collector way more expensive that its flat plate counterparts [12].

1.1.3 Solar concentrators

Solar concentrators can be made in several forms but share the same operational concept. Mirrors intercept the solar radiation to reflect and concentrate it onto a receiver, in which a working fluid is heated up by the energy collected. Thanks to this concentration the fluid can reach high enough temperature to feed thermodynamic cycles [15].

There are four different concentrator technologies: *parabolic through collector (PTC), solar power tower (SPT), linear Fresnel reflector (LFR), solar parabolic dish (SPD)*, each of them using different concentration mechanisms that allow to feed several energy producers.

Figure 1.4: Evacuated tube collector. Constituent parts are highlighted: the heat pipes in the transparent evacuated tubes, the manifold in which heat is exchanged from heat pipes to fluid, and the metallic support frame (Source [14]).

Parabolic trough collector (PTC)

The device is composed by a long parabolic-shaped canal coated on the internal surface by reflecting materials. The focus of the parabolic is occupied by an absorber tube painted to maximise the absorbing capacity, since the tube is hit by the reflected solar radiation (Figure 1.5). Inside the tube a heat carrier flows, typically oil or molten salts, that the reflected radiation heats up. The trough is built on a one-axis tracking system that follows the motion of the sun in the sky from east to west, to make sure that the reflected solar radiation is constantly directed on the receiver pipes [15].

The alignment of the receiver tube in the focal point and the absorption ratio are the two crucial issues of the technology and when they are well tackled the fluid temperature can reach 400°C [16].

This kind of collectors is usually paired with steam turbines and alternators by means of an heat exchanger, and the solar-to-electric efficiency is of about 15% [15]. Among the advantages of this collector are the possibility to store the heat carrier to ensure continuity in the energy production, decoupling it from the day/night cycle, and the best land use in the solar harvesting technologies [17].

Parabolic through is the oldest concentrating solar collector, since the first rudimental plant was built in 1912 in El Cairo, Egypt [18] and nowadays 77 power plants operates around the world of which 39 in Spain only [15].

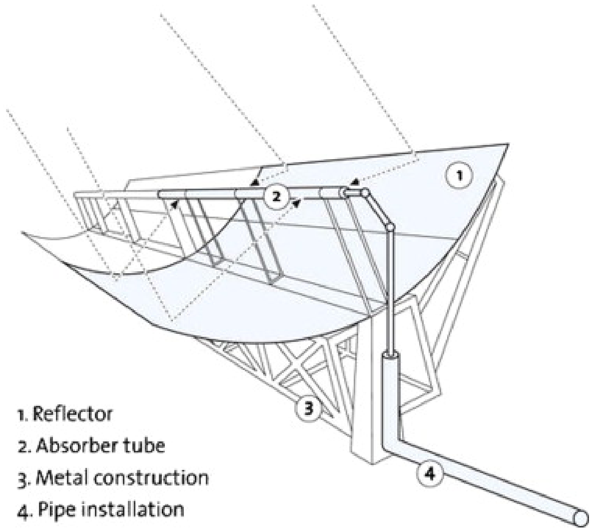

Figure 1.5: Construction schematics of parabolic trough concentrator. The parabolic concentrator reflects solar radiation onto the focal adsorber tube, in which circulates the heat carrier; The assembly tilts around the trough axis in order to follow the sun, to have normal incident radiation on its surface (Source [19])

Solar power-tower (SPT)/central receiver

This technology of CSP presents some important difference compared to the others, since it works on a very larger scale. The plant is constituted by a considerable number of flat mirrors equipped with a two-axis tracking system, called heliostats, that follow the Sun and reflect its radiation to a receiver posed on a tower building (Figure 1.6).

The receiver is usually made of metals or ceramic materials stable at high temperature, to be able to withstand irradiations in the range from 200 to 1000 kW/m^2 [21]. Into the receiver the heat carrier flows, it can be water, molten salts, gases, liquid sodium, that takes the heat from the receiver to the power block in which the heat is used to evaporate water to produce steam, then sent to steam turbines and alternators, producing electric power [23].

In the case of water or molten salts as heat carrier, an energy storage is widely adopted, in which, respectively, hot steam or hot molten salts are conserved, to have a continuous electric output regardless of the meteorological weather [15].

The efficiency of the systems depends on several factor, the most important of them are the optical properties and the cleanliness of the mirrors, the accuracy of the sun tracking system, the absorption properties of the receiver. Usually efficiency varies from 20% to 35% solar-to-electric conversion rate [23]. Since every heliostat is computer-controlled and motorized, and the solar field is typically constituted by thousands of mirrors, they represent the major capital cost in these CSP plants, that needs to produce power in the order of 50-100 MW to be economically viable and sustainable [15].

One way to reduce the financial risk of the SPT project is the hybridisation with conventional natural gas-fired turbines, oil-fired Rankine cycles or, a more recent way, with PV systems

Figure 1.6: 10 MW PS-10 solar power tower at Seville, Spain. It is possible to see the heliostats field surrounding the solar tower, on which is built the concentrated solar energy receiver, and the steam turbine locale at its base (Source [15]).

[22].

There are drawbacks in this technology that have limited its diffusion, the more severe are the needs of great water supply, to feed the steam turbines, and the largest land area confronted to other CSP technologies [15]. Nevertheless, it is the fastest growing CSP technology, with 6 new plants nowadays under construction for an expected power of 632 MW, and a prevision of 900 MW new capacity in the near future, the majority of them located in China [15].

Linear Fresnel reflector (LFR)

LFR power plants use as reflectors flat mirror strips relying on the Fresnel lens mechanism, to concentrate the solar radiation on linear receivers. The water flowing into the receivers is evaporated to feed steam turbines and generators to produce electric power (Figure 1.7). The radiation is kept concentrated onto the receivers thanks to a one-axis tracking system to exploit the maximum power from the sun [24].

The Fresnel reflector design is able to lower sensibly the capital cost of the plant [25]. However, this advantage is balanced by the lower efficiency that the plant can achieve, normally around the solar-to-electric 8-10% for plants that varies in capacities from 10 to 200 MW [23].

The largest operational LFR-CSP plant was built in 2014 in India, with a 125 MW capacity [15].

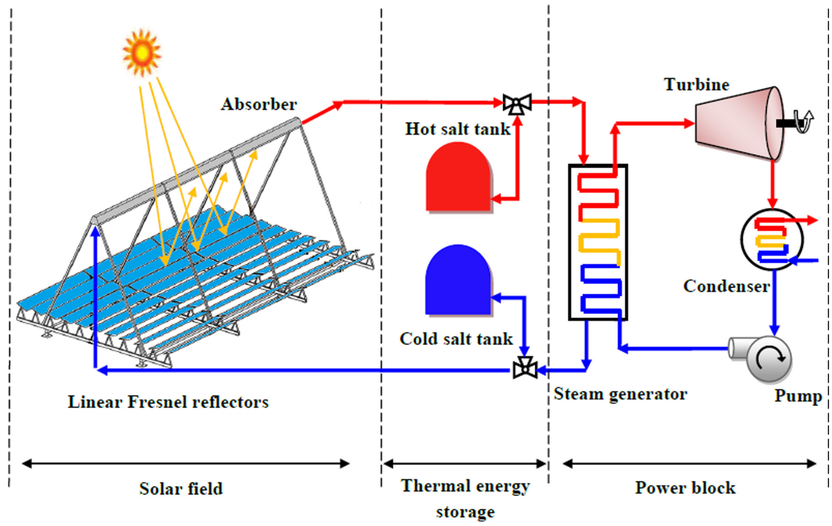

Figure 1.7: Linear Fresnel reflectors power plant outline. On the left side is depicted the typical LFR system design, with solar radiation concentrated onto a central receiver by means of Fresnel lens mechanism reflectors; In the receiver an heat carrier fluid flows and heats up and then brings heat to the steam turbines to produce electric power (Source [20]).

Solar parabolic-dish (SPD)

A parabolic-dish concentrator consists in a mirror parabolic-shaped surface at which focal point a receiver is collocated. The concentrator is put together with a two-axis tracking system to follow the sun through the day. In the power plants that use this technology, a Stirling or Brayton thermal engine is fixed at the receiver, to transform the solar radiation in mechanical and then electric power [15].

The mirror dish can have a diameter from 5 to 10 metres and is composed of silver or aluminium covered by transparent plastic or glass (Figure 1.8). The best configuration is a thin layer of silver of 1 micro metre coated with iron-added glass in order to reach the 90-94% of reflection [21].

An inherent advantage of SPD is the capacity to be always normal to incident radiation and so to be not affected by cosine losses typical of other technologies. For this reason, it can achieve a solar-to-electric efficiency of 25-30%, which is one of the highest in all the solar energy panorama [21]. The construction shape allows the installation on non-levelled ground, making SPD suitable for nearly all terrains that present the right irradiation during the year. The two previous features contribute in making the dish concentrator an ideal candidate for installation in remote areas of the world, with limited, insulated or even absent power grid [15].

Two SPD-CSP plants have been constructed to the present day: one is located at Toele, Utah with a 1.5 MW capacity using 429 parabolic-dishes equipped with Stirling engines, the other was built in Peoria, Arizona and it is no longer in activity, it featured a 1.5 MW capacity [15].

Figure 1.8: 1.5 MW Toele army depot plant, Utah. The solar parabolic dish is composed by several mirror slices that focus the sun rays onto the Stirling thermal engine positioned at the focal point of the parabolic. Several SPD arrays are needed to reach the nominal power capacity (Source [15]) .

Table 1.1: Trinum physical and energetic main parameters (Source [26]).

Gross capturing area	11.23 m^2
Net capturing area	9.58 m^2
Optic efficiency	89.0%
Maximum Pressure	6 bar
Flow rate	7-19 l/min
Voltage required	230 V 50 Hz
Thermal peak power (DNI 1000 W/m^2)	7.4 kW
Weight	550 kg
Focal distance	2.26 m

1.1.4 Trinum Turbocaldo by Innova (IT)

Trinum by Innova is the selected solar device for the system modelling. It is a Solar Parabolic-Dish concentrator of small size and it is designed to have two possible configurations, one features at the focus a Stirling engine, the other a receiver for thermal energy. The thermal receiver configuration is called Turbocaldo version and it is the one considered by this work.

The concentrator has an effective dish area of 9.58 m^2 and a focal distance of 2.26 m. The device is equipped with a two-axis tracking system to follow the sun and collimate perpendicularly with the solar radiation. Its thermal peak power is 7.4 kW with a Direct Normal Irradiance of 1 kW/m^2. The employed heat carrier fluid defines the maximum operative temperature, 110 °C with water-glycol mixture, 250 °C with diathermic oil.

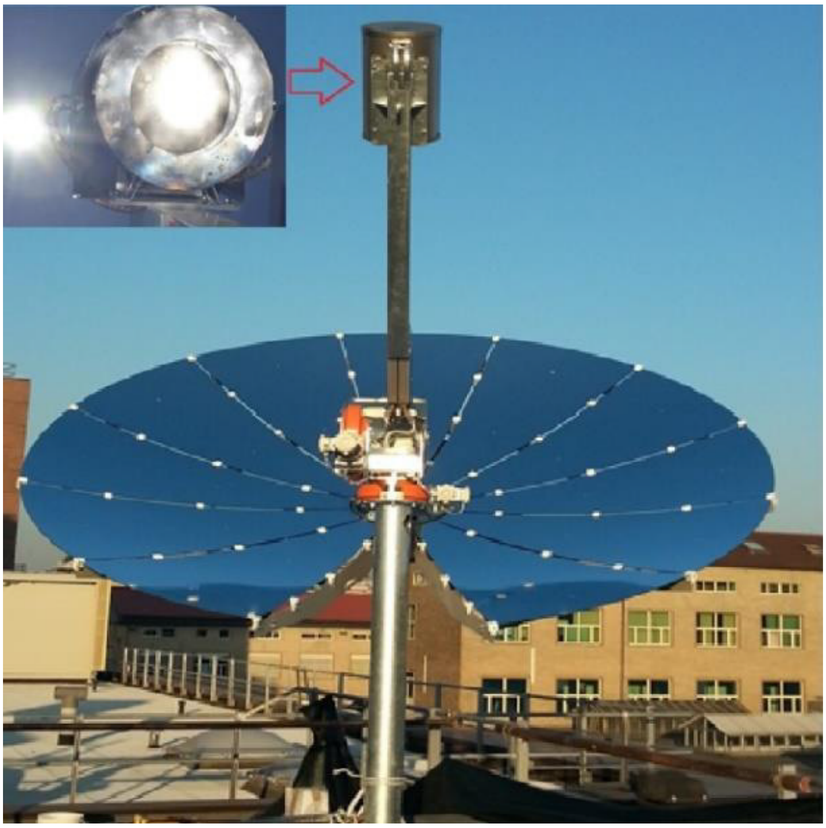

Figure 1.9: The Trinum unit installed at Politecnico di Torino. It is possible to see the mirror dish, the two-axis tracking system motors and the focal receiver; in the top-left corner a particular shoving the receiver cavity hit by concentrated sun rays (Source [44]).

1.2 Saltwater Desalination

Saltwater Desalination covers a broad variety of processes, different one from each other with respect to energy source needed, involved physical phenomena, complexity, efficiency and costs. In this section, the most diffuse technologies will be reviewed, while membrane distillation will be better analyzed in its fundamental. Also a description of the Membrane distillation lab unit by Aquastill is carried out, since this device will be implemented into the general system model.

1.2.1 Multi stage flash desalination (MSF)

In Multi stage flash desalination the heated saltwater passes across different tanks in which the pressure is set in descending order.

When saltwater enters one tank, it experiences a flash evaporation, being at high temperature and lower pressure than the stage before. Steam condenses in each tank on the external surface of a pipes bundle, inside of which saltwater is circulating before entering the series of tank and so using the latent heat to increase its temperature (Figure 1.10). In this way is possible to have a heat recovery, and the only part in which heat is added is the Brine Heater right before the first stage, to reach the top brine temperature of the system.

Thanks to heat recovery with 1 kg of low pressure steam sent to the Brine Heater it is possible to produce 8-10 kg of freshwater [1].

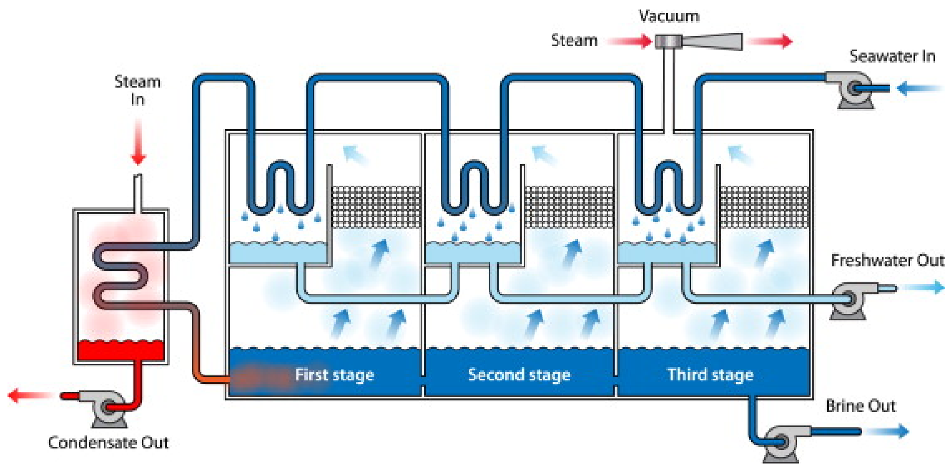

Figure 1.10: Schematic diagram of a MSF desalination unit. Different stages are depicted, with the links between them; water passing from one tank to another flashes thanks to the descending pressures in the different tanks (Source [27]).

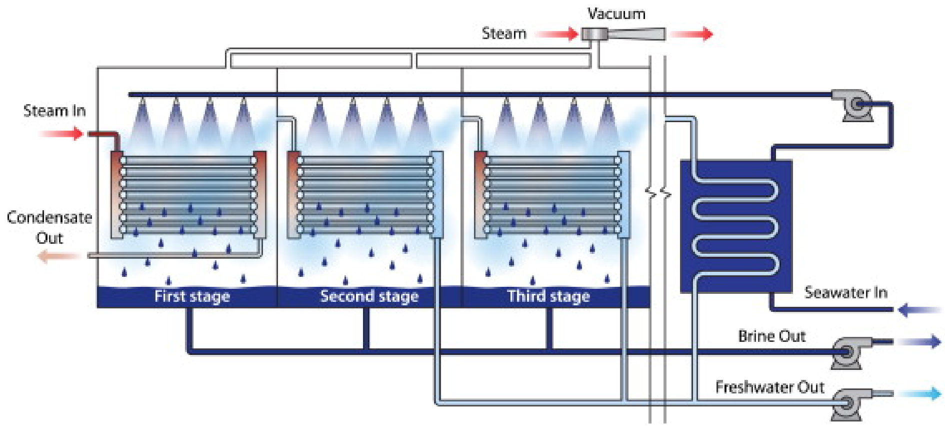

Figure 1.11: Schematic diagram of a MED desalination unit. Saltwater is evaporated using condensing motive steam; the steam of one effect is used as motive for the following one, in which the pressure is lower and evaporation is possible at lower temperatures (Source [27]).

1.2.2 Multi effect distillation (MED)

This arrangement features the evaporation on the external surface of a tube bundle heated by the condensation of motive steam into it, that takes place in a low pressure effect tank. The steam created is then used as motive in the next effect, in which the boiling point is lower since the operative pressure is lower (Figure 1.11).

The configuration allows for a very effective heat management, resulting in a product of 10-12 kg of freshwater for kg of motive steam fed. To further increase the efficiency of the process is possible to use two techniques: Thermal vapour compression and mechanical vapour compression. Both rely on a compression of the last effect vapour and its recirculation to the first effect, one by the mean of a steam ejector (TVC), the other with a mechanical compressor (MVC). Consequently, the efficiency rises to 15-16 kg of fresh water per kg of motive steam [1].

1.2.3 Reverse osmosis (RO)

Reverse osmosis consists in a filtration process driven by pressurisation of water. The filter used is a semi-permeable membrane that lets the water pass, rejecting the salts. In this way, only freshwater can reach the other side of the membrane (Figure 1.12).

The process needs electric power to operate the pumps for pressurisation, the typical pressure values being 17 to 27 bar for brackish water and 55 to 82 bar for seawater. Since reaching such high values is very energy consuming, coupling with renewable energy sources or organic Rankine cycles has been investigated in research and development environment [27].

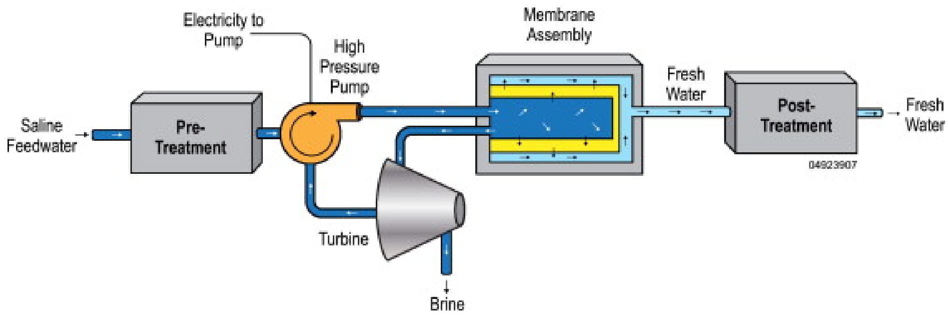

Figure 1.12: Schematic diagram of a RO desalination unit. In the membrane assembly the high pressure water is pushed across the hydrophilic membrane, leaving salt behind; pre- and post-treatment is needed to avoid fouling and scaling of membrane (Source [27]).

1.2.4 Electro-dialysis (ED)

Electro-dialysis relies on an electro-chemical process that use direct electric power to drive ions through a membrane, leaving freshwater behind. The core of the system consists in a container in which membranes are disposed to form channels; at the boundary of these channels electrodes connected to a direct source of electric current are built. As the saltwater flows into the channels, salt ions are forced to go towards the electrodes by the difference of potential, resulting in freshwater in the inner channel and concentrated brine in the outer channels (Figure 1.13).

A process variant called electro-dialysis reversal consists in periodical change of polarity at the electrodes. This behaviour helps to increase electrodes lifetime and to clean the membranes, as precipitants can build up on the concentrate sides [27].

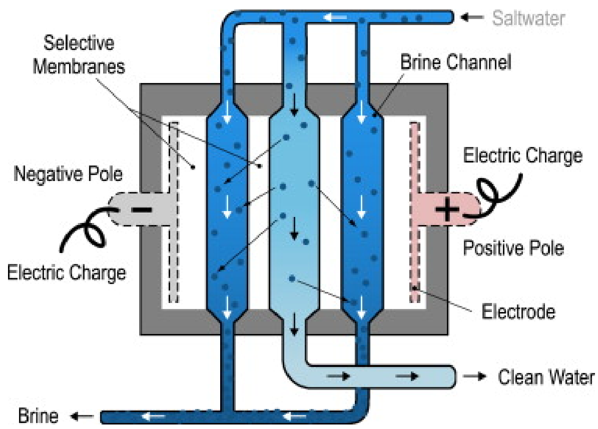

Figure 1.13: Schematic diagram of a ED desalination unit. The electrodes create a difference of potential that drives salt ions respectively to their opposite polarization electrode leaving the central freshwater channel (Source [27]).

1.2.5 Membrane distillation (MD)

Membrane distillation is a hybrid thermal-membrane process. Thermal energy is used in water evaporation, while a hydrophobic membrane is used as a mean of separation of the vapour from the liquid phase [5].

Several characteristics of this technology, treated in detail later in this work, make MD well compatible with solar thermal energy technologies.

The basic configuration of MD is composed by a hydrophobic membrane that separates two channels: in one of them flows the hot saltwater feed, while in the other the freshwater permeate is collected. At the feed side of the membrane the water changes phase into vapour thanks to thermal energy and transits across the micro-porous hydrophobic membrane; at the same time the high surface tension of the water on the membrane prevents the liquid phase to infiltrate in the pores. Once arrived at the opposite side of the membrane, the vapour condensates giving its energy to a cold stream [28]. The driving force that moves vapour across the membrane is the difference of vapour pressure at both sides of the membrane, given by the difference of temperature between the hot and cold streams.

Several advantages arise from this process. In the first place the operational temperature of the hot feed is in the range from 50 to 90 °C [29], thus it is possible to couple the process with waste process heat or solar thermal system and the device can be built with polymeric materials, reducing costs and corrosion problems. The complexity of the system is low, unlike MSF or MED, and the membrane does not suffer from dry period, allowing start and stop operation that are not possible with RO.

Large membrane pores and absence of applied hydraulic pressure make MD process more resistant to fouling compared to Reverse Osmosis, allowing less intensive pretreating and less frequent membrane cleaning [30].

All these factors contribute in making Membrane Distillation a well-suited technology to deploy in stand-alone solar-powered systems, that can be installed in remote areas of the world, affected by water scarcity issues.

Mass and heat transfer in direct contact membrane distillation

Membrane distillation can be applied using several technological concepts. The simplest one is called Direct Contact Membrane Distillation (DCMD). In this configuration the saltwater feed side is separated from the freshwater permeate side only by the hydrophobic membrane. The lab unit considered in this work relies on DCMD configuration, thus, in order to have a better comprehension of the physical process that allow for a correct modelling for simulations, heat and mass transfer mechanisms occurring in DCMD are analyzed in detail (Figure 1.14).

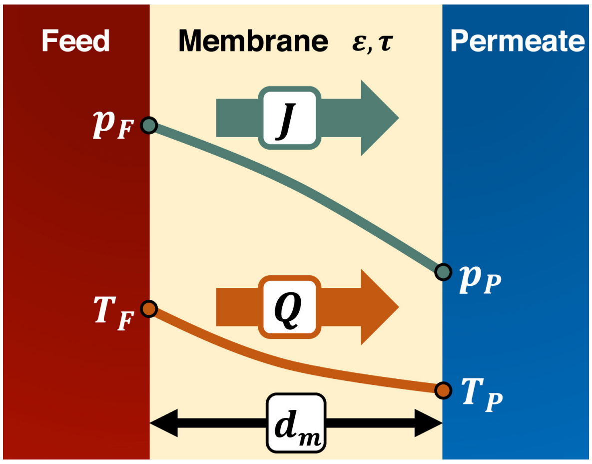

Figure 1.14: Schematic of mass and heat transfer through a membrane in direct contact membrane distillation. Water evaporates at the feed-side membrane solution interface (MSI) before diffusing through the membrane and condensing at the permeate-side MSI; heat transfer across the membrane comprises latent heat flux carried by the vapour mass flux, and a conductive flux, arising from the temperature difference across the membrane. (Source [29]).

Mass transfer Mass transfer in MD is based on the convection and diffusion of the water molecules in vapour phase [5].

Dusty Gas Model (DGM) is typically employed to describe the vapour flux across the membrane. In DGM are considered four type of diffusion mechanisms, viscous flow, molecular diffusion, Knudsen diffusion, surface diffusion. In the case of MD viscous flow and surface diffusion are in general neglected [31].

More commonly, the average pore diameter of 0.2 micrometre stands in both the transition regions of the models, making necessary the superposition of the two mechanisms to correctly describe the physic of the process. Knudsen diffusion is used when the average pore size is lower than the mean free path of the vapour molecules, while it is possible to employ molecular diffusion only if the pore size is 100 times larger than the mean free path [5].

However, experimental evidences derived from gas permeation tests on membranes demonstrate that the Knudsen mechanism is dominant in vapour diffusion [5]. Following this assumption, the mass transfer across the membrane can be expressed, knowing membrane properties and geometry, as

$$N_w = -\frac{2r\epsilon}{3\tau}\sqrt{\frac{8R\bar{T}}{\pi M}}\frac{M}{R\bar{T}}\frac{dp}{dx} \tag{1.1}$$

where

- N_w Mass flux [kg/(s m^2)];
- r Mean pore radius [m];
- ϵ Membrane porosisty [-];

- τ Membrane tortuosity [-];
- M Water molar mass [kg/mol];
- R Gas constant [J/(mol K)];
- $\bar{T}$ Membrane mean temperature [K];
- $\frac{dp}{dx}$ Vapour pressure differential [Pa/m].

The geometry term, composed by $\frac{r\epsilon}{\tau}$, the molecular velocity $\sqrt{\frac{8R\bar{T}}{\pi M}}$, and the temperature term can be included in one Knudsen coefficient C_k [5]. The transport resistance exercised by the air present in the membrane can, on the other hand, be evaluated using the molecular diffusion approach, considering air as a stationary component [32]. The mass flux opposing this resistance can be computed by

$$N_w = -\frac{\epsilon}{\tau}\frac{PD}{P_a}\frac{M}{R\bar{T}}\frac{dp}{dx} \tag{1.2}$$

where

- D Diffusion coefficient [m^2/s];
- P Membrane pressure [Pa];
- P_a Air pressure [Pa].

Combining all the terms before the vapour pressure differential $\frac{dp}{dx}$, it is possible to write a molecular diffusion coefficient C_d. Both coefficients are then used to take into account the two different diffusion mechanisms in a general expression of the mass flux moving across the membrane.

$$N_w = -\frac{1}{\frac{1}{C_k}+\frac{1}{C_d}}\frac{dp}{dx} \tag{1.3}$$

To stress the importance of the diffusion driver, the difference or vapour pressure, the above formulation is rewritten as

$$N_w = K\Delta p \tag{1.4}$$

The membrane coefficient K, whose physical units are kg/(s m^2 Pa) , can assume values in the order from $3{\cdot}10^{-7}$ to $4{\cdot}10^{-6}$, as reported in literature [33]. The last formulation is the one considered when modelling the Aquastill membrane distillator that is part of the simulation model object of this dissertation.

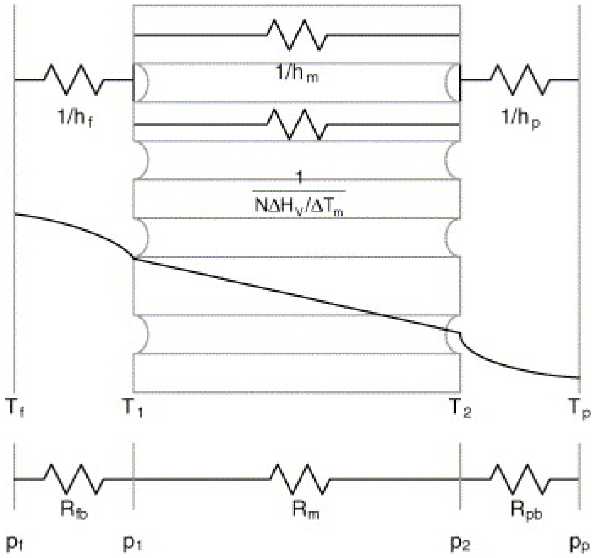

Figure 1.15: Schematic of heat transfer through a membrane in direct contact membrane distillation; Electric analogy resistances of the heat transfer process are depicted in the location in which they occur; also the temperature profile is plotted from feed bulk to permeate bulk (Source [31]).

Heat transfer In MD the driving force of mass transfer is the difference of vapour pressure between the two sides of the membrane. To have this difference the two streams divided by the membrane must be at different temperatures, since vapour pressure is a function of temperature (and activity). Having this temperature difference triggers heat transfer from the hot side to the cold side. The heat transfer process can be divided into three phases, corresponding to different mechanisms.

The first phase is the convective heat transfer in the thermal boundary layer between the hot saltwater bulk and the membrane interface. The heat flux can be written as [31] :

$$Q_f = h_f(T_{fb} - T_f) \tag{1.5}$$

with

- Q_f Heat Flux [W/m^2];
- h_f Convective heat transfer coefficient [W/(m^2 K)];
- T_{fb} Feed side bulk temperature [K];
- T_f Feed side membrane temperature [K];

The second phase is the heat transfer across the membrane. It is composed by two contributions, the conductive heat transfer across the membrane material and the latent heat carried by the vapour flux into the pores. The conductive transfer is described as [31] :

$$Q_s = u_m(T_f - T_p) \tag{1.6}$$

where

- Q_s Heat Flux [W/m^2];
- u_m Conductive heat transfer coefficient [W/(m^2 K)];
- T_p Permeate side membrane temperature [K];

The conductive heat transfer coefficient is calculated as $u_m = \frac{k_m}{\delta}$ with k_m the heat conductivity [W/(mK)] and δ the thickness [m].

The latent heat flux is written as [31] :

$$Q_l = N_w \Delta h_v \tag{1.7}$$

where N_w is the vapour flux [Kg/(m^2 s)] and Δh_v is the water latent heat of vaporization [J/kg].

The total heat flux across the membrane is:

$$Q_m = Q_s + Q_l = h_m(T_f - T_p) + N_w \Delta h_v \tag{1.8}$$

The third phase is the convective heat transfer in the thermal boundary layer between the membrane interface and the permeate bulk. The heat flux can be written as [31] :

$$Q_p = h_p(T_p - T_{pb}) \tag{1.9}$$

with

- h_p Convective heat transfer coefficient [W/(m^2 K)];
- T_{pb} Permeate side bulk temperature [K];
- T_p Permeate side membrane temperature [K];

The three formulations are linked by the heat flux continuity in the membrane channel [31]

$$Q_f = Q_m = Q_p \tag{1.10}$$

The above equation is important to calculate both temperatures at the membrane interfaces, once determined the heat transfer coefficients.

1.2.6 Membrane distillation lab unit by Aquastill (NL)

The lab unit is a direct contact membrane distillation device. The unit is composed by modular aluminum elements which can be adapted to the needed application. It is composed

Figure 1.16: Aquastill Lab Unit installed in the DIATI department Laboratory (Courtesy of Francesco Ricceri).

by two tanks, one for the saltwater feed and the other for the permeate side freshwater. The first one is equipped with an electric resistance, to heat up the saltwater, the second one is cooled down by a chiller (Figure 1.17a). The resistance heats up the saltwater, while the chiller is needed to cool down the return water from the membrane channel to maintain the temperature difference that drives the desalination process.

From each tank, a plastic pipe departs to the related membrane channel, both channels encased in an assembly set on one side of the devices. In the membrane channels (Figure 1.17c), the two streams are set in counterflow, with only the membrane to divide them. Here, the saltwater evaporation occurs, and the vapour travels across the membrane, condensing in the permeate side stream. The two streams then return into their respective tanks using plastic pipes.

Under the tanks, the circulating pumps are located and the opposite side with respect to membrane channels is occupied by the datalogging system (Figure 1.17b), that permits to set operative values and to read signals from the device sensors. In the middle of the inlet pipe of both sides, a pressure sensor, a temperature sensor and a flow sensor are located (Figure 1.17d), while at the outlet a temperature sensor on both sides is inserted.

During the device operations, the saltwater in the feed tank concentrates itself, while at the permeate tank an increase of volume is experienced. This volume increase heightens the the tank level until it reaches an overfill pipe that discharge the excess freshwater into another recipient [34].

Main characteristics of the lab unit are listed in Table 1.2.

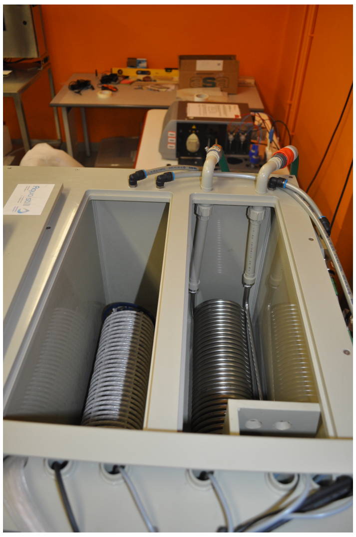

(a) *Salt- and freshwater tanks*

(b) *datalogging system*

(c) *membrane channel assembly*

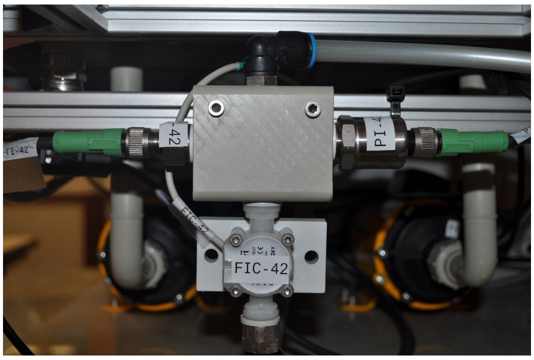

(d) *sensors at feed inlet*

Figure 1.17: Details from the Aquastill Lab Unit (Courtesy of Francesco Ricceri).

Table 1.2: Aquastill lab unit characteristics (Source [34]).

Feed side:	
Tank (material PP)	60x160x350 mm
Electrical heating	3 kW (220 V)
Pump Q_{max}	10 l/min
Distillate side:	
Tank (material PP)	60x160x350 mm
RVS spiral cooling exchanger	d125x410 mm
Pump Q_{max}	10 l/min
Distillate return:	
Tank (material PP)	100x105x350 mm
Pump Q_{max}	10 l/min
Membrane module element (2 channels) (material PP):	
External dimensions	650x200x50 mm
Internal dimensions	500x100x4 mm
Spacer thickness	2 mm

1.3 Thermal energy storage

Intermittence is one of the drawbacks affecting solar energy. Thermal energy storage is able to contribute in intermittence mitigation, allowing energy availability during low solar energy production periods and a more stationary operation of the solar powered systems in which it is implemented [40].

Thermal energy storage (TES) is usually a low-cost technology and may be used in a vast range of applications, ranging from energy production to industrial processes to buildings heat management [41]. TES concept can be applied in three modes: *sensible heat storage, latent heat storage* and *physical/chemical heat storage*. All of them offer advantages and present issues and different development stages.

The three technologies will be reviewed in this section and the main characteristics of the selected sensible thermal storage tank chosen for implementation in the system modeled will be presented.

1.3.1 Sensible heat thermal storage

In sensible heat storage systems , the thermal energy is accumulated by the internal energy increase in a suitable storage material, induced by temperature changes [42]. Several materials, in solid and liquid phase, may be used to store sensible heat depending on their properties and fields of application. In general, high specific heat and high thermal conductivity are favoured [40], one to store large energy amounts and the other to have an efficient heat transfer in the material. Water is one of the most used fluids in sensible heat storage, thanks to its high specific heat and the transport easiness that permit to use it as both heat carrier fluid and thermal energy storage. However, it is not possible to use water for applications above 100 °C due to its boiling point, unless pressurization is considered. For temperature above water boiling point, it is possible to utilize thermal oils, that present lower thermal properties with respect to water but retain their liquid phase up to 250 °C. Thermal oils are subject to slow degradation during high temperature operation and may be enhanced using nano-additives like graphene, graphite and metal oxides [40]. Molten salts and liquid metals are less common fluids used for high temperature operation [40]. Also solid materials are used to store energy, the more common are rocks, gravel and concrete blocks [40].

Sensible heat storage technologies are currently the most popular solution, since they are low in cost and in complexity. However, they present low energy density, in the range from 10 to 50 kWh/m^3, that in turn increases the needed storage volume for a certain system [42]. Sensible TESs also experience considerable heat losses to the environment, driven by the temperature difference, that affects the storage efficiency.

1.3.2 Latent heat thermal storage

Latent heat storage involves the latent energy associated with phase change, the sensible heat needed to reach phase change temperature and possible sensible heat involved in exceeding this temperature. This technology typically involves solid-liquid transitions but also liquid-gas transformation is used, for example in direct steam storage [41].

The materials involved in latent TES all share good values of latent heat to store the highest possible amount of energy and are called with the acronym PCM (phase-changing materials). Since great efforts are put into latent TES research, several materials have been considered to implement the concept. For low temperature applications, organic materials are typically used, since their melting points stay below 100 °C. At higher temperatures, these materials decompose and they present poor heat conductivity [40]. Among their advantages, organic materials are chemically stable, non-toxic, non-corrosive and easily available [40]. The most common class of organic materials are Paraffins, but also Fatty Acids, Esters, Alcohols and Glycols are used [40]. For high temperature applications, inorganic materials are preferred. Eutectic salts are mixtures that presents sharp melting point and have expanded the PCMs temperature range pushing up to higher temperatures, while Salt hydrates are used in the human thermal comfort range and are the most popular inorganic PCMs in commercial applications [40]. When high temperatures and volume reduction are the design criteria, it can be convenient to rely on Metals and Alloys, thanks to their highest heat capacity per unit volume and highest heat conductivity among PCMs. However, they require inert atmosphere, to avoid oxidation, special containers, and they suffer repeated thermal cycle, that can change their microstructure and consequently their physical properties, including latent heat and melting point [40].

The main advantage of PCMs is the higher energy density with respect to sensible heat storage material, while they still present several issues as difficult confinement into the storage system, chemical instability (for some materials), uncertainties on long term behaviours, high costs. These drawbacks need further research and development to be overcome, to produce reliable and effective phase change materials [42].

1.3.3 Physical/chemical thermal storage

Thermo-chemical energy storage is an emerging technology that may overcome the present sensible and latent storage drawbacks. This technology in usually based on thermo-chemical storage and adsorption storage in micro-porous materials [42]. In thermo-chemical storage, thermal energy is stored into chemical bonds, such as covalent or ionic bonds, through reversible reactions and it is released once the reactions are reversed. In adsorption in micro-porous materials, liquids or gases form bonds, such as van der Waals forces, on the surface of another material. [41]. The interest for these phenomena also stems from the high energy density that can be reached using chemical bonds as a mean of storage (around 1000 MJ/m^3 [42]), and the possibility to store indefinitely the energy at nearly ambient temperature without losses [40].

Currently, most of the research efforts are devoted to adsorption. It involves the sorption of liquid or gas molecules on the surface of a porous and solid material, involving an endothermic reaction during desorption to store energy and its exothermic reversal during adsorption to release energy. The fluid is called adsorbate, while the solid is called adsorbent [42]. One of the research lines concerns the coupling between different types of adsorbate and adsorbent, to find suitable couple presenting high energy density while being not difficult to manage [42]. Among others, the most popular adsorbates are water, ammonia, carbon dioxide and hydrocarbons and adsorbents like activated carbon, silica gels, natural and synthetic zeolites are tested [42].

Chemical thermal energy storage presents advantages such as highest energy density, long storage duration and low losses, but currently, important challenges as sintering and grain growth in storage material and low rehydratation rate are still not resolved [40]. Adsorpion processes share the same benefits, while presenting different challenges due to the physics of the phenomenon, such as adsorbent instability and system variability [42]. Thus, both technologies are in a status of material characterization, laboratory-scale systems and pilot-scale prototypes and research community continues to make efforts in order to develop further these processes [42].

1.3.4 AllSTOR VPS 800/3 sensible heat storage tank by Vaillant (GE)

AllSTOR VPS 800/3 is a multifunction thermal storage, featuring good flexibility and hot water capacity. It serves as a buffer for heating water directed to other heating circuits. An highly efficient thermal insulation concept allows to reduce standby losses to low values. Also, it permits several connections simultaneously. The previous characteristics make the allSTOR tank very suitable to the system concept described in the present work. On Table 1.3 its main attributes are listed and Figure 1.18 shows the device.

Table 1.3: AllSTOR VPS 800/3 characteristics (Source [43]).

Nominal storage capacity	778 l
Approv. heating function overpressure	3 bar
Max. heating water temp.	95 °C
Standby energy loss	<2.4 kWh/24 h
Dimensions:	
Height with insulation	1944 mm
Height without insulation	1846 mm
Diametre with heat insulation	1070 mm
Diametre without heat insulation	790 mm
Weight	130 kg

Figure 1.18: AllSTOR VPS 800/3 sensible heat storage tank by Vaillant (GE) (Source [43]).

Chapter 2

Simulink model of the solar desalination system

This chapter of the work is devoted to describe the system model used to evaluate the performances of the coupling between the solar parabolic-dish (SPD) concentrator Trinum by Innova (IT) and the direct contact membrane distillation (DCMD) unit by Aquastill (NE).

2.1 The Tool: MATLAB Simulink

Simulink is a block diagram software for simulation and Model-Based Design. It is able to perform system-level design, simulation, automatic code generation, continuous test and verification of systems.

Simulink includes a graphical editor, customizable block libraries, and solvers for modeling and simulating dynamic systems. Its strong integration with MATLAB enables to incorporate MATLAB algorithms into models and export simulation results for further post-processing. To push on simulation performances, it is equipped with fixed-step and variable-step ODE solvers and model analysis tools for refining model architecture [45].

Since the goal of the thesis work is to evaluate the performances of a thermal system powered by solar energy, which suffers of daily and seasonal variation, a simulation over a significant period of time, e.g. one year, is needed. Simulink offers all the essential tools to handle this task and elaborate the results in a convenient way.

2.2 Model outline

The system under consideration has four main parts: the solar concentrator, a sensible heat storage, a back-up conventional boiler and the MD unit.

The solar concentrator captures the solar radiation energy and converts it into thermal energy provided to a heat carrier fluid. The fluid transports the heat from the receiver of the concentrator to the thermal storage. In the storage tank the thermal energy is partly accumulated as mass internal energy and party sent to the MD unit thanks to another heat carrier fluid. The second fluid heats up the saltwater contained in the MD unit feed tank, that is pumped into the hot channel of the membrane assembly. Here, at the membrane interface, water evaporates, vapour moves across the membrane and condenses at the other side of the membrane, producing freshwater. If the thermal storage temperature falls under a chosen value of 55 °C, the back-up boiler activates and heats up the water in the storage. The temperature value is chosen because 50°C is the lower boundary of the temperatures range of application for membrane distillation. Figure 2.1 shows the layout of the system the model simulates.

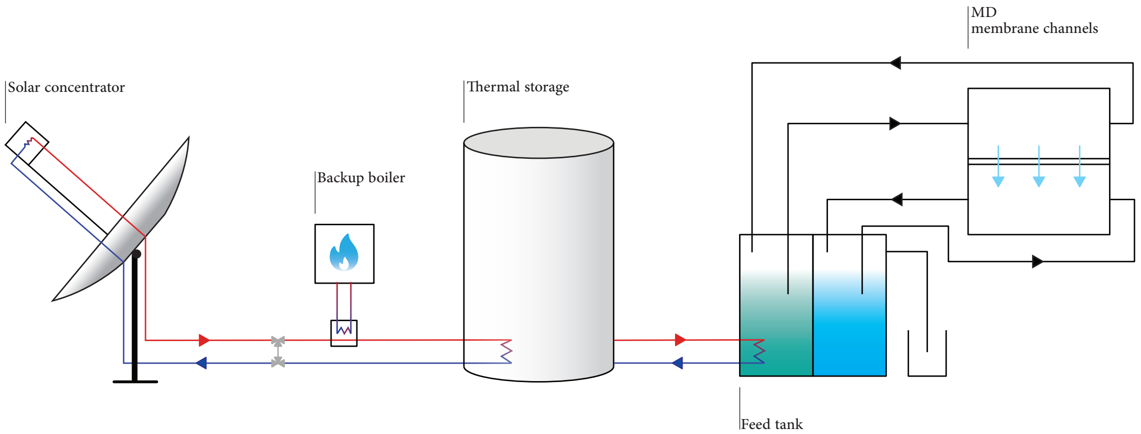

Figure 2.1: Outline of the physical system modeled. From left to right, the parabolic-dish concentrator, to collect solar energy, the conventional back-up boiler, to integrate heat and maintain suitable operational temperatures, the sensible heat thermal storage, to store solar energy and to allow MD unit continuos functioning, the MD unit feed tank, in which saltwater is heated up, and the membrane channels, in which the membrane distillation process occurs and freshwater is produced.

The model is composed by the mathematical representation of these main components and of the links between them. As stated above, the blocks and lines composing the Simulink diagram do not represent the physical outline of the system, rather mathematical (e.g. additions, integrations, etc.) or logical (e.g. if/else. . . then, etc.) operations at elementary scale, and physical relations as properties, quantities and parameters calculations at a larger scale. In Simulink it is possible to group elementary blocks linked between them into subsystems to increase order in the diagram and to eventually reuse the subsystem block in another part of the diagram. As an example, the mathematical expression of saltwater density with respect to temperature and salinity can be represented with the combination of elementary mathematical blocks, then grouped as a Subsystem block that have input and output ports.

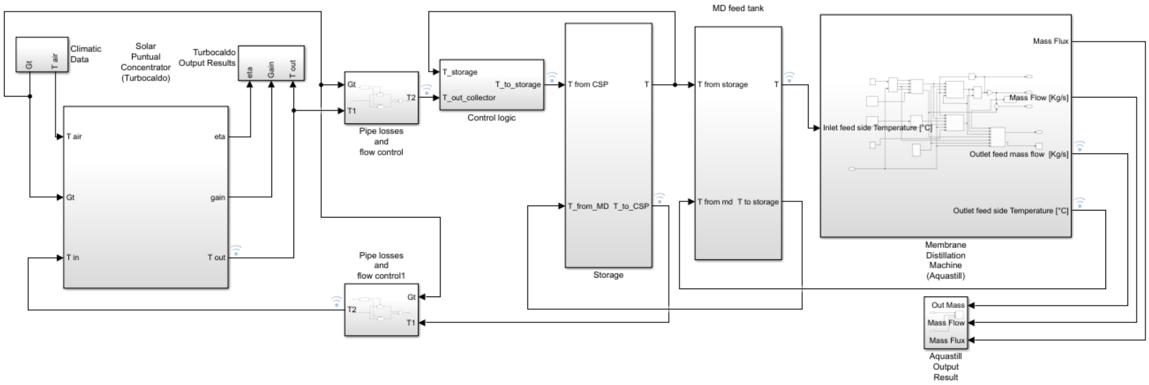

Figure 2.2: Simulink model of the presented system. The block diagram shows the main blocks corresponding to the main components of the system; inside these blocks there are the logical and mathematical relationships that compute the outputs (on the right side of the blocks) using the input given (on the left side of the blocks); the lines represent the signal transfers among blocks, allowing the use of output data as inputs for other blocks.

Figure 2.2 shows the highest level of grouping in the model of the system developed for the present work.

The shaded blocks contain other subsystem blocks that contribute in generating the block outputs processing the block inputs.

In the context of a collaboration, the author personally designed and built the climatic data block, the saltwater properties correlations blocks (embedded in the MD unit block, thus not visible at the highest model level), the SPD concentrator block, the pipe losses and flow control blocks and the MD unit block. control logic block, storage block and feed tank block were designed and built by Anna Mate, fellow student at Politecnico di Torino.

2.3 Climatic data

Climatic data are important variable inputs in the model. The considered data are the Direct Normal Irradiation (DNI) and the ambient air temperature. The two data are both collected by the European Union database PVGIS [46] for a great number of location around the world, allowing the modelled system to be virtually located in several places to assess its performances. The data can be consulted using a free web application with integrated map and several options regarding the available data. More specifically for this work, it is possible to obtain a typical meteorological year (TMY) DNI in W/m^2 and ambient air temperature in °C with an hourly resolution. These data are used to evaluate the solar power collected in the solar concentrator block and to compute heat losses to the environment in the storage tank block and in the MD feed tank block.

Since the DNI and temperature data represent quantities dependent on time, Simulink needs to receive them encoded in Time Series (.ts) format, to correctly interpret them for the simulation purposes. The encoding is made by a simple Matlab script, using .csv format data provided from PVGIS, previously loaded on a Excel sheet. The time series data are introduced into the Simulink model by From File elementary blocks, that synchronize the values with the simulation time.

2.4 Saltwater properties correlations

The salts diluted in the water changes the physical and thermal properties of the fluid, sometimes to a great extent. Thus, it is very important to take into account these variations when modelling a system. In this work, we make use of saltwater properties correlations, a popular topic in scientific literature devoted to desalination. Saltwater density, viscosity and vapour pressure correlations are taken from Sharqawy et al. [35] while specific heat and thermal conductivity are taken from Nayar et al [36]. These correlations have as input variables the Salinity of salt water expressed in kg/kg or g/kg and the saltwater temperature in K or °C, very important for a thermal process like Membrane Distillation.

Since correlations are algebraic formulation is simple to implement them into Simulink using elementary Math Operations blocks. In Figure 2.3 are shown the block diagrams for the correlations.

2.5 SPD Concentrator: Trinum vers. Turbocaldo by Innova (IT)

The Turbocaldo concentrator is modelled starting from the equation comparing the solar power collected and the enthalpy increase in the heat carrier fluid that states:

$$\eta A_{rea} I = \dot{m}_f c_{p_f} (T_{f_{out}} - T_{f_{in}}) \tag{2.1}$$

with

- η Concentrator efficiency [-];
- A_{rea} Net capturing area of the parabolic dish [m^2];
- I Direct Normal Irradiance (DNI) [W/m^2];
- $\dot{m}_f$ Heat carrier mass flow [kg/h];
- c_{p_f} Heat carrier specific heat [J/(kg K)];

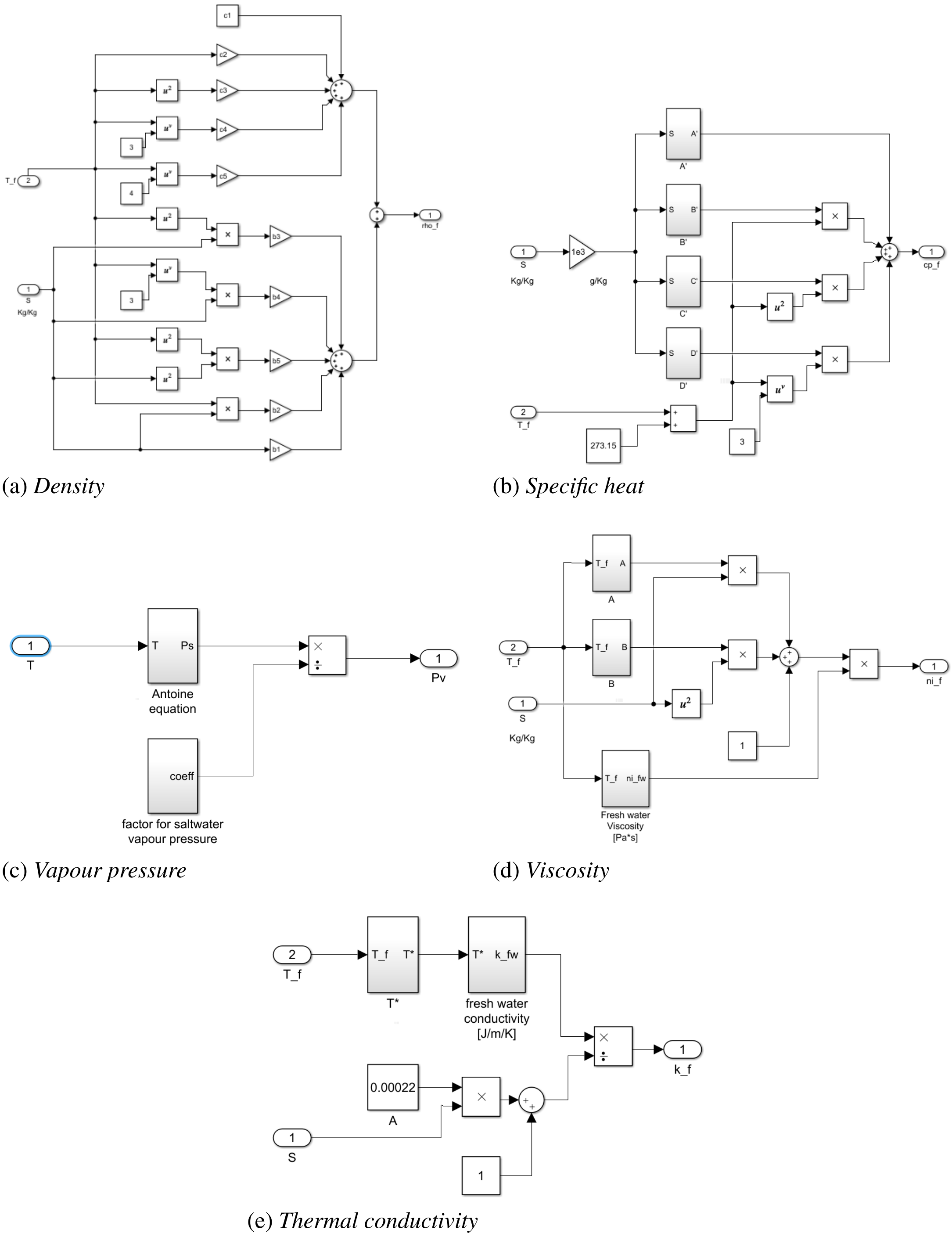

(a) *Density*

(b) *Specific heat*

(c) *Vapour pressure*

(d) *Viscosity*

(e) *Thermal conductivity*

Figure 2.3: Saltwater properties correlations block diagrams.

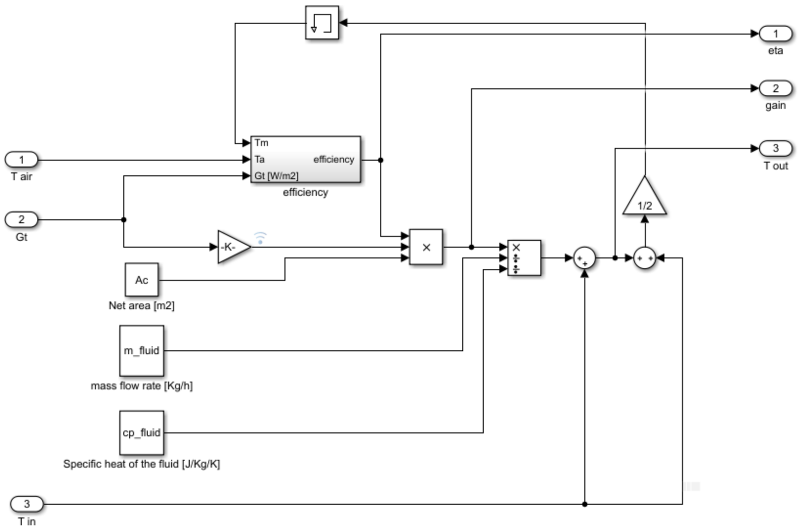

Figure 2.4: Solar concentrator block diagram. The block receives as inputs the Solar Irradiance, the Ambient air temperature and the Inlet temperature to compute the outlet temperature and the solar power harvested; it is present a subsystem devoted to evaluate efficiency, its structure visible in Figure 2.5

.

- $T_{f_{out}}$ Heat carrier outlet temperature [K];
- $T_{f_{in}}$ Heat carrier inlet temperature [K].

Figure 2.4 depicts the implementation as block diagram of Eq. 2.1 to simulate the Concentrator operations.

The efficiency η is computed in a subsystem using the general empiric formula of the efficiency of a solar thermal collector [47] :

$$\eta = \eta_0 - a_1 \frac{(\bar{T} - T_a)}{I} - a_2 I \left(\frac{(\bar{T} - T_a)}{I} \right)^2 \tag{2.2}$$

where

- η_0 Optical losses loefficient [-];
- a_1 Thermal losses linear coefficient [K/(W/m^2)];
- a_2 Thermal losses parabolic coefficient [K^2/(W/m^2)];
- $\bar{T}$ Mean fluid temperature computed as $\frac{(T_{f_{out}} + T_{f_{in}})}{2}$ [K];
- T_a Ambient air temperature [K].

The Eq. 2.2 is implemented as a block diagram in Figure 2.5.

The model computes the outlet temperature of the fluid using as inputs the DNI and the inlet fluid temperature. It also calculates the solar power collected, useful for energy evaluations.

The values of the block parameters are listed in Table 2.1.

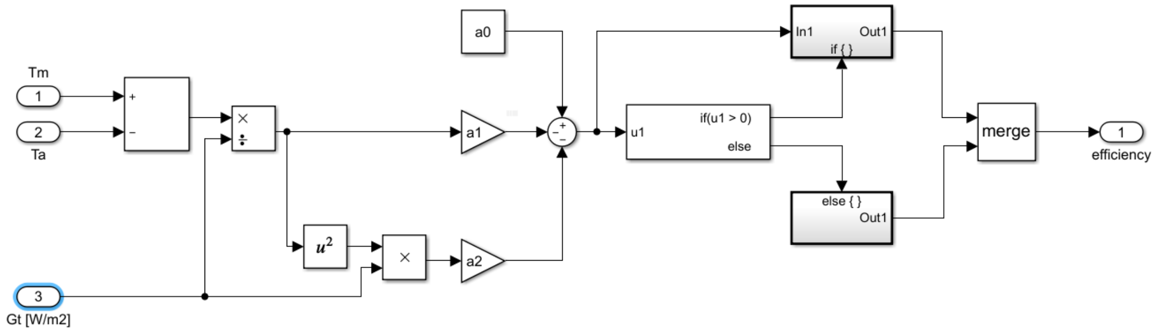

Figure 2.5: Concentrator Efficiency block diagram. Beyond the algebraic formulation, logical blocks are implemented to correctly simulate the system. the efficiency goes to 0 automatically if its mathematical evaluation results in negative (and so non-physical) values, to mimic the concentrator behaviour during nighttime (no gain).

Table 2.1: SPD Concentrator Trinum vers. Turbocaldo model parameters [26].

Parameter	Definition	Value
`Ac`	Net receiving area [m^2]	9.58
`m_fluid`	Fluid mass flow rate [kg/h]	576.288
Efficiency coefficients:		
`a0`	Optical losses coefficient [-]	0.769
`a1`	Thermal losses linear coefficient [K/(W/m^2)]	0.66
`a2`	Thermal losses parabolic coefficient [K^2/(W/m^2)]	0.008

2.6 Control logic

Control logic llock performs checks on the heat carrier that connects the solar concentrator and the sensible thermal storage. First it is in charge to check whether the heat carrier temperature is above a set value (95°C for the water-glycol mixture) to avoid biphasic flow. Then, it checks if the heat carrier fluid temperature is larger than the storage temperature; if it is not the case, the block computes the thermal power that is needed to heat up the fluid flow to a set minimum temperature, chosen to have a suitable storage temperature to feed the desalination process. This thermal power from a conventional source, combined with the solar energy value from the Concentrator block, is useful to evaluate the energy performances of the system.

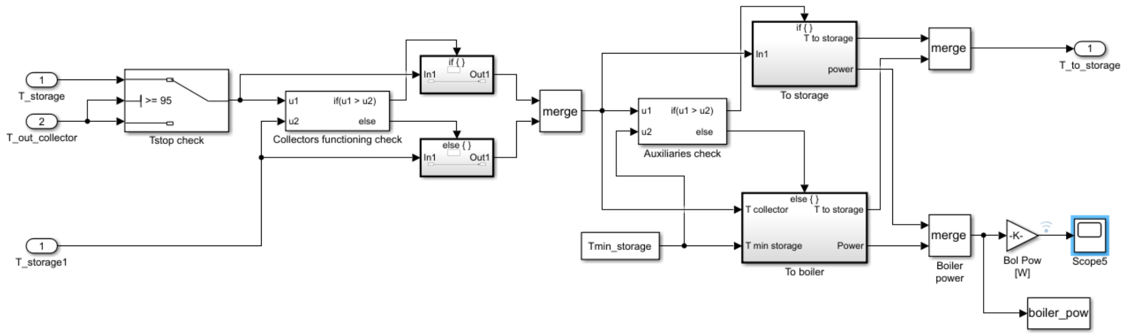

Figure 2.6: Control logic block diagram. It is possible to observe the three logical steps embedded in the block; From left, the check on fluid temperature to avoid biphasic flow and system damage, then the check on the collector functioning,and at the the right end of the figure the check on fluid temperature, its eventual increase and the evaluation of the conventional heat used.

2.7 Pipe losses and flow control

The block simulates the thermal losses of the heat carrier when flowing into the connection pipes from the SPD concentrator to the thermal storage tank and on the returning path. The losses are represented by a temperature drop over pipe length coefficient, multiplied by the connection pipes length (Figure 2.7 b). The block also performs an irradiance check to simulate the fluid pump turning off during night time.

On Table 2.2 block parameters are listed.

Table 2.2: Pipe losses and flow control block parameters.

Parameter	Definition	Value
Cp	linear temperature drop coefficient [°C/m]	0.1
Lp	pipe length [m]	10

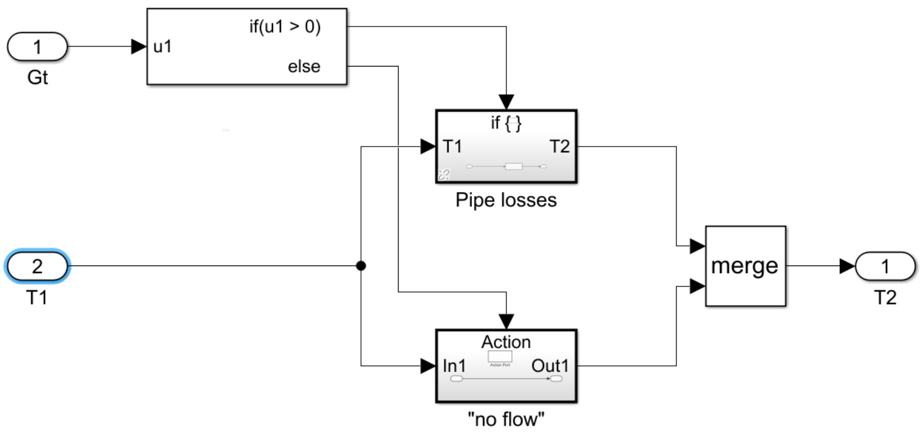

(a) *Pipe losses and flow control block diagram*

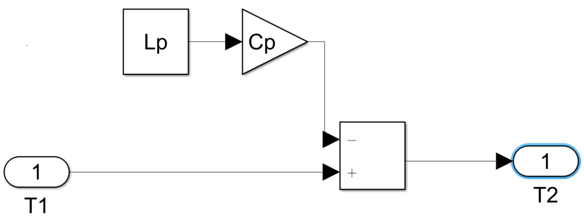

(b) *pipe losses formulation block diagram*

Figure 2.7: Pipe losses and flow control block diagram. The block consists essentially in a logic "if" control on the solar irradiance: if it is larger than 0 the fluid flows through the pipe, thus having its temperature decreased by thermal losses; if irradiance is lower than 0, "the pumps stops"; thermal losses are evaluated in the Pipe Losses subsystem, shown in Figure 2.7 b.

2.8 Sensible thermal storage

The sensible thermal storage block implements the first law of thermodynamics for the specific application (Figure 2.8). The main assumption of the implementation consists in the perfect mixing of the water mass inside the tank, that allows to consider a homogeneous mass temperature over all the tank volume. As another assumption, efficiency value of the heat exchanger that provide the heat from the solar concentrator to the storage tank is set to one. It is a strong assumption taken in order to simplify the formulation.

The first law of thermodynamics represents the conservation of energy and is usually expressed as

$$\Delta U = Q - W \tag{2.3}$$

with

- ΔU Internal energy variation in the system [J]
- Q Thermal energy provided to the system [J]
- W Work done by the system on its surroundings [J]

Since no work is done by the storage tank, our system in discussing, the W term can be removed from the equation. The equation can be expressed in differential form as

$$\frac{dU}{dt} = \dot{Q} \tag{2.4}$$

The $\dot{Q}$ term includes in it all the heat flow contributions, both entering and leaving the system. This term is replaced with the expression of the actual heat flow affecting the storage tank, the entering terms are placed in the left hand side while the leaving terms are placed into the right end side with the differential internal energy term, that assumes the form $Mc_{p_s}\frac{dT_s}{dt}$ to point out the storage temperature. This results in equation 2.5:

$$\dot{m}_f c_{p_f}(T_{f_{in}} - T_{f_{out}}) = Mc_{p_s}\frac{dT_s}{dt} + Q_{dis} + \dot{m}_{MD}c_{p_s}(T_s - T_{MD_{in}}) \tag{2.5}$$

with

- $\dot{m}_f$ Heat carrier mass flow [kg/h];
- c_{p_f} Heat carrier specific heat [J/(kg K)];
- $T_{f_{in}}$ Heat carrier inlet temperature in storage [K];
- $T_{f_{out}}$ Heat carrier outlet temperature from storage [K];

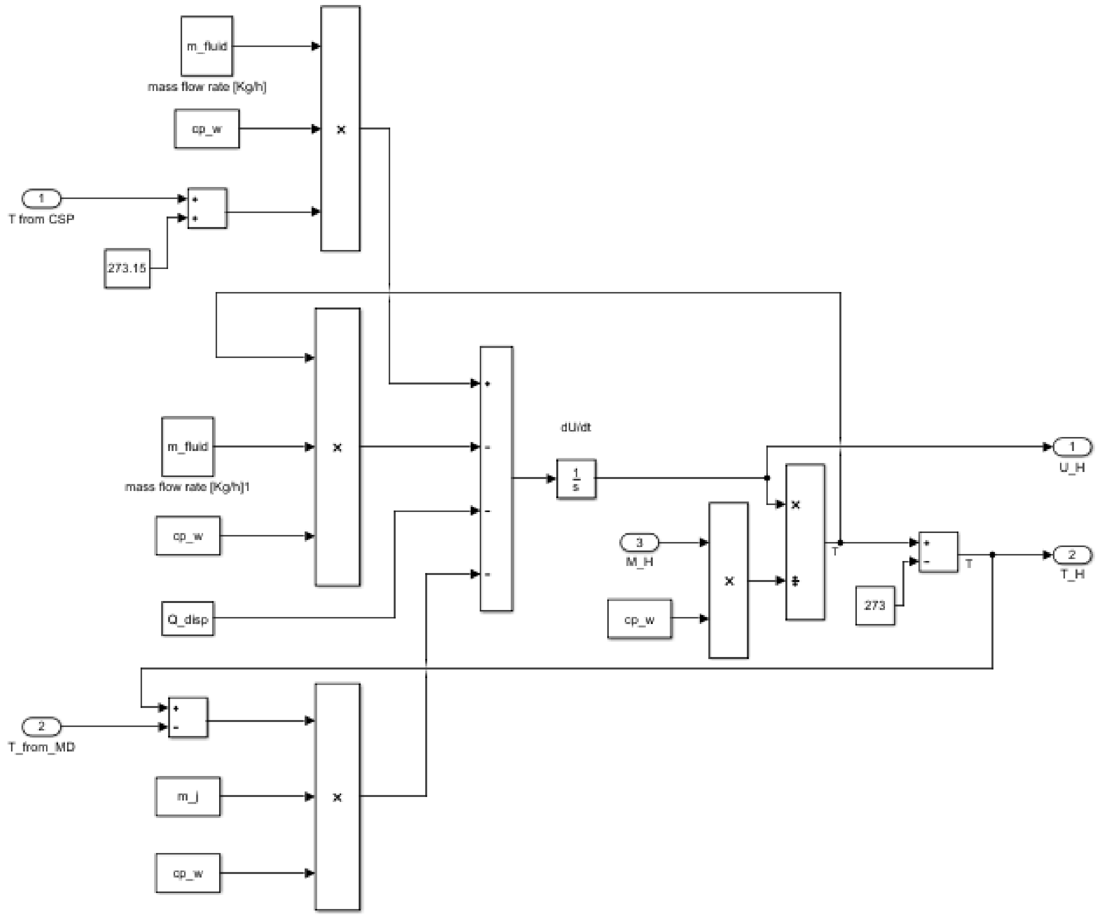

Figure 2.8: Implementation of the first principle on the storage control volume. At the left side are represented the energy flow contributions. At the core of the diagram the Integrator elementary block performs the resolution of the differential equation.

- M Storage mass [kg];
- c_{p_s} Storage mass specific heat [J/(kg K)];
- T_s Storage temperature [K];
- Q_{dis} Thermal losses to the environment [J/h];
- $\dot{m}_{MD}$ Mass flow rate to and from MD feed tank [kg/h];
- $T_{MD_{in}}$ inlet temperature of returning mass flow from MD feed tank [K].

The block returns as output the storage temperature, used both as input in other blocks and as a simulation result of interest.

2.9 MD feed tank

The MD feed tank is modelled as a very small size sensible heat storage. The perfect mixing assumption is made for the tank mass, supported by the small size of the volume and efficiency value of the heat exchanger that provide the heat from the solar concentrator to the storage tank is assumed one. It is a strong assumption taken in order to simplify the formulation. Hence another first law of thermodynamics application is implemented to describe it, stating:

$$\dot{m}_{MD} c_{p_s} (T_s - (T_{ft} + \Delta T_{min})) = M_{ft} c_{p_{sw}} \frac{dT_{ft}}{dt} + Q_{dis} + \dot{m}_{feed} c_{p_{sw}} (T_{ft} - T_{feed_{in}}) \quad (2.6)$$

where

- $\dot{m}_{MD}$ Mass flow rate to and from storage [kg/h];
- T_{ft} Feed tank temperature [K];
- ΔT_{min} Temperature difference at the heat exchanger pinch point [K];
- M_{ft} Feed tank mass [kg];
- Q_{dis} Thermal losses to the environment [J/h];
- $\dot{m}_{feed}$ Mass flow rate to and from MD membrane feed side [kg/h];
- $T_{feed_{in}}$ Inlet temperature of returning mass flow from MD membrane feed side [K].

The given output is the bulk temperature of the saltwater sent to the membrane, a crucial value to estimate the freshwater permeate flux, and the consequently produced freshwater flow. Figure 2.9 shows the block diagram implementation.

2.10 MD unit

The membrane distillation block is the most complex part of the model. It represents the processes that take place into the membrane channels of the Aquastill's DCMD lab unit (Figure 2.10).

The core of the block is the subsystem that computes the fresh water mass flux using the difference of vapour pressures across the membrane as:

$$N_w = K(p_v(T_f, S) - p_v(T_p)) \quad (2.7)$$

with

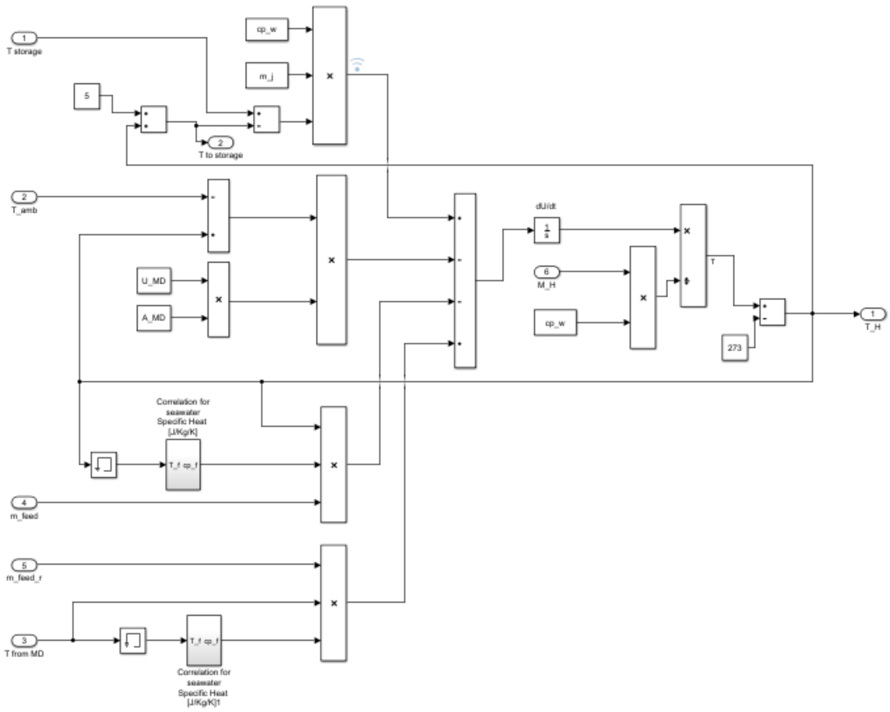

Figure 2.9: Implementation of the first principle on the MD feed tank control volume. At the left side are represented the energy flow contributions. At the core of the diagram the Integrator elementary block performs the resolution of the differential equation.

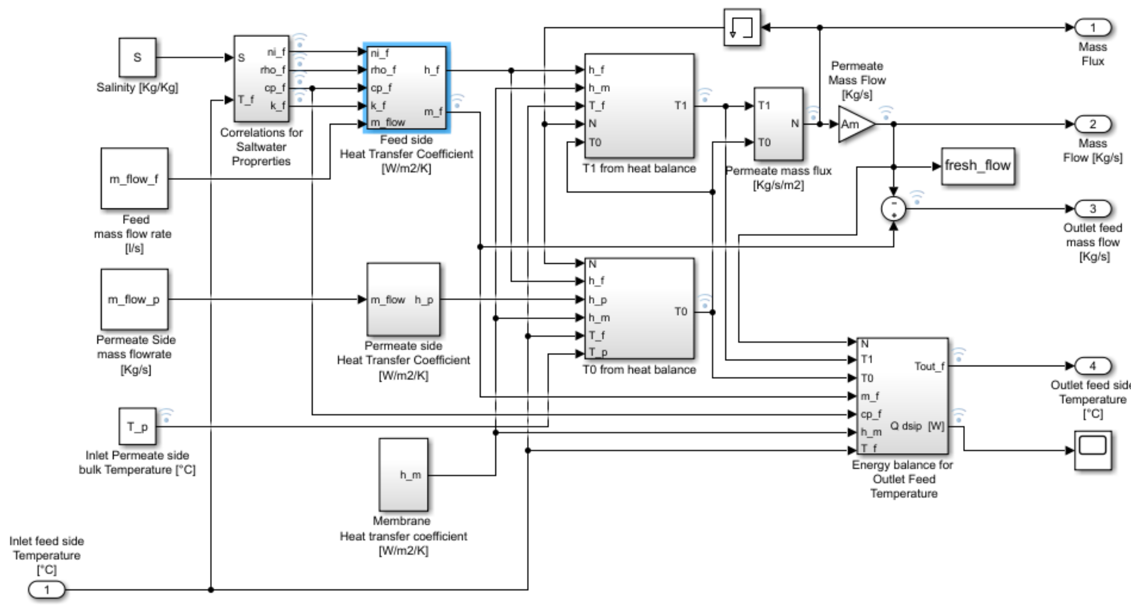

Figure 2.10: Membrane Distillation Unit block diagram. The block diagram is composed by several subsystems, of which diagrams are shown in Figure 2.11. From left to right it is possible to observe the saltwater properties correlation block, the three subsystem blocks devoted to the evaluation of the heat transfer coefficient for each heat transfer phenomena occurring into the channels (Figure 2.11a shows feed side heat transfer coefficient block as example), the two subsystem blocks devoted to the evaluation of membrane temperatures (Figure 2.11b shows feed side membrane temperature block as example), the subsystem block devoted to the computation of the freshwater mass flux (Figure 2.11c) and the subsystem block devoted to evaluation of the feed side outlet temperature by means of a steady state energy balance equation (Figure 2.11d).

- N_w Freshwater mass flux [kg/(s m^2)];
- K Membrane coefficient [kg/(s m^2 Pa)];
- p_v Vapour pressure [Pa];
- T_f Saltwater temperature at the membrane interface [K];
- S Saltwater salinity [kg/kg];
- T_p Permeate side temperature at the membrane interface [K];

The saltwater vapour pressure is computed using literature correlation that takes into account temperature and salinity, while the permeate side vapour pressure is computed using the Antoine Equation based on temperature.

The temperatures at the membrane interfaces must be computed imposing the continuity of the heat flux from the hot side bulk to the cold side bulk, passing through the membrane. The mathematical model of this phenomenon is already discussed in this work in section 1.2.5. Here the temperatures computation is carried by coupling two of the equation resulting from continuity [31] and by putting in evidence the two needed temperatures.

$$T_p = \frac{N_w \Delta h_v \left(1 - \frac{1}{1+\frac{h_f}{h_m}}\right) + h_p T_{pb} + \frac{h_f T_{fb}}{1+\frac{h_f}{h_m}}}{h_p + h_m - \frac{h_m}{1+\frac{h_f}{h_m}}} \tag{2.8}$$

$$T_f = \frac{h_f T_{fb} + h_m T_p - N_w \Delta h_v}{h_m + h_f} \tag{2.9}$$

This computation is made by two dedicated subsystems, one for each temperature value.

The heat transfer coefficients present in the formulations above have to be computed taking into account the flow regime experienced in the two channels by the water, for the convective heat transfer in the bulk-interface transfers, and by evaluating the membrane heat transfer coefficient, for the conductive transfer across the membrane.

The first task is performed by two dedicated subsystems, one for channel. The subsystems receive as input the mass flow rate values and the physical and thermodynamic properties of the water, salt and fresh respectively. These are used to evaluate, using the dimensionless Reynolds number, whether the flow regimes are laminar or turbulent and choose accordingly what correlation is to be used to calculate the dimensionless Nusselt number, from which is possible to calculate the heat transfer coefficient [37].

Scientific literature about MD [39] [38] [31] suggests some Nu correlations, in this work were used:

For laminar flow the Graetz-Leveque correlation

$$Nu = 1.86\Big(RePr\frac{d_h}{L}\Big)^{0.33} \tag{2.10}$$

where

- Re Reynolds number [-];
- Pr Prandtl number [-];
- d_h Hydraulic diameter of the channel [m];
- L length of the channel [m].

For turbulent flow the Dittus-Boelter correlation

$$Nu = 0.023Re^{0.8}Pr^n \tag{2.11}$$

where

- n Constant equal to 0.4 for heating and 0.3 for cooling [-].

The membrane coefficient K is computed following the physical description of the mass transfer phenomena in the membrane discussed in section 1.2.5. In brief:

$$N_w = -\frac{1}{\frac{1}{C_k}+\frac{1}{C_d}}\frac{dp}{dx} \tag{2.12}$$

It is worth noting that thePD factor in C_d formulation (see section 1.2.5) is computed using the correlation based on temperature that states:

$$PD = 1.19 \cdot 10^{-4}\bar{T}^{1.75} \tag{2.13}$$

in which $\bar{T}$ is the mean temperature across the membrane, while the tortuosity τ used in both C_k and C_d is computed as:

$$\tau = \frac{(2-\epsilon)^2}{\epsilon} \tag{2.14}$$

Using the porosity ϵ [31].

MD block also computes the outlet temperature of the feed mass flow in a subsystem, that rely on a heat power balance on the hot feed channel that can be written as:

$$\dot{m}_{feed}c_{p_{sw}}(T_{feed_{in}} - T_{feed_{out}}) = Q_{disp} + A_m h_m(T_f - T_p) + N_w A_m \Delta h_v \tag{2.15}$$

where

- $T_{feed_{in}}$ Inlet bulk temperature at the channel entrance [K];
- $T_{feed_{out}}$ Outlet bulk temperature at the channel exit [K];
- A_m Membrane surface Area [m^2].

The termal losses to environment Q_{disp} are calculated by a correlation based on experimental values from the Aquastill module. As input variable uses the inlet feed bulk temperature and its validity range is from 50 to 80 °C.

Table 2.3 shows parameters values of the whole block.

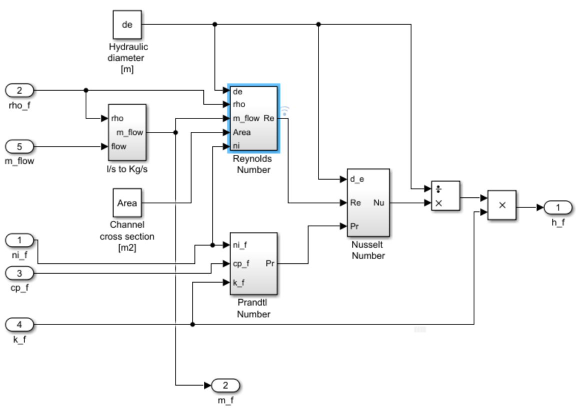

(a) *Feed side heat transfer coefficient block diagram*

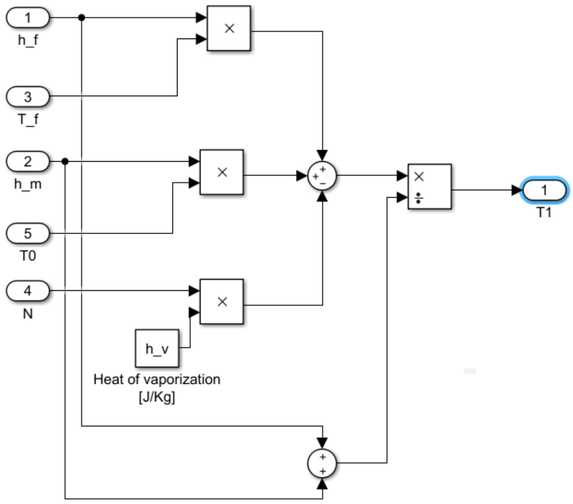

(b) *Feed side membrane temperature block diagram*

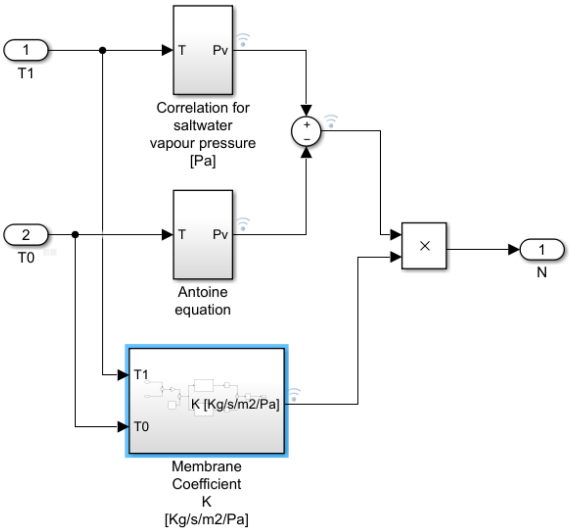

(c) *Freshwater mass flux block diagram*

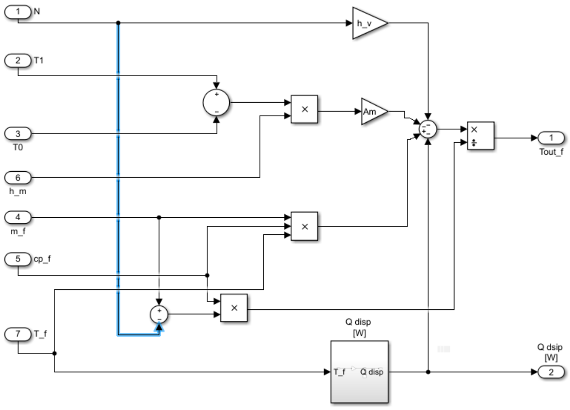

(d) *Feed side outlet temperature block diagram*

Figure 2.11: Block Diagrams of the main subsystems composing the MD unit block.

Table 2.3: MD unit block parameters [34]

Parameter	Definition	Value
Feed side:		
`m_flow_f`	Flow rate [l/s]	0.0278
`S`	Salinity [kg/kg]	0.0350
Permeate side:		
`m_flow_p`	Flow rate [l/s]	0.0278
`T_p`	Bulk temperature [°C]	20
`rho_p`	Density [kg/m^3]	1000
`ni_p`	Dynamic viscosity [Pa s]	$0.4024 \cdot 10^{-3}$
`cp_p`	Specific heat [J/(kg K)]	4186
`k_p`	Thermal conductivity [J/(m K)]	$675.3 \cdot 10^{-3}$
`Pr_p`	Prandtl number [-]	2.4944
Membrane (Aquastill PTFE from [48]):		
`thick`	Thickness [μm]	77
`rad_m`	Mean pore size [μm]	0.17
`epsilon`	Porosity [-]	0.83
`k_m`	Thermal conductivity [J/(m K)]	0.0382
`Am`	Surface area [m^2]	0.05
Geometry:		
`Area`	Channel cross-section [m^2]	$1 \cdot 10^{-4}$
`de`	Hydraulic diameter [m]	0.002
`L`	Channel length [m]	0.5

Chapter 3

Membrane distillation unit model validation

In the following part of the work, the Membrane Distillation unit SimuLink model is validated. To correctly estimate the validity of the MD unit model the used method is to compare its outputs with data obtained by experimental activities. Experiments and simulations must be carried out in the same condition to relate results to each other.

The MD Lab Unit by Aquastill comes from manufacturer with samples of different membrane types, to carry out several experimental activities. The experiments are executed imposing a steady state operation of the MD unit. In detail, inlet feed temperature, inlet permeate temperature, feed flow rate and permeate flow rate are kept fixed for the time needed to correctly evaluate the figure of merit for membrane distillation devices, the freshwater hourly surface flow rate [l/h/m^2]. Inlet and outlet temperatures for both feed and permeate flow are measured by the experimental instruments. The inlet feed temperature is then varied to investigate performances at different steady state conditions.

On model side the input values for inlet feed temperature, inlet permeate temperature, feed flow rate and permeate flow rate are kept fixed at the same values used for experiments, to simulate steady state conditions. The geometry of the physical device is implemented into the model, prominently to determine the flow regimes into the membrane channels. Since the model evaluates the membrane coefficient starting from the membrane parameters of porosity, thickness, mean pore diameter, and thermal conductivity, it is necessary to find those values. These data do not come with the membranes from manufacturer and are difficult to evaluate using experimental processes. However, Eykens et al. [48] have characterized several commercial membranes in their work , including a Polytetrafluoroethylene (PTFE) membrane from Aquastill.

Hence, to judge if the model represents accurately the experimental results, experimental freshwater flux with PTFE membrane at 50°C, 60°C and 70°C inlet feed side temperature

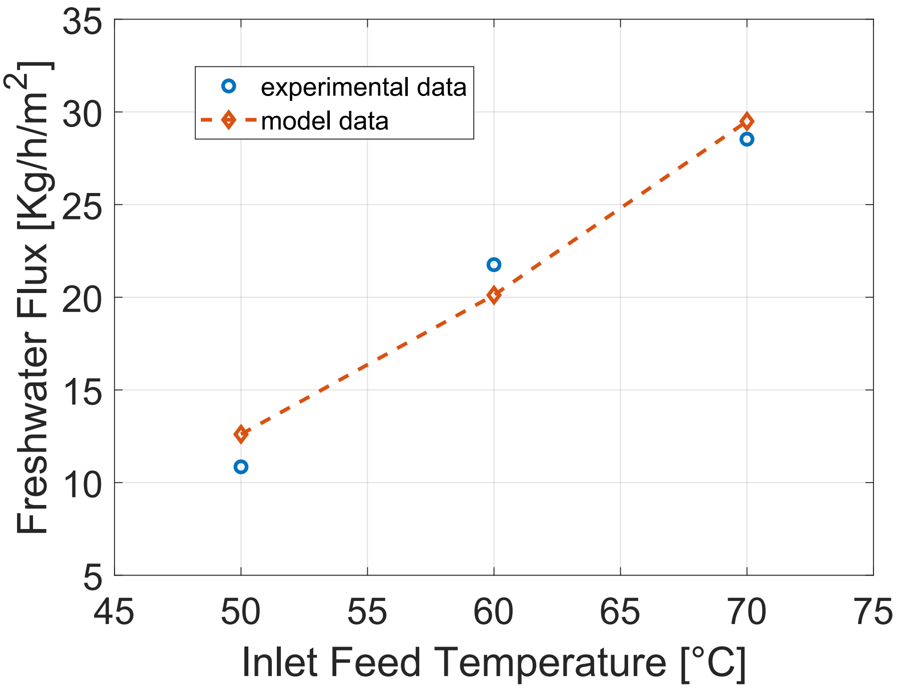

Figure 3.1: Comparison on Freshwater Flux between experimental data and model results. In a qualitative way, it is possible to appreciate the model results accuracy with respect to the experimental data collected. The trend of the model results follows the vapour pressure curve trend, which is the driver of the phenomenon.

are compared with the computational results with same condition of operation computing the errors on the single experimental values and their mean value. Another comparison is made on the outlet feed temperature values, computing the errors on the single experimental values and their mean value for this quantity too, to check also the consistence of an important thermal result, in term of device integration with the overall system.

The results are summarized in Figure 3.1 and Figure 3.2 for the freshwater flux and in Figure 3.3 and Figure 3.4 for the outlet feed temperature.

Analizing the comparisons and the related relative errors, it is possible to observe a good concordance between model computiations and experimental data.

The mean error on the freshwater flux is around 9% with a minimum at the highest considered operative temperature below 4%. 70 °C are a typical operative temperature for steady state functioning, so having the relative error minimum at this temperature can lead to very precise prediction of productivity in the most typical configuration.

Even better results are achieved on the outlet feed temperature, with a mean relative error below 2.5% and a minimum at 60 °C below 1.5%. The heat losses correlation, which presents a low standard deviation, contributes to the computational accuracy.

In conclusion, the model can be trusted in its computation and it is suitable to simulate the MD unit behavior, allowing its implementation on the general model of solar desalination.

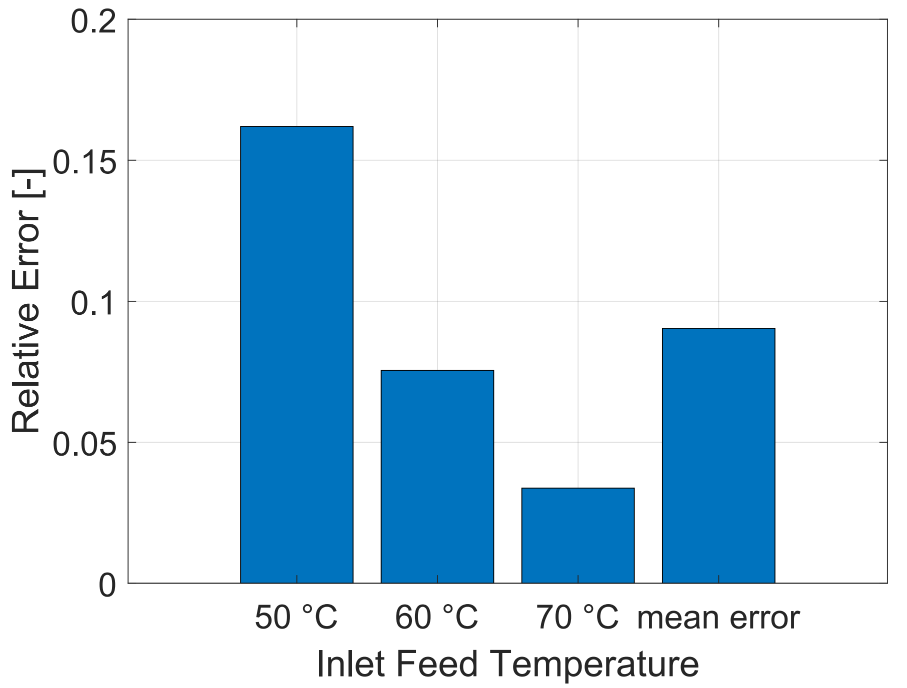

Figure 3.2: Model error on Freshwater Flux experimental data. The bar plot shows a descending trend in the error value with respect to the increasing temperature. The mean value attests at 0.09, assuring a good overall accuracy on the freshwater flux computation.

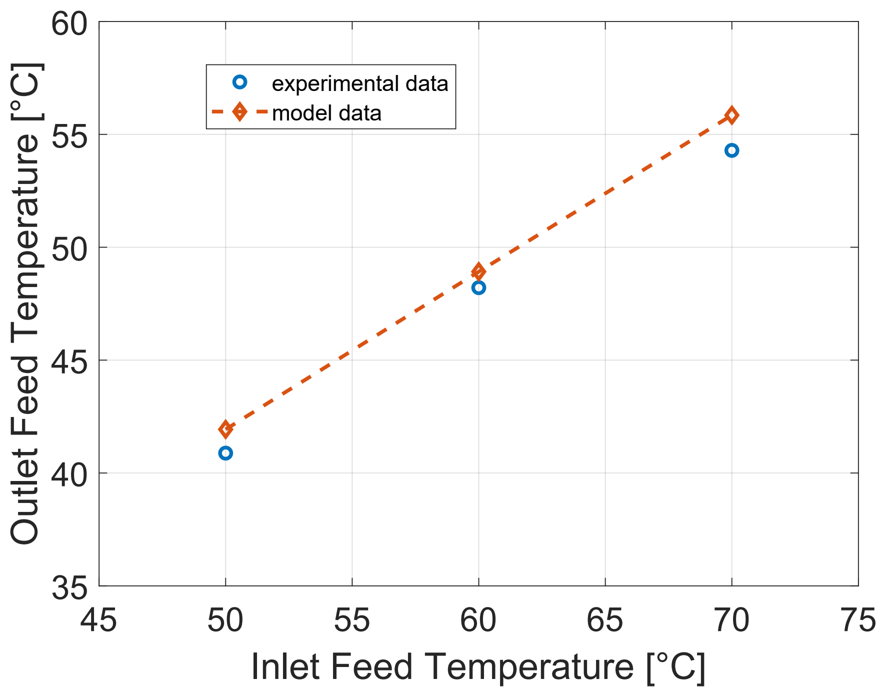

Figure 3.3: Comparison on Outlet Feed Temperature between experimental data and model results.The model results trend is almost linear, due to the preponderance of the ambient losses (computed with a linear correlation) with respect to the heat transfer from feed side to permeate side.

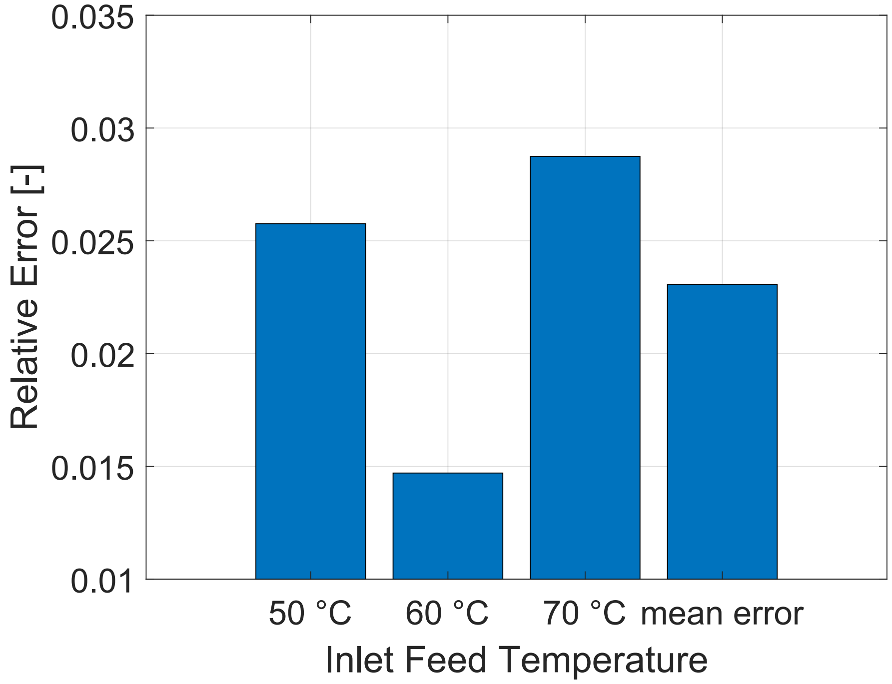

Figure 3.4: Model error on Outlet Feed Temperature.

Chapter 4

Model results

In the previuos chapters the solar desalination model has been outlined and validated. In this chapter the model is used to perform simulations in three geographical location to evaluate the system behaviours and performances.

The chosen location are Turin, Piedmont in Italy, Palermo, Sicily in Italy and Abu Dhabi in the United Arab Emirates. Climatic data of these places can be taken from the European Union PVGIS database [46]. The data are used to carry out a simulation along a year and to evaluate four main values: the renewable energy portion on the total fed energy to have suitable minimum operational temperatures in the system, as discussed in Chapter 2, the freshwater annual yield, the mean hourly production during the year and the energy consumption per cubic metre of produced freshwater.

The three case studies behaviours are now presented, taking into account a weekly period of both winter and summer seasons. Subsequently, comparison on the the renewable energy portion on the total fed energy and the freshwater annual yield are presented and discussed.

4.1 Turin, Piedmont (ITA)

Turin (45.068 N; 7.682 W) is a major city in the north-west of Italy. This location since a Trinum concentrator unit is installed at Politecnico di Torino, to have a brief comparison between experimental data and model computations [44].

Turin neither experiences freshwater shortage nor has saltwater reservoirs, but it is worth noting that membrane distillation process can be used to purify wastewater in a certain range of wastewater composition [5]. Thus, it may be interesting to evaluate system performance in the perspective of the deployment of this technology in the city wastewater processing cycle.

4.1.1 Trinum solar concentrator

The relevant values for the component are the inlet and outlet fliud temperatures (Figure 4.1), to investigate the time variation and to verify that no biphasic flow occurs in the fluid circuit, and the concentrator efficiency (Figure 4.2), to evaluate its performance.

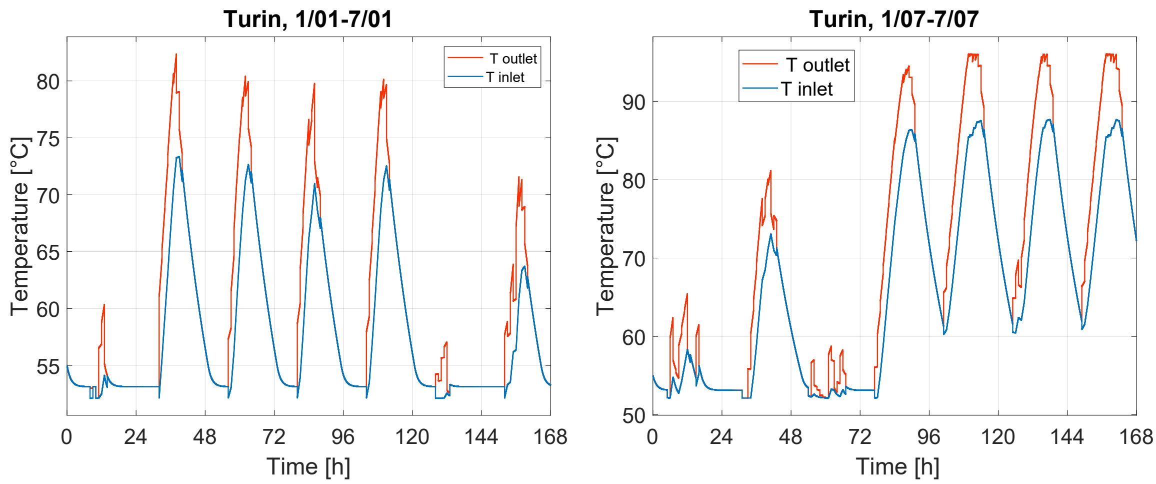

(a) *Wintertime week* (b) *Summertime week*

Figure 4.1: Concentrator fluid temperatures in Turin: the seasonal differences are well represented by the reached maximum temperatures during day and the curve shapes along the week

During wintertime in Turin, the fluid outlet temperature reaches values above 80 °C only in a few days for the season.

Moreover, cloudy or rainy days further reduce the solar power collected, a reduction that is clearly visible not only on the outlet fluid temperature but also on the inlet temperature, because the returning fluid from the thermal storage reflects the decrease in storage temperature due to a lack of energy contribution.

Even if Turin is located in the temperate portion of the northern hemisphere, the good performance of the solar concentrator allows the outlet fluid temperature to reach values over 95 °C in summertime. However, days with low irradiation values continue to influence noticeably the outlet temperature.

Concentrator efficiency (Eq. 2.2) values hardly reach 0.7 value in winter (Figure 4.2a), due to the combination of low ambient air temperature and low irradiation typical of the period. During summertime the efficiency is larger compared to winter values (Figure 4.2b), for the opposite reasons, but still present large variations along the day as in wintertime.

For both wintertime and summertime, the efficiency value is set to 0 when irradiance is 0, since no solar energy can be collected during nighttime.

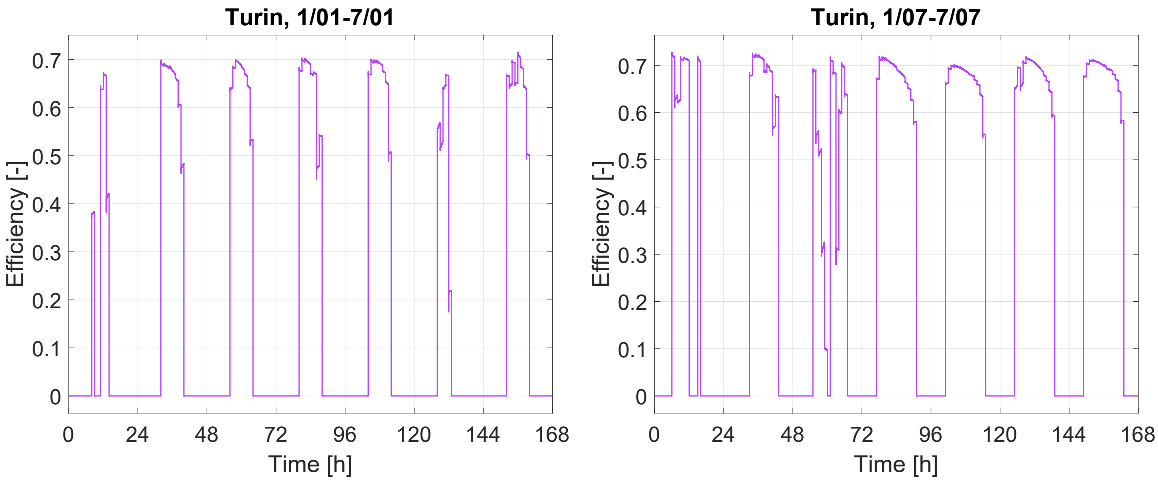

(a) *Wintertime* (b) *Summertime*

Figure 4.2: Efficiency in Turin during a week. Thanks to the higher irradiance and warmer ambient temperature, efficiency during summertime is larger than in wintertime.

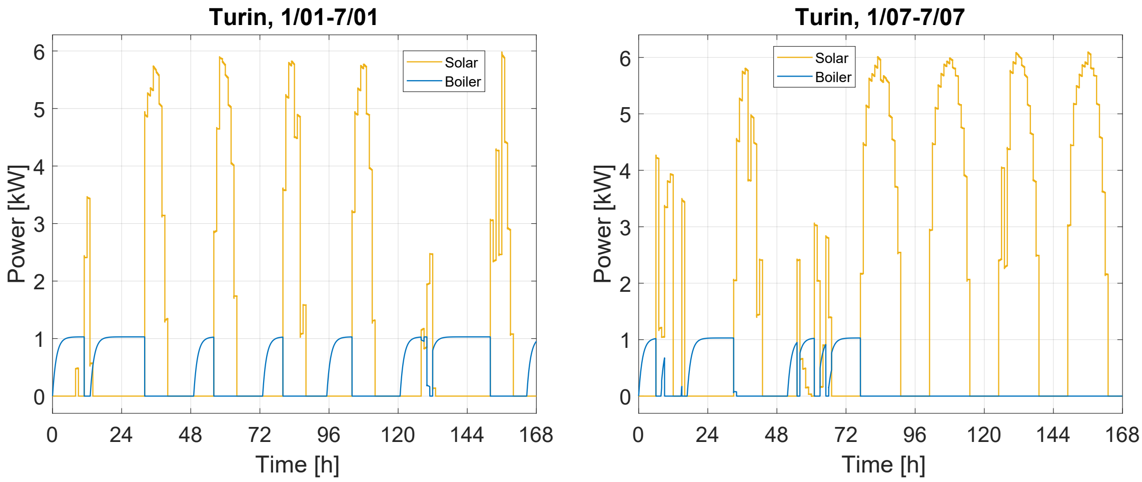

(a) *Wintertime* (b) *Summertime*

Figure 4.3: Inlet power into the system in Turin during a week. Since in summertime the irradiance is higher and the insolation time is longer, the back-up boiler is able to not intervene for even consecutive days, while in wintertime daily contribution are needed.

4.1.2 Power contributions

The Figure 4.3 shows the contribution of both solar and conventional power to the system, to check the correct intervention of the back up boiler. These results are used, on the whole year period, to compute the energy and to evaluate the solar ratio on total energy fed.

Wintertime climatic conditions do not permit the solar concentrator to harvest more than 6 kW even in peak irradiation hours, forcing the back-up boiler to turn on in order to keep storage temperature to the set minimum value of 50 °C. As it can be expected, the boiler turns on usually during the nighttime, with longer operation time after low irradiation days, and during particularly low irradiation days.

The situation is different during summertime. In fact, the higher irradiance values, that permit to exceed 6 kW of peak power, and the longer exposition time to the sun allow to harvest a larger quantity of energy, that in turn makes not necessary the intervention of the back-up boiler, if not in case of rainy or cloudy days.

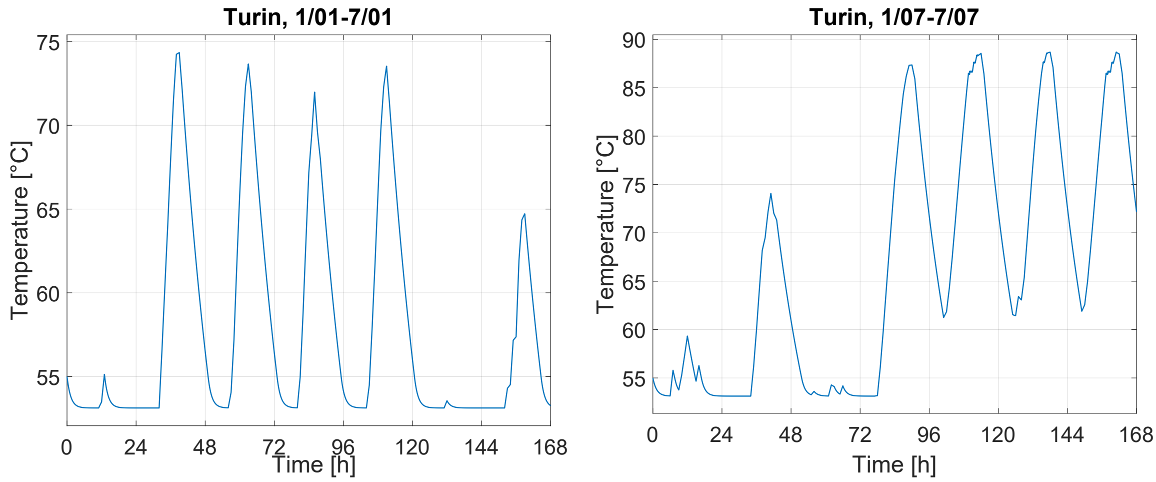

(a) *Wintertime* (b) *Summertime*

Figure 4.4: Storage temperature in Turin during a week. As it can be expected, storage temperature can reach higher values and oscillate in an higher range during summertime; still, low irradiance days greatly effect the storage, leading to low temperature near the set minimum.

4.1.3 Thermal storage and MD feed tank

The interesting output for this two components is their mass temperature (Figures 4.4 and 4.5) that permits to evaluate the good functioning and to check whether the back up boiler succeeds in maintaining the storage temperature above the set minimum value.

During the winter week considered, the storage temperature is subject to daily oscillations that spans along 20°C and have their baseline at the set minimum temperature, and they would be even lower if a back-up boiler was not installed. Consequently, also the feed tank saltwater temperature shows variations during the time period, assuming values that spans from 44°C to 62°C. These range of temperatures imposes to desalination unit a low freshwater flux at the membrane, since it is tied to the vapour pressure difference, dependent on saltwater temperature.

Thanks to the higher energy harvest, storage temperature assumes higher values in summer. Its value can reach almost 90°C, and its minimum values during a series of sunny days is above 60°C, allowing higher temperature also in the saltwater feed tank of the membrane distillation unit, that enables larger freshwater mass flux across the membrane. Feed tank temperature in sunny days spans from above 50°C to nearly 75°C , a proper operative range for the desalination device.

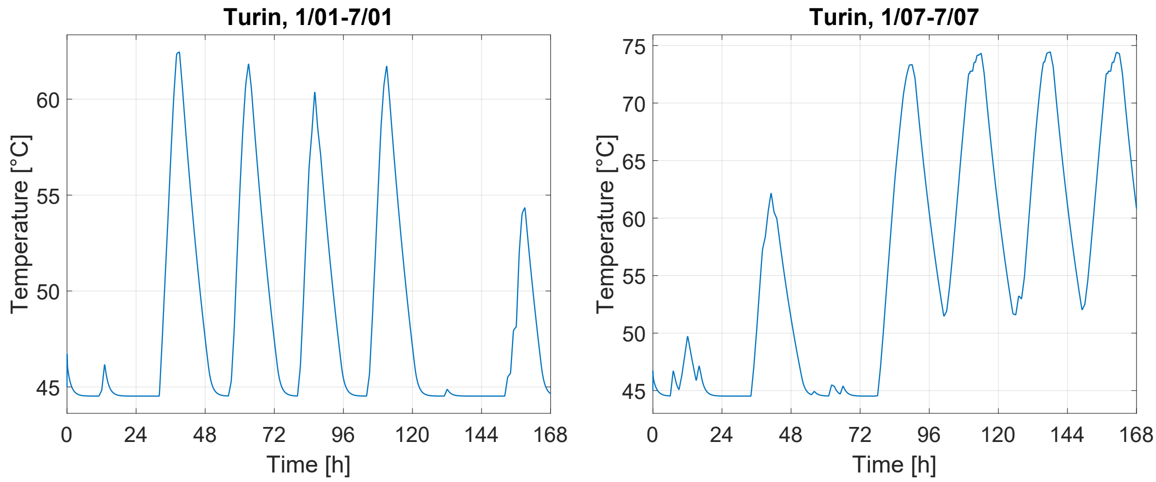

(a) *Wintertime* (b) *Summertime*

Figure 4.5: Feed tank temperature in Turin during a week. The tank temperature behaviour follows closely the storage one (Figure 4.4), with summertime values assuring MD unit good operations.

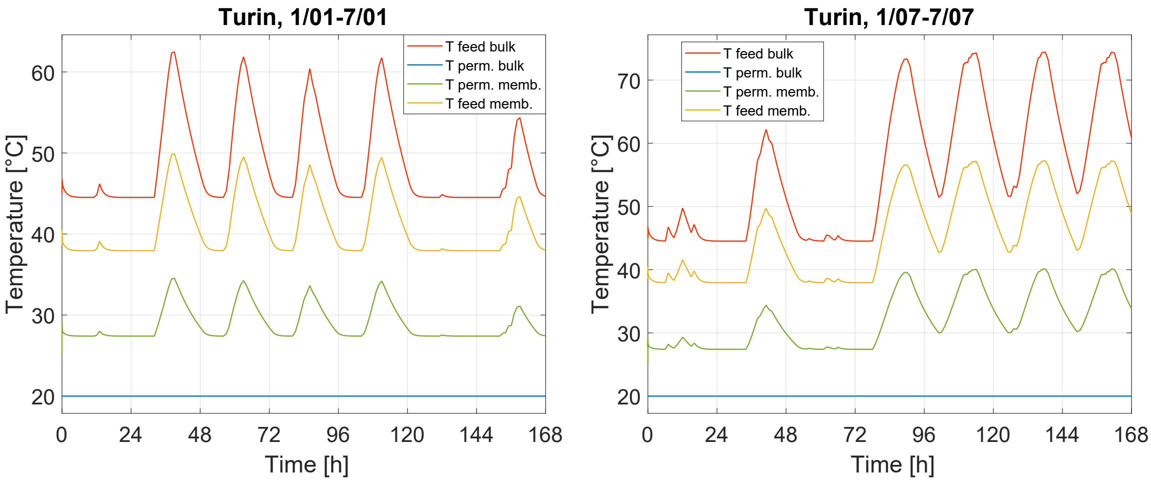

(a) *Wintertime* (b) *Summertime*

Figure 4.6: Channels temperatures in Turin during a week. The pictures represent the temperature trends during operations. The membrane temperatures permits to evaluate the vapour pressure and the freshwater flux across the membrane consequently.

4.1.4 Membrane distillation channels

In this part of the model,membrane channels, in which distillation occurs, temperatures (Figure 4.6) are evaluated, to correctly compute the freshwater mass flux (Figure 4.7), one of the main output of the entire model. To connect this block to the rest, also another thermal value is computed, the outlet feed bulk temperature(Figures 4.9) , that indirectly shows the heat in part used in the process and in part lost to the environment.

The values for the feed and permeate membrane temperatures depend on the heat transfer mechanisms from the bulk to the membrane interface and on the mass flux across the membrane. Since the flow in both channels is of laminar type (Re< 2100), the heat transfer coefficients are low, inducing a quite high temperature difference from bulk to interface.

The freshwater mass flux follows the trend of the membrane interface temperatures, that influence it both determining the vapour pressure difference and affecting the membrane coefficient.

In wintertime, the mass flux assumes values from $2.1{\cdot}10^{-3}$ Kg/s/m^2 to $6.2{\cdot}10^{-3}$ Kg/s/m^2, denoting a low process efficiency due to low temperature.

In summer, values can rise above $9.0{\cdot}10^{-3}$ Kg/s/m^2 with a minimum for low irradiance days around $4.0{\cdot}10^{-3}$ Kg/s/m^2, thanks to the consequent increase of membrane coefficient and vapour pressure difference.

Regarding the bulk temperatures on the feed side (Figure 4.9), it is possible to see, both in wintertime and in summertime, the increase in the inlet-outlet temperature difference as the inlet temperature of the feed bulk increase, denoting a larger heat transfer from the saltwater

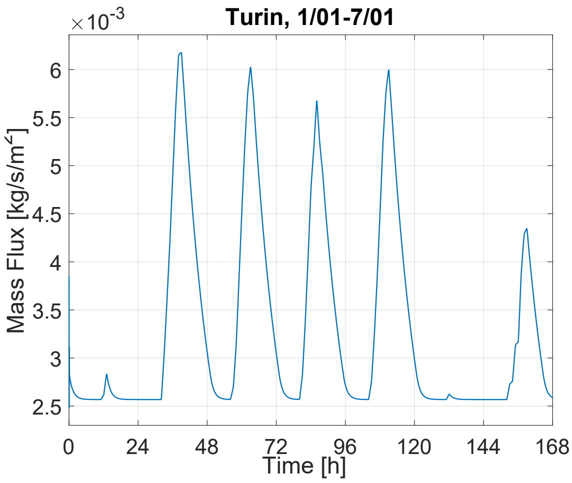

(a) *Wintertime*

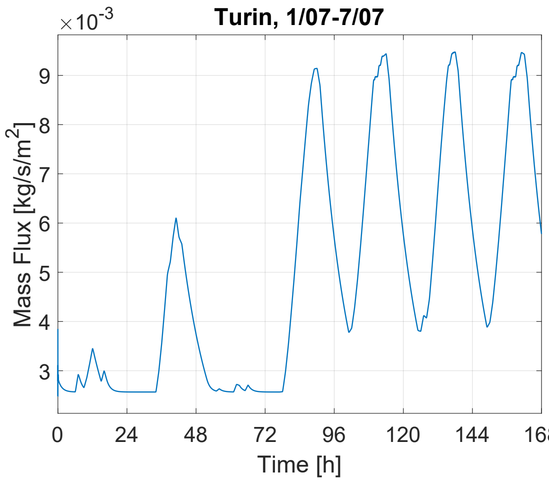

(b) *Summertime*

Figure 4.7: Freshwater mass flux in Turin during a week. The values vary with respect to the vapour pressure difference on the membrane, depending on the feed temperature.

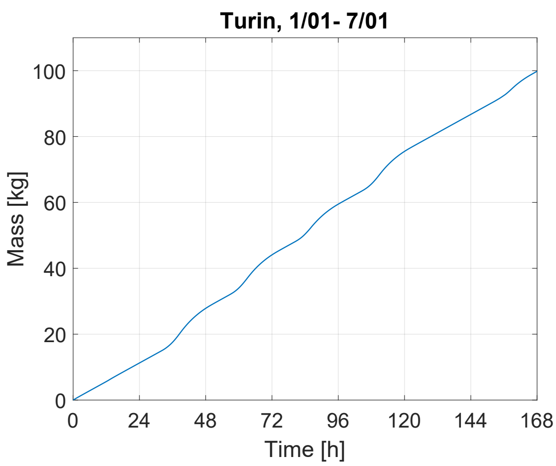

(a) *Wintertime*

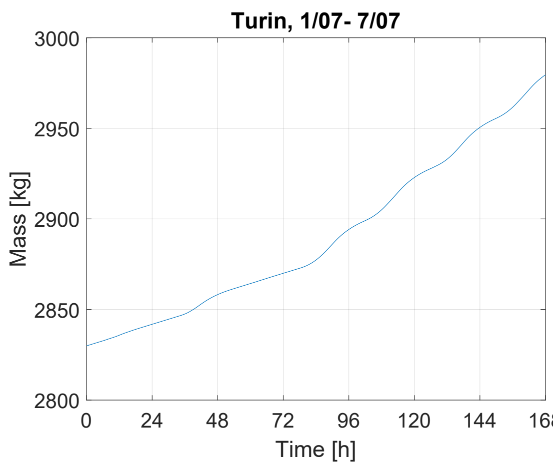

(b) *Summertime*

Figure 4.8: Freshwater mass cumulative in Turin during a week. The plots shows the total produced mass for every time step in the two weeks; in the summertime plot, it is interesting to note the fast increase of the quantity during time.

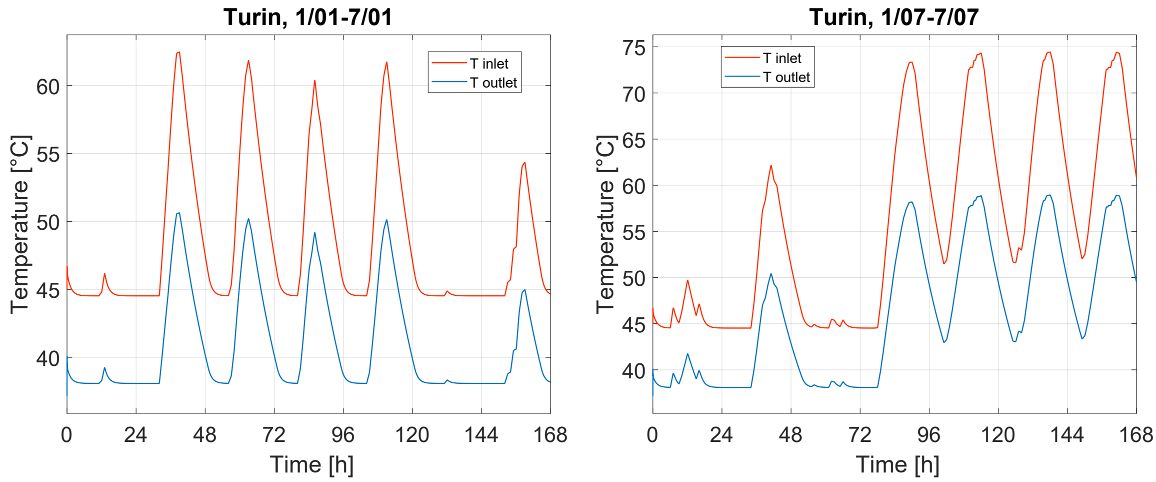

(a) *Wintertime* (b) *Summertime*

Figure 4.9: Feed bulk temperatures in Turin during a week. The difference from inlet to outlet are due to the latent heat transfer associated with the freshwater flux and the heat losses to the environment from the channel.

flow both to environment and to the other side of the membrane. The latter heat flux is directly dependent on the mass flux, since it carries away its associated latent heat of vaporization, and on the temperature difference across the membrane that drives a conductive heat transfer through the membrane, both again dependent on the feed saltwater temperature.

4.1.5 Main results

The yearly calculation states that in Turin it is possible to produce with the Lab Unit $5.6699{\cdot}10^3$ kg of freshwater using the 71.62% of solar energy and the 28.38% of conventional thermal energy provided by the back-up boiler. The mean hourly yield during the simulated year is 0.65 l/h. The energy consumption per cubic metre of freshwater produced is 2538.3 kWh/m^3 of which 694.9 kWh/m^3 are provided by the back-up boiler.

Even if Turin is not characterized by high values of irradiance along the year, it is possible to consider a good result the latter values. The freshwater flow can be increased setting a higher set minimum temperature in the storage, but it will mean to decrease the percentage of solar energy, since back up boiler intervention will be needed more often.

4.2 Palermo, Sicily (ITA)

Palermo (38.111 N; 13.351 W), on the northern coast of Sicily, is the capital city of the region. The whole island often suffering freshwater shortages and Palermo location on the seaside can justify desalination plants. Moreover, due to its latitude, solar irradiance along the year has quite high values. The city conditions suggest the implementation of a solar desalination plant, making interesting to perform a simulation of the system operations.

4.2.1 Trinum solar concentrator

The relevant values for the component are the inlet and outlet temperatures (Figure 4.10), to investigate the time variation and to verify that no biphasic flow occurs in the fluid circuit, and the concentrator efficiency (Figure 4.11), to evaluate its performance.

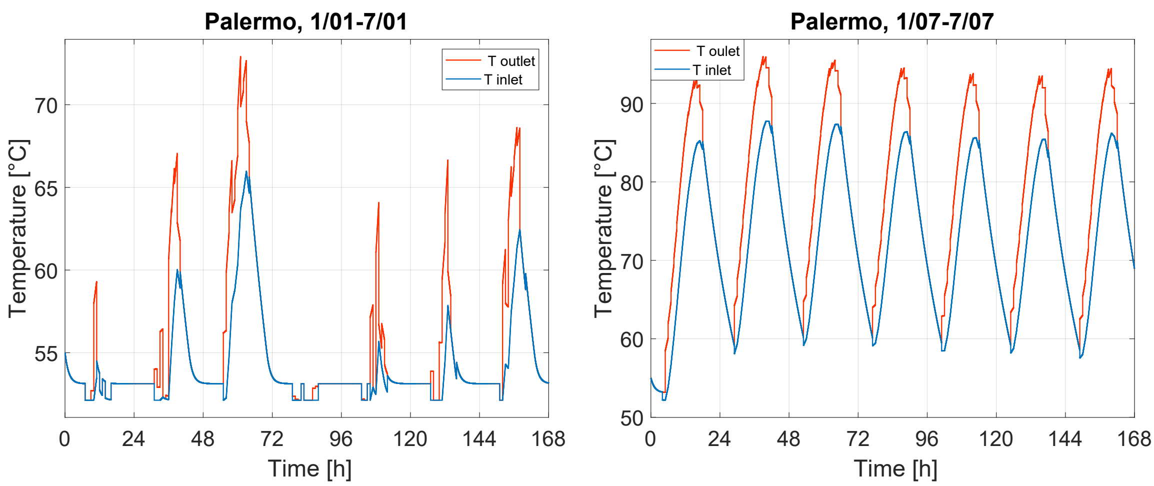

(a) *Wintertime* (b) *Summertime*

Figure 4.10: Concentrator fluid temperatures in Palermo during a week. Seasonal differences are well represented , both by peak temperatures reached and by the presence of nearly no irradiance periods in the wintertime plot.

Along the wintertime week considered for Palermo, the location experiences days with low or nearly absent irradiation leading to maximum outlet fluid temperatures below 70°C with only one weekly exception.The inlet temperatures shows indirectly the storage temperature decrease due to lack of inserted solar energy. On the other hand, during summertime week, the great amount of clear sky days determines peak temperatures always higher than 90°C and close to 95°C.

Concentrator efficiency (Figure 4.11) is affected by the low irradiation series of days during winter too. Its value is barely over 0.7 at peaks and it drop below 0.1 in its worst record. The typical summertime conditions rise the concentrator efficiency above 0.7 for nearly half the

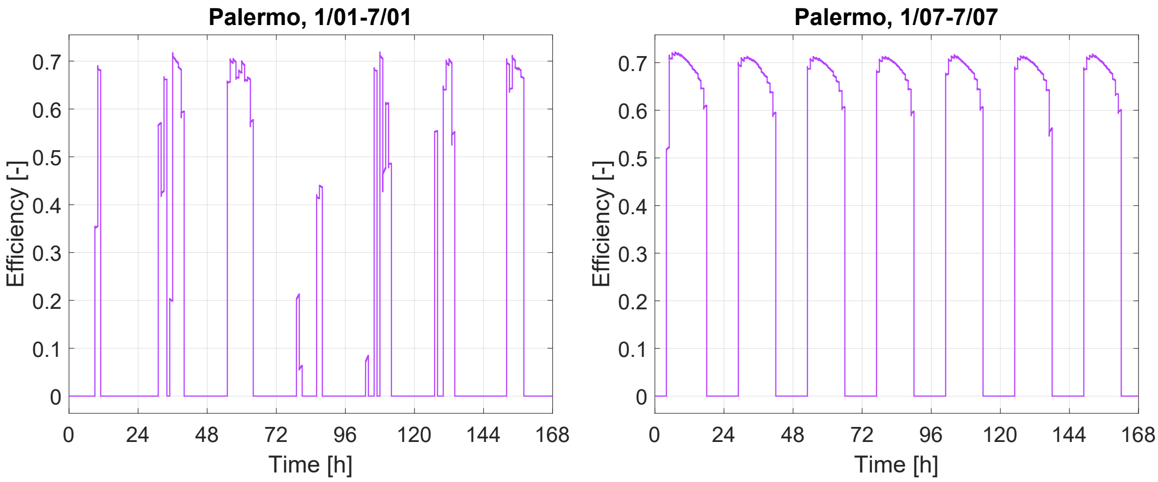

(a) *Wintertime*

(b) *Summertime*

Figure 4.11: Efficiency in Palermo during a week. Season drastically affects concentrator efficiency both in values and operative periods.

insolation period, thanks to both higher irradiance and ambient air temperature, that limit the thermal losses to the environment.

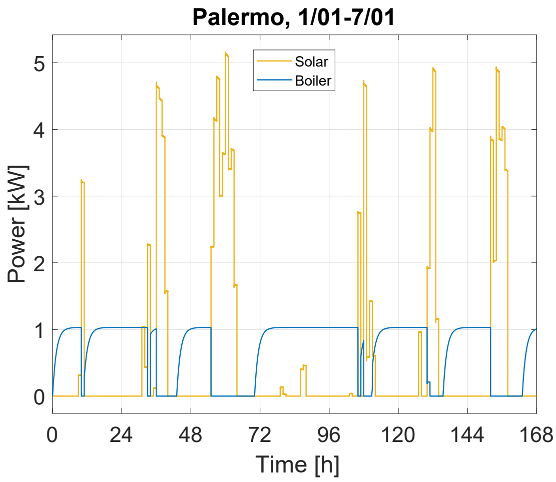

(a) *Wintertime*

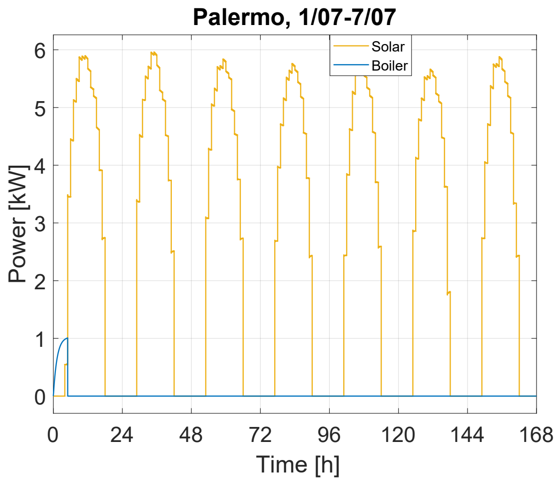

(b) *Summertime*

Figure 4.12: Inlet power into the sytem in Palermo during a week. Very good solar performances can be observed in summertime, making not necessary the back-up boiler intervention. Conversely during wintertime week the boiler intervention are frequent and prolonged, due to low solar power harvested.

4.2.2 Power contributions

Figure 4.12 shows the contribution of both solar and conventional power to the system, to check the correct intervention of the back up boiler. These results are used, on the whole year period, to compute the energy and to evaluate the solar ratio on total energy fed.

The lack of irradiance in the wintertime week in question forces the back-up boiler to intervene often during the period. Solar power collected exceeds 5 kW only once in the week, and the boiler maintain steady operation during all the nights and for a large part of the daytime. Conversely, during summer, after a brief turn on of the back-up system, the solar power alone is able to feed the system without letting the storage temperature descend below the set minimum value. Even if the solar power value never overcomes 6 kW , the long period of daily insolation associated with summertime contributes in harvesting the needed energy.

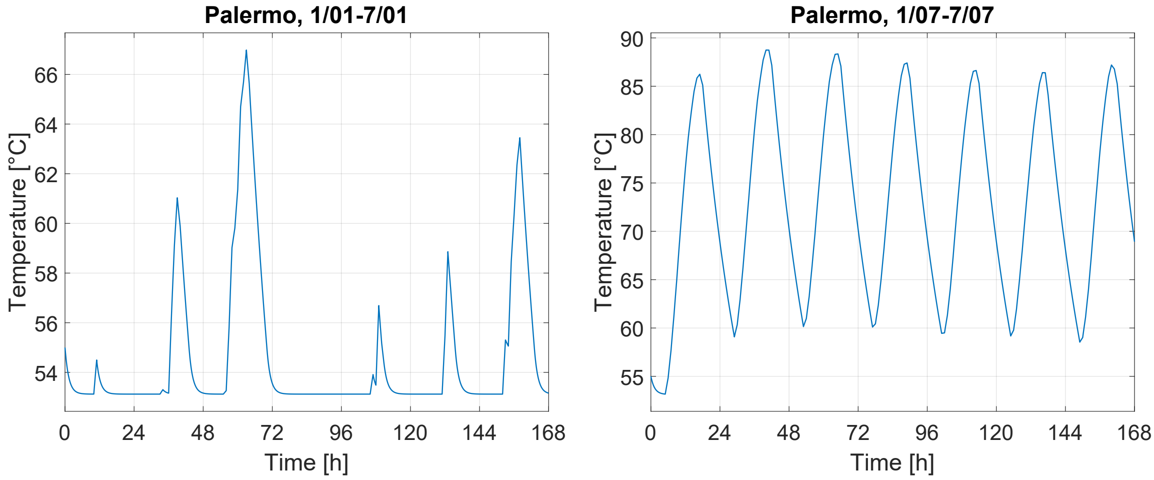

(a) *Wintertime* (b) *Summertime*

Figure 4.13: Storage temperature in Palermo during a week. During wintertime the temperature rarely rises significantly above set minimum. During summertime the temperature has optimum values to feed the distillation process, thanks to the increase solar energy collected.

4.2.3 Thermal storage and MD feed tank

The interesting output for this two components is their mass temperature (Figures 4.13 and 4.14) that permits to evaluate the good functioning and to check whether the back-up boiler succeeds in maintaining the storage temperature above the set minimum value.

As the previous quantities computed with winter climatic data, also thermal storage temperature, and subsequently saltwater feed tank temperature are affected by the week low irradiance values. Storage temperature rises above 60°C only for limited time during the week in exam. In summertime, the situation changes drastically as the storage temperature presents minimum values around 60°C and can reach more than 85°C during peak irradiance hours, thanks to high efficiency values due to lower concentrator heat losses to the environment.

The feed tank temperature follows the same generic trend of the thermal storage both in wintertime and summertime week. During wintertime the temperature is so low that is actually suitable for the membrane distillation process only for limited periods. In the summertime week the temperature of the saltwater in the feed tank always stays within the range from 50°C to 75°C, that allows for a good freshwater production.

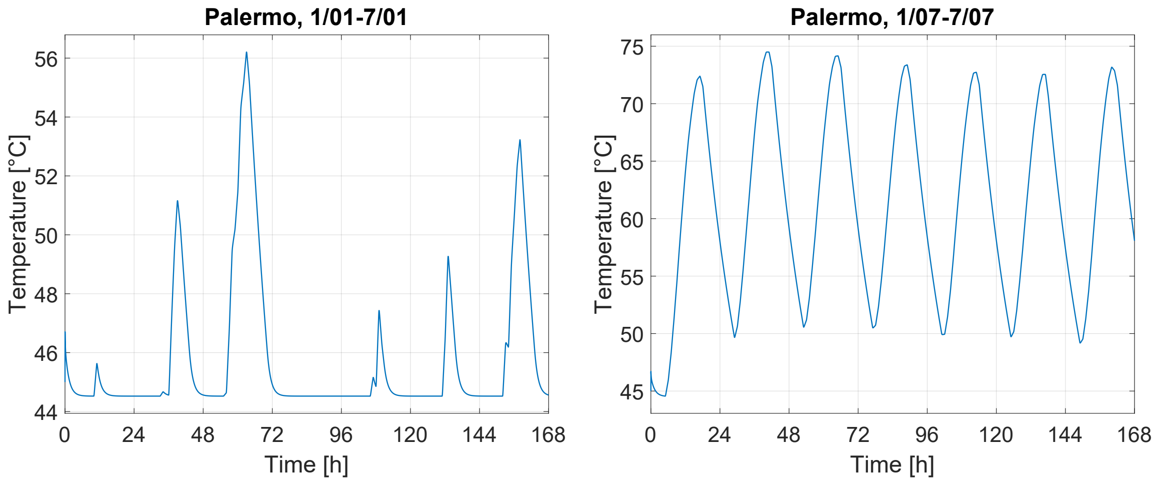

(a) *Wintertime* (b) *Summertime*

Figure 4.14: Feed tank temperature in Palermo during a week. This temperature drives the membrane distillation process, and its low wintertime values do not allow for a good freshwater yield. Particularly high temperature are reached in summertime. permitting higher freshwater production.

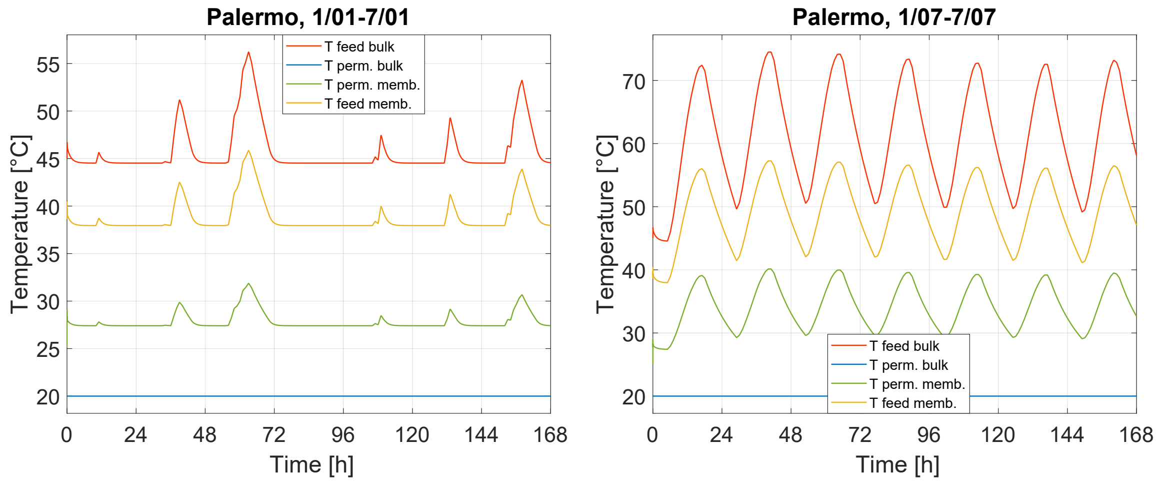

(a) *Wintertime* (b) *Summertime*

Figure 4.15: Channels temperatures in Palermo during a week. Trends in the channels are determined by the heat transfer mode occuring into them. The membrane temperatures are evaluated to compute the vapour pressure difference that drives the membrane distillation process.

4.2.4 Membrane distillation channels

In this part of the model, membrane channels, in which distillation occurs, temperatures (Figure 4.15) are evaluated, to correctly compute the freshwater mass flux (Figure 4.16), one of the main output of the entire model. To connect this part to the rest, also another thermal value is computed, the outlet feed bulk temperature (Figures 4.18) , that indirectly shows the heat in part used in the process and in part lost to the environment.

The low irradiance condition during wintertime week is reflected also on the temperatures inside the membrane channels of the membrane distillation unit, with feed membrane temperature rarely exceeding 40°C. This situation leads to a low vapour pressure difference and a lower membrane coefficient. Freshwater mass flux is directly related to both the previous quantities, so also its values along the week are low, with values above $4.0{\cdot}10^{-3}$ Kg/s/m^2 only for very limited amount of time.

The production of freshwater experiences a cospicuous drop during wintertime week in exam, due to the low inlet temperature determined by the lack of insolation of the period. In the summertime week the mass flux fluctuates, and can reach considerable values exceeding $9.0{\cdot}10^{-3}$ Kg/s/m^2 and rarely fall below $4.0{\cdot}10^{-3}$ Kg/s/m^2. These values allows good freshwater yields during the summer. It is worth noting that the winter values here reported are more of an exception in the typical wintertime. This is confirmed by the annual yield, that is greater than the yield computed for the Turin case study.

As noted in the Turin case study, the outlet feed bulk temperature follows the oscillations of the inlet feed bulk temperature and the increase of the latter also increase the temperature

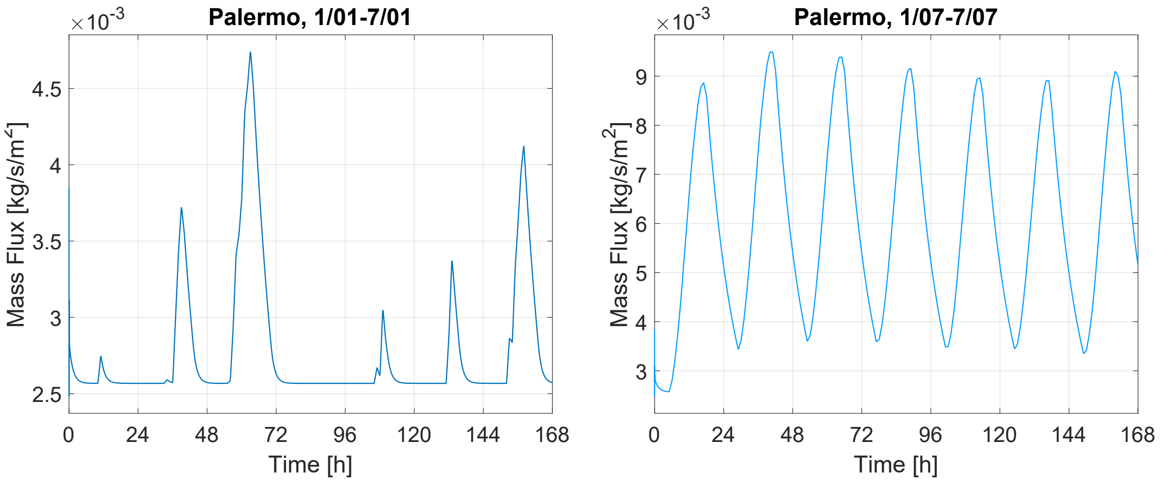

(a) *Wintertime* (b) *Summertime*

Figure 4.16: Freshwater mass flux in Palermo during a week. As it can be expected observing the feed tank temperature, mass flux presents low values during wintertime, while can assure a notable freshwater production in summer.

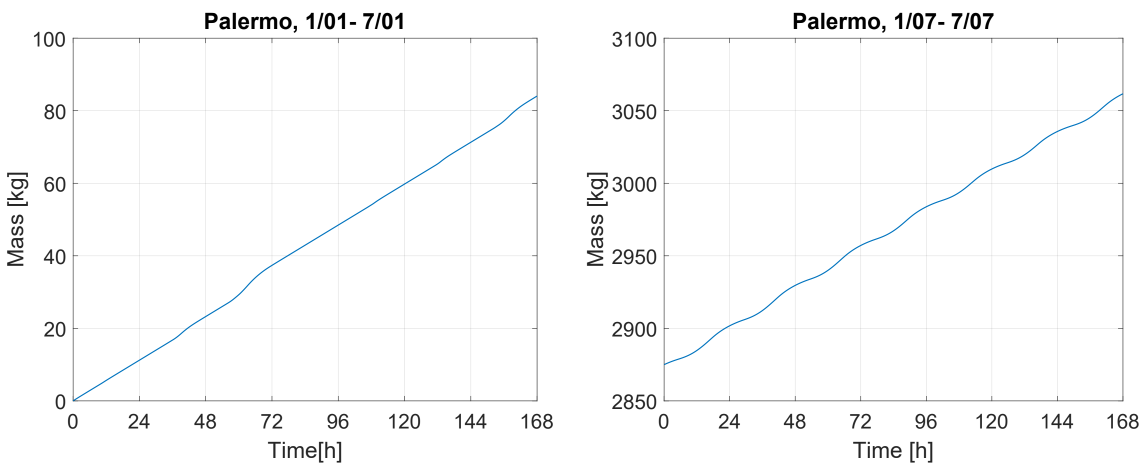

(a) *Wintertime* (b) *Summertime*

Figure 4.17: Freshwater mass cumulative in Palermo during a week. The plots shows the total produced mass for every time step in the two weeks.

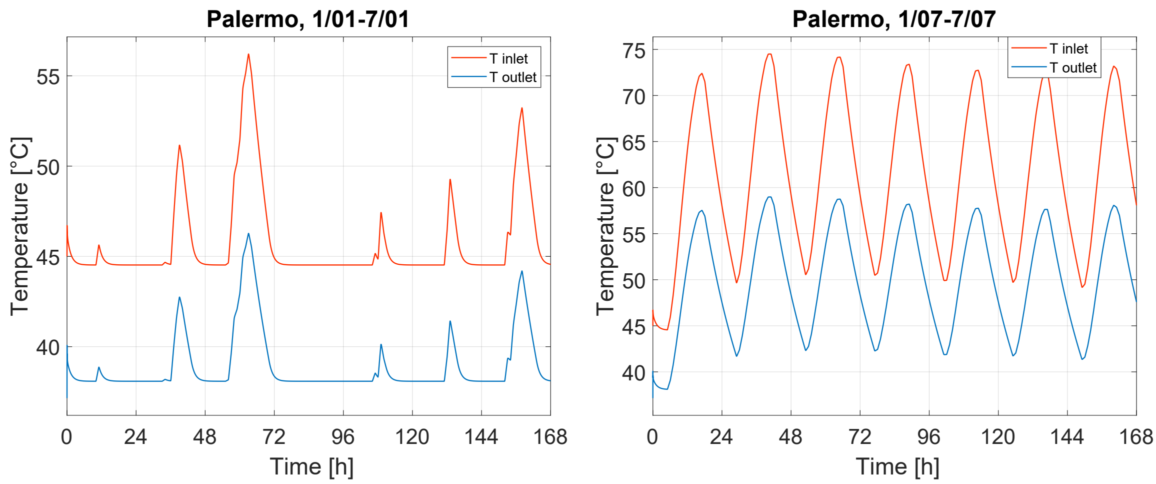

(a) *Wintertime* (b) *Summertime*

Figure 4.18: Feed bulk temperatures in Palermo during a week. The temperature difference experienced through the feed channel is caused by the heat losses to the environment, dependent on inlet temperature, and by the latent heat carried by the mass flux across the membrane.

difference between them, as the lost heat to the environment and the latent heat associated to the mass flux across the membrane increase.

4.2.5 Main results

The yearly calculations states that in Palermo is it possible to produce with the Lab Unit $5.9526 \cdot 10^3$ kg of freshwater using the 79.49% of solar energy and the 21.51% of conventional thermal energy provider by the back-up boiler. The mean hourly production during the simulated year is 0.68 l/h.The energy consumption per cubic metre of freshwater produced is 2585.6 kWh/m^3 of which 530.3 kWh/m^3 are provided by the back-up boiler.

The solar percentage shows that a solar desalination plant can be a proper way to reduce the water stress in the city and on the island, particularly for the agricultural use of freshwater, since the primary sector occupies a large portion of island economy.

4.3 Abu Dhabi (UAE)

Abu Dhabi (23.998 N; 53.644 W) is the capital city of the United Arabic Emirates, a confederation situated on the South East of the Arabic Peninsula. The peninsula is for the most part desert and the city is built over a tiny sea island.

Desalination technologies are widely adopted, since the cost drawback is overcome by the profuse country wealth. The almost tropical latitude of the place ensures proper irradiance values along all the year. The location is thus ideal for solar desalination plants.

4.3.1 Trinum solar concentrator

The relevant values for the component are the inlet and outlet temperatures (Figure 4.19), to investigate the time variation and to verify that no byphasic flow occurs in the fluid circuit, and the concentrator efficiency (Figure 4.20), to evaluate its performance.

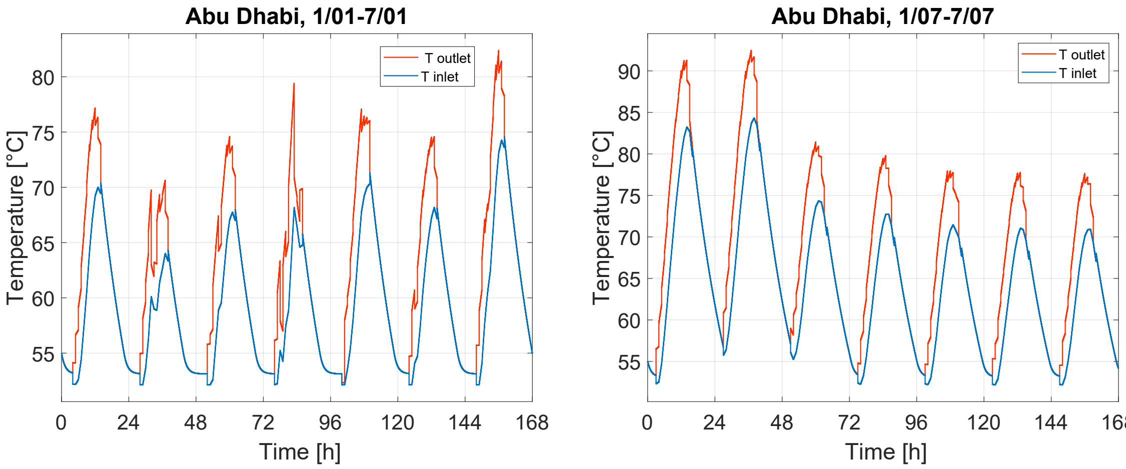

(a) *Wintertime*

(b) *Summertime*

Figure 4.19: Fluid temperatures in Abu Dhabi during a week. The favorable weather of the location assures considerable fluid temperatures along all the year.

The outlet fluid temperature temperature reaches rather high values along both wintertime and summertime week, with peaks that never fall below 70°C. These performances are due to the moderate variation of irradiance during the whole year, since the low latitude of the location. Is interesting to note that , unlikely the two previous case study locations, in July the peak outlet temperatures have a descending trend, that is not caused by a bad weather period, but by the typical sun behaviour of the almost tropical latitude.

Collector efficiency presents jagged curve for a couple of days in wintertime week (Figure 4.20a), due to cloudy weather, but always reaches peak values of 0.7. Along summertime week the efficiency values stays above the 0.7 values (Figure 4.20b), except for the dusk

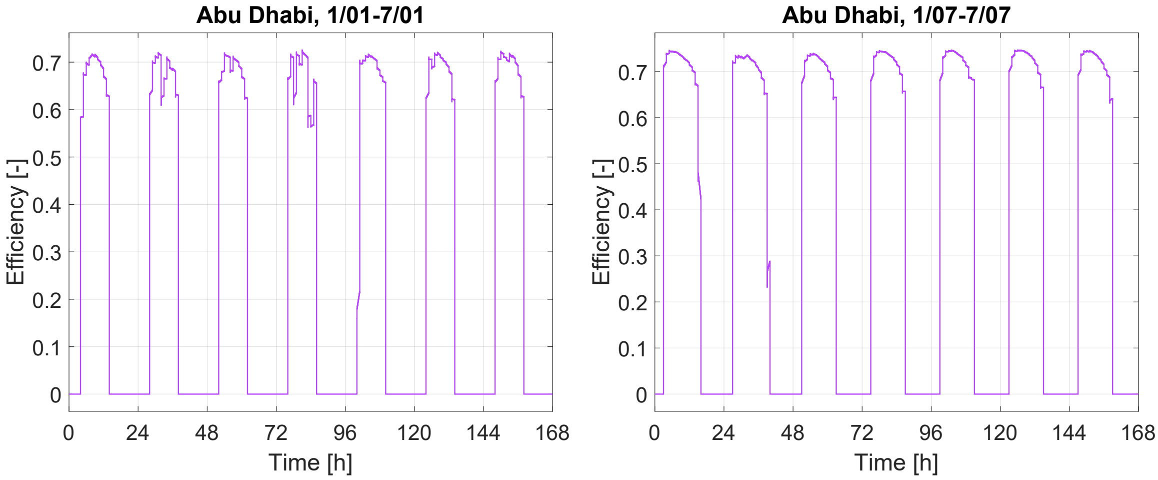

(a) *Wintertime*

(b) *Summertime*

Figure 4.20: Efficiency in Abu Dhabi during a week. The plots shows the efficiency behaviour along two different season weeks, that presents appreciable values in both cases, thanks to the combination of high irradiance and hot climate.

hours. These high values, the best of all the three case studies, are explainable as the combination of quite high irradiance and hot ambient temperatures, that reduce the concentrator thermal losses to the environment.

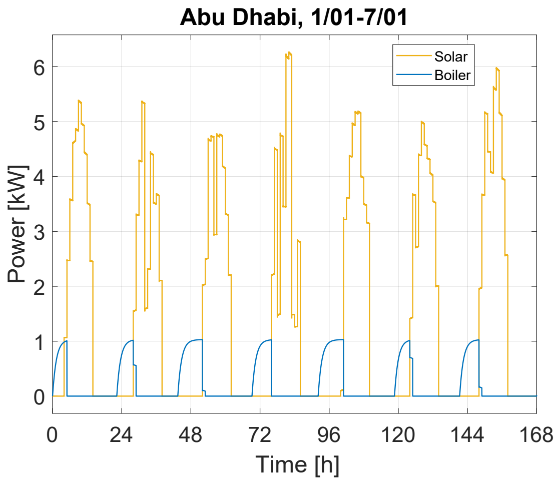

(a) *Wintertime*

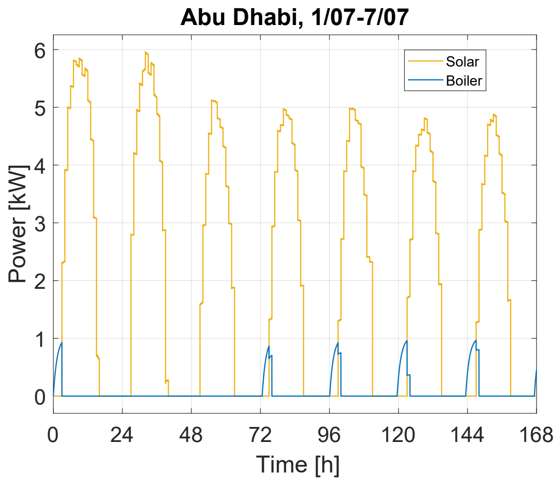

(b) *Summertime*

Figure 4.21: Inlet power into the system in Abu Dhabi during a week. As for the previous case, summer higher solar power collection allows the system to not take advantage of the back-up boiler intervention, if not for brief periods.

4.3.2 Power contributions

Figure 4.21 show the contribution of both solar and conventional power to the system, to check the correct intervention of the back up boiler. These results are used, on the whole year period, to compute the energy and to evaluate the solar ratio on total energy fed.

The cloudy weather experienced during the winter time affects the solar power collected by the concentrator, as it is possible to deduce from the irregular shape of its plotted curve. As a consequence, the back-up boiler must intervene in the last hours of the nights to prevent the falling of the storage temperature below the set minimum. The more regular irradiance during summertime results in a more regular and abundant solar power collection, that allows a moderate boiler intervention. Regardless of the season, the solar peak power rarely stands over 6kW, but has a regular behaviour along the year that permits to obtain high system performance.

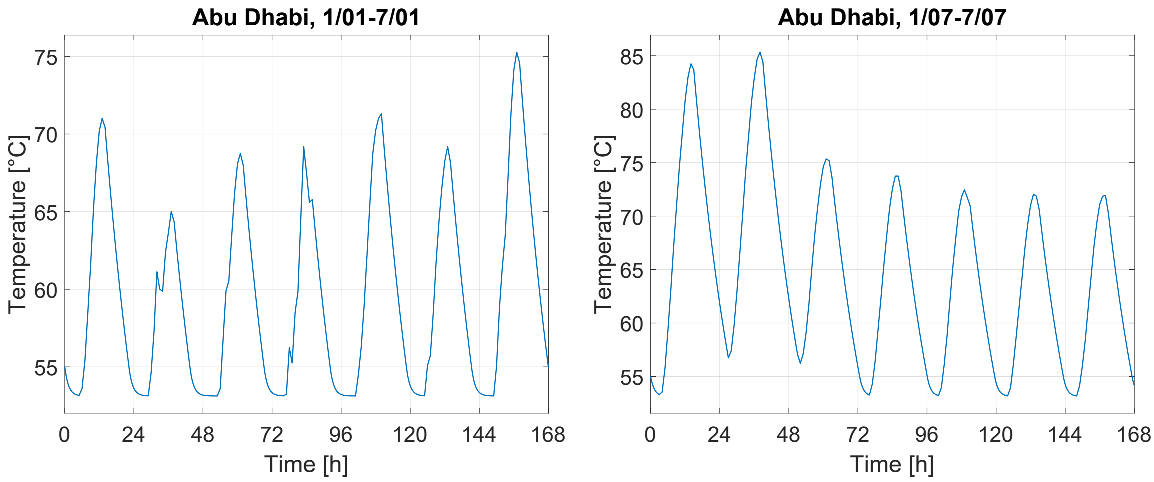

(a) *Wintertime* (b) *Summertime*

Figure 4.22: Storage temperature in Abu Dhabi during a week. The temperature values remain high for the most part of the year, while in the winter week considered they may drop near the set minimum, due to low solar energy collected.

4.3.3 Thermal storage and MD feed tank

The interesting output for this two components is their mass temperature (Figures 4.22 and 4.23) that permits to evaluate the good functioning and to check wheter the back up boiler succeeds in maintaining the storage temperature above the set minimum value.

As the previous case studies, the temperatures in the thermal storage and in the membrane distillation feed tank shows a strong dependence on the concentrator outlet fluid temperature. During wintertime week, the storage temperature spans in the range from 50°C to 70°C, with an absolute maximum around 75°C. This trend is hold for the summertime period too, but in this week the absolute maximum reaches around 85°C due summer irradiation peaks.

The same trends can be noticed in the feed tank temperature, that in wintertime rarely reaches 60°C at its peaks, while in summertime week it can reach values around 70°C, a temperature eligible to produce a high freshwater flux.

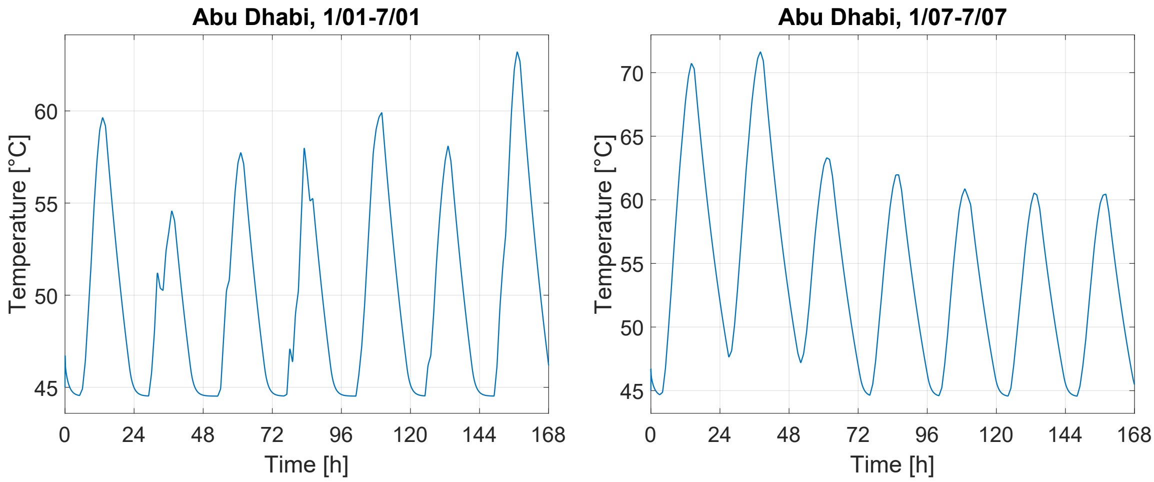

(a) *Wintertime* (b) *Summertime*

Figure 4.23: Feed tank temperature in Abu Dhabi during a week. The values oscillate into a proper range for the membrane distillation process in both the weeks considered, thanks to the favorable climatic condition of the location.

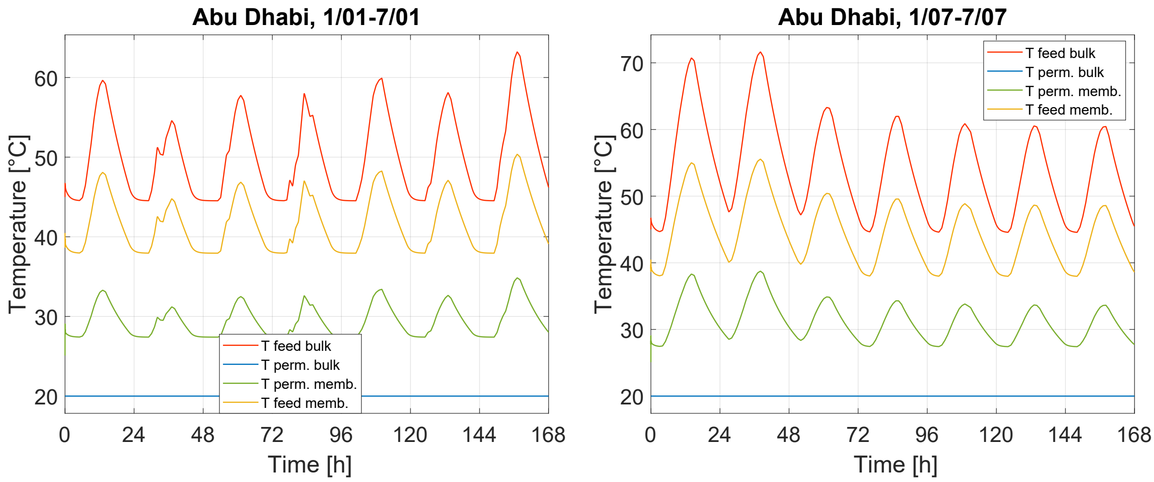

(a) *Wintertime* (b) *Summertime*

Figure 4.24: Channels temperatures in Abu Dhabi during a week. Heat transfer phenomena occuring determine the temperature diffecence among differnt points of the membrane channels. The membrane temperature are used to evaluate the freshwater mass flux.

4.3.4 Membrane distillation channels

In this part of the model channels temperatures (Figure 4.24) are evaluated, to correctly compute the freshwater mass flux (Figure 4.26), one of the main output of the entire model. To connect this part to the rest, also another thermal value is computed, the Outlet feed bulk temperature(Figure 4.27) , that indirectly shows the heat in part used in the process and in part lost to the environment.

The temperatures in the membrane channel reflect the feed tank temperatures curve shape both in winter and in summer. It is interesting to notice that the temperature difference between bulk and membrane increase as the feed bulk temperature increases, due to the poor heat transfer coefficient that the laminar flow regime provides. This behaviour affects negatively the freshwater mass flux, that is directly dependent on temperature through vapour pressure, and thus decreases the process efficiency.

As noted for other computed quantities in the Abu Dhabi case study, the freshwater mass flux value spans in a range from $2.5 \cdot 10^{-3}$ Kg/s/m^2 and $6.0 \cdot 10^{-3}$ Kg/s/m^2 along the whole year, with occasional peaks exceeding $8.0 \cdot 10^{-3}$ Kg/s/m^2.

The computed outlet feed bulk temperature presents values from 35°C to 45°C. In principle, a low outlet temperature would be an indicator of good performances, since indicates a large latent heat transfer caused by an high mass flux, but in this case, the low temperature is not consequence of proper operation, but of low inlet temperature. The heat losses to the environment are directly related to the inlet temperature, resulting in their low value. This can be noticed on the difference of temperatures at the feed membrane channel ends.

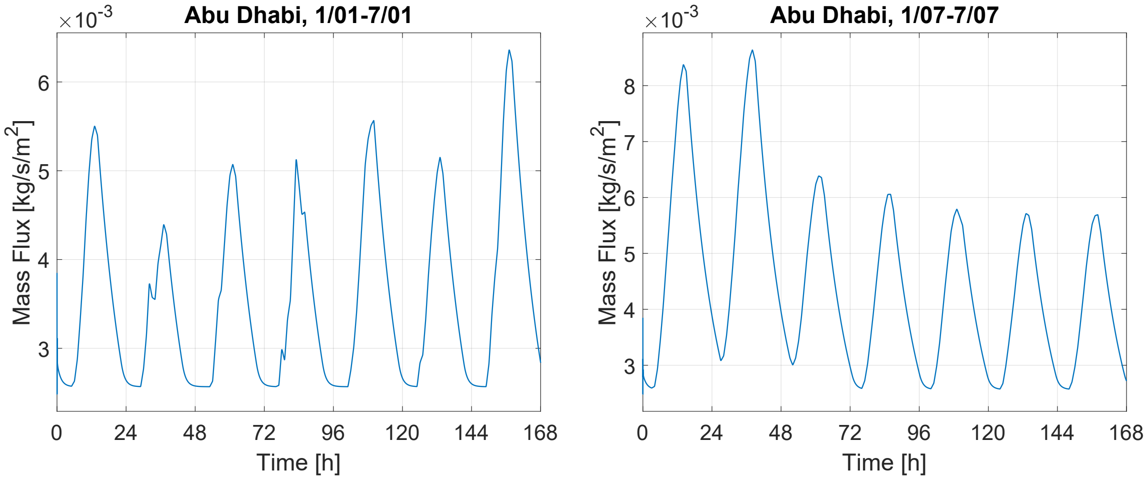

(a) *Wintertime*

(b) *Summertime*

Figure 4.25: Freshwater mass flux in Abu Dhabi during a week. While oscillating, the mass flux values remain into a convenient range for long period, determining the highest freshwater yield among the case studies.

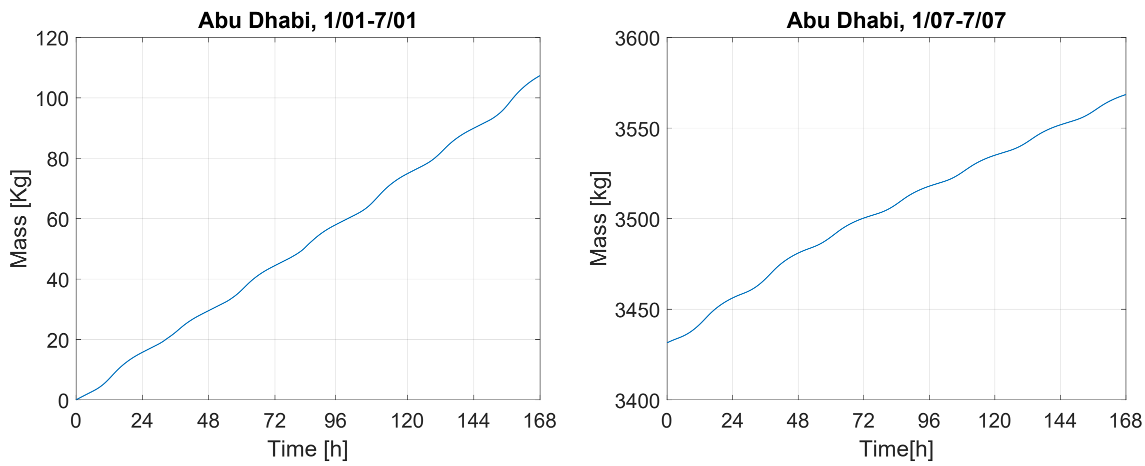

(a) *Wintertime*

(b) *Summertime*

Figure 4.26: Freshwater mass cumulative in Abu Dhabi during a week.The plots shows the total produced mass for every time step in the two weeks.

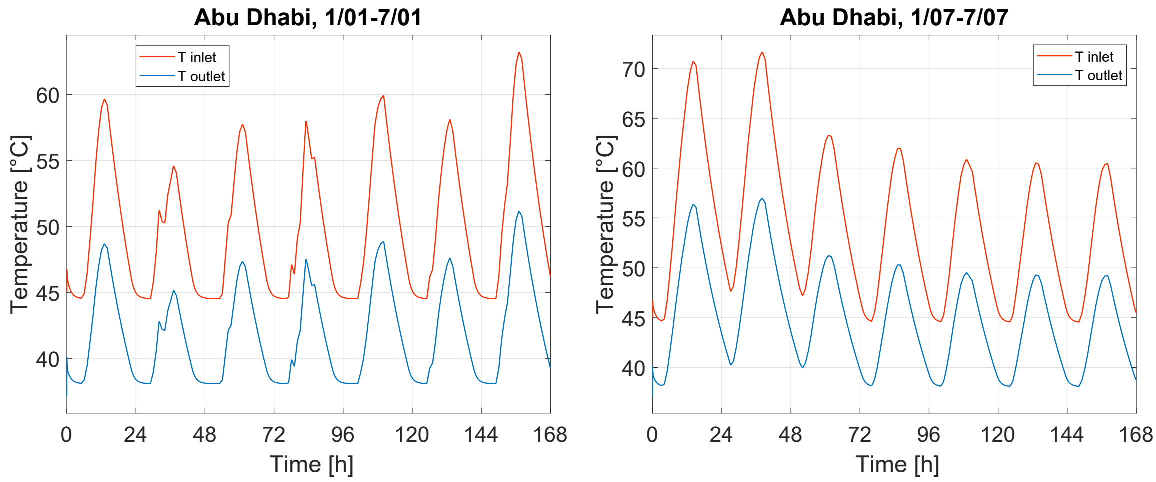

(a) *Wintertime* (b) *Summertime*

Figure 4.27: Feed bulk temperatures in Abu Dhabi during a week. The usual behaviour in the computed values can be observed, with greater temperature differences between inlet and outlet temperatures as inlet temperature rises.

4.3.5 Main results

The yearly calculations states that in Abu Dhabi is it possible to produce with the Lab Unit $6.76 \cdot 10^3$ kg of freshwater using the 93.68% of solar energy and the 6.32% of conventional thermal energy provided by the back-up boiler. the mean hourly yield during the simulated year is 0.77 l/h. The energy consumption per cubic metre of freshwater produced is 2577.5 kWh/m^3 of which 162.7 kWh/m^3 are provided by the back-up boiler.

The results confirm Abu Dhabi as an ideal location for seawater desalination, thanks to its very considerable value of solar energy ratio. Setting aside environmental sustainability, a higher set minimum temperature could increase the freshwater yield, crucial for the location, lowering the solar percentage to a value that is anyway good, for example to 75% or 80%.

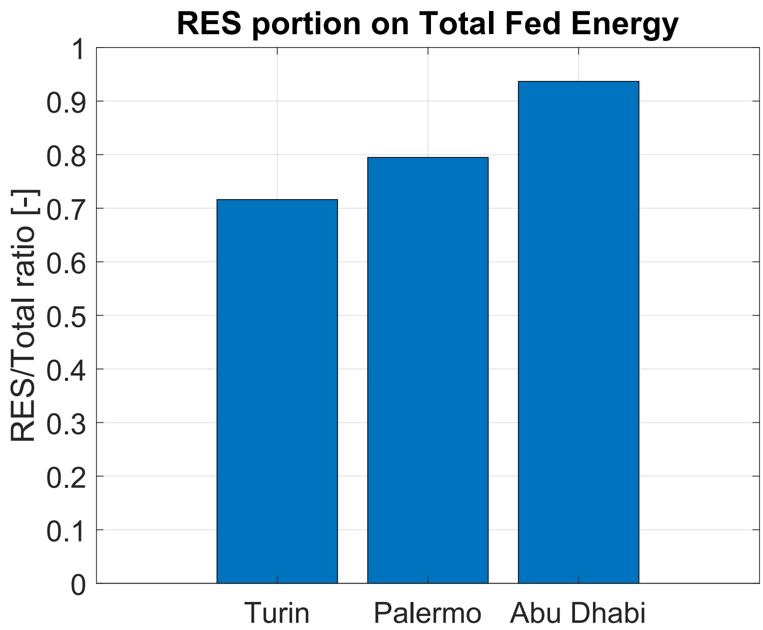

Figure 4.28: Solar to total energy ratio. The difference on the solar portion of energy fed can be interpreted as the difference in latitude of the case studies locations; as latitude decrease, insolation periods and irradiance values increase determining warmer climates of which system energy performances benefit.

4.4 Results comparison

The solar energy portion on total energy fed (Figure 4.28), the energy consuption per cubic meter (Figure 4.29), the annual freshwater yield (Figure 4.30) and the mean hourly production along the year (Figure 4.31) for the different locations are grouped to have a comparison at a glance.

Figure 4.28 clearly indicates that the grographical location plays a fundamental role on energetic performance of the system. The more close to the Equator, the more solar to total ratio is large, not only due to the increasing solar irradiance values, but also to the warmer ambient temperatures, that limit the storage thermal losses. The energy consumption per cubic metre doesn't vary considerable in the different case studies, while the boiler contribution decreases, in concordance with the solar to total ratio values (Figure 4.29). Going toward equator also increase the freshwater yield as Figure 4.30 shows, thanks to the increase of the mean operation temperature, that allows a larger mass flux at the membrane. The same trend affects the mean hourly production shown in Figure 4.31.

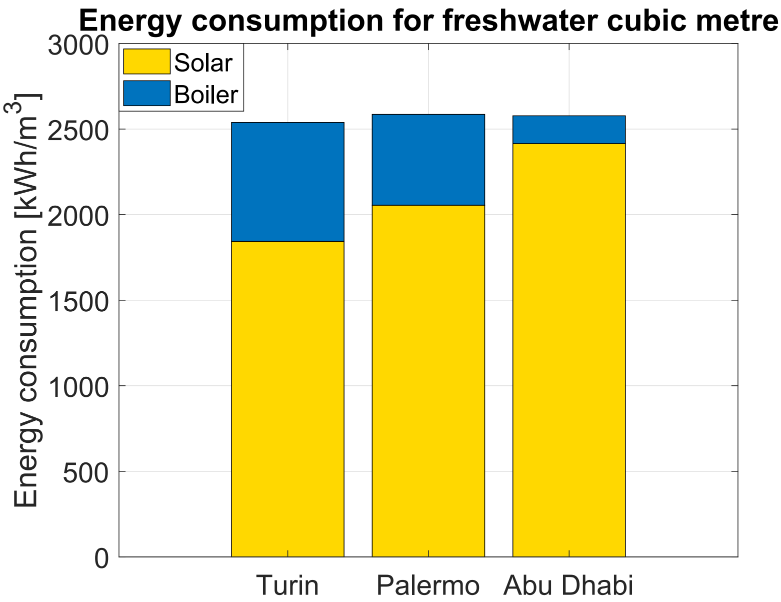

Figure 4.29: Energy consumption per cubic meter. While the total amount of energy to produce one cubic metre of freshwater changes only slightly, the conventional boiler contribution decrease as latitude decrease thanks to the warmer climate, the higher irradiance values and longer insolation periods.

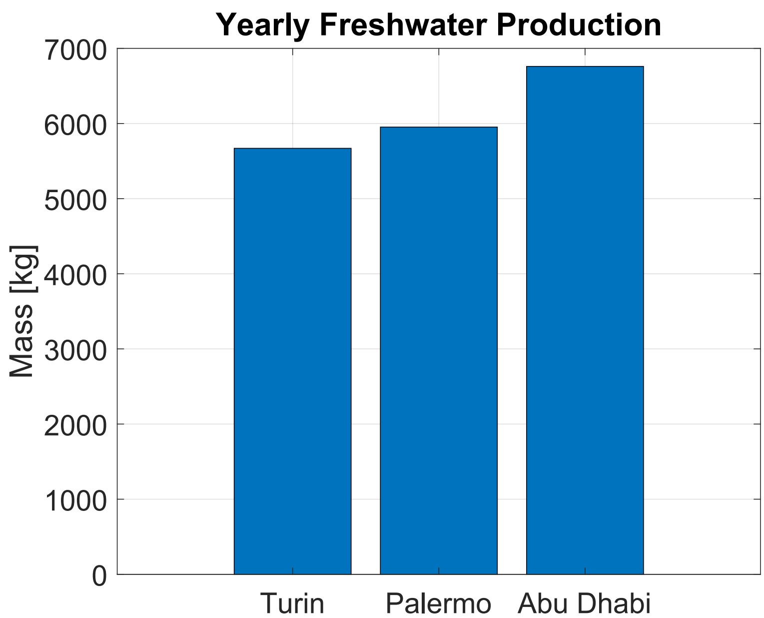

Figure 4.30: Annual Freshwater Yield. As latitude decrease, insolation periods and irradiance values increase determining warmer climates of which system freshwater yield benefits, functioning for longer period at suitable temperature.

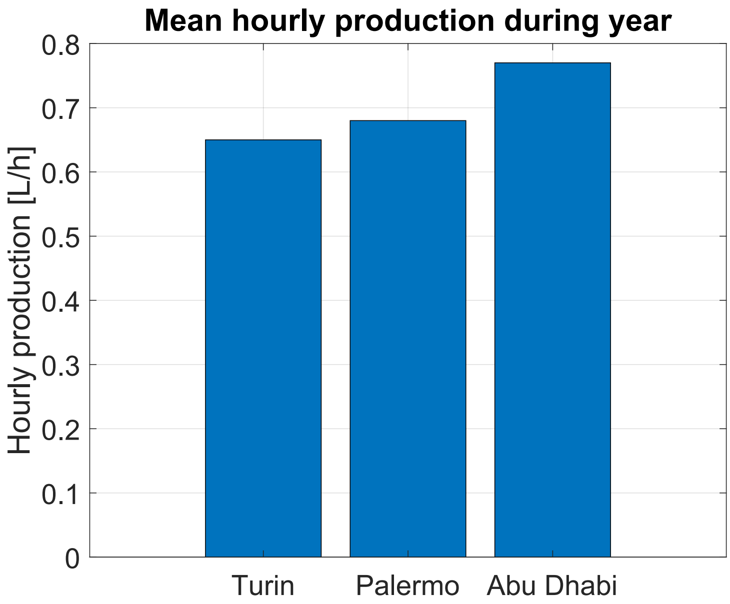

Figure 4.31: Mean hourly freshwater production. As latitude decrease, insolation periods and irradiance values increase, increasing the freshwater yields and consequently the mean hourly production.

Conclusion

The work is motivated by the recognition of the contemporary presence in several places around the world of water scarcity, saltwater reserves and solar irradiation abundance, and of the opportunity to reduce freshwater stress adopting solar desalination processes. Among the various technologies, a coupling between solar concentration and membrane distillation may fulfill the characteristics of low cost, simplicity and self-reliance that the installation locations require, being them remote and/or underdeveloped.

A system concept composed by solar parabolic-dish concentrator, back-up boiler, thermal storage and membrane distillation unit is designed and a simulation model is built to study its behaviour. In the system model, Trinum SPD concentrator by Innova, allSTOR sensible heat storage by Vaillant and MD Lab Unit by Aquastill are implemented into the Simulink software to carry out dynamic simulations.

To validate the model accuracy, the MD Lab Unit model has been compared with data from experimental activities on the actual device, led in the DIATI department of Politecnico di Torino by assistant researcher Francesco Ricceri. The comparison on freshwater hourly flux and outlet feed temperature of the unit demonstrated trustworthy concordance, with mean relative error on the hourly flux around 9% and on the outlet feed temperature around 2.3%.

The system model was used to compute two main indexes to evaluate the system performances: the solar portion on the total energy fed to the process and the annual freshwater yield. Turin (ITA), Palermo (ITA) and Abu Dhabi (UAE) are chosen as case studies to perform simulations and assess the two aforementioned values.

In Turin case study 5.6699 m^3 of freshwater production were computed and the solar on total energy ratio was estimated as 71.62% . In Palermo case study both values rise to 5.9526 m^3 of freshwater using the 79.49% of solar energy. Abu Dhabi case study shows the best computed performances reaching 6.76 m^3 of freshwater production with 93.68% of solar energy, thanks to its favorable climate. The results disclose that the solar concentration and membrane distillation coupling possesses potentialities in reducing water stress using renewable energy to tackle the energy consumption issue that affects desalination processes.

It is possible to engage in further research and concept development to gain more insight. Larger membrane distillation devices may be implemented into the system model to make a step out from laboratory-scale, modeling commercial size units. Also, latent thermal storage, that requires more complex mathematical models, may substitute the simple sensible thermal storage implemented into the model to improve performances. An optimization study may be carried out on storage size and on MD unit size, to understand whether it is more convenient to store thermal energy for a small size desalination unit or to increase the MD unit size and couple it with smaller energy storage size. Lastly, economic feasibility analysis is a necessary study to be carried out, since it permits to have a better picture on cost and benefits of the concept studied in the present work.

Bibliography

[1] Micale G, Cipollina A, Rizzuti L. Chapter 1 - Seawater Desalination for Freshwater Production. In: Micale G, Cipollina A, Rizzuti L, eds. *Seawater Desalination*. London, UK: Springer; 2009:1-15.

[2] Pugsley A, Zacharopoulos A, Mondol JD, Smyth M. Global applicability of solar desalination. *Renewable Energy*. 2016;88:200-219. doi:10.1016/j.renene.2015.11.017.

[3] INNOVA ENERGY SOLUTIONS S.P.A. http://www.innova.co.it/

[4] Aquastill B.V. http://aquastill.nl/

[5] Koschikowski J, Wieghaus M, Rommel M. El-Nashar A. Chapter 7 - Membrane Distillation for Solar Desalination. In: Micale G, Cipollina A, Rizzuti L, eds. *Seawater Desalination*. London, UK: Springer; 2009:.165-187.

[6] van Weert F, van der Gun J, Reckman J. Global Overview of Saline Ground - water Occurrence and Genesis. http://www.un-igrac.org/resource/global-overview-saline-groundwateroccurrence-and-genesis-0. Published 2009.

[7] Soil and Water Conservation Society of Metro Halifax. Saline Lakes: the Largest, Highest and lowest Lakes of the world! Halifax, Canada: SWCSM; 2006: 1-32.

[8] SolarGIS: World Map of Global Horizontal Irradiation. Bratislava,Slovakia: GeoModel Solar; 2013. http://solargis.info/doc-pics/freemaps/1000px/ghi/SolarGIS-Solar-map-World-map-en.png

[9] International Energy Agency. World Energy Outlook.

[10] Dhar S, Sridhar R, Mathew G. Implementation of PV cell based standalone solar power system employing incremental conductance MPPT algorithm. *2013 International Conference on Circuits, Power and Computing Technologies (ICCPCT)*. 2013. doi:10.1109/iccpct.2013.6528926.

[11] Ee publishers. Solar PV module faults and failings. http://www.ee.co.za/article/solar-pv-module-faults-failings.html

[12] Settino J, Sant T, Micallef C, Farrugia M, Spiteri Staines C, Licari J, Micallef A. Overview of solar technologies for electricity, heating and cooling production. *Renewable and Sustainable Energy Reviews*. 2018;90:892-909. https://doi.org/10.1016/j.rser.2018.03.112

[13] Sarsam WS, Kazi S, Badarudin A. A review of studies on using nanofluids in flat-plate solar collectors. *Solar Energy*. 2015;122:1245-1265. doi:10.1016/j.solener.2015.10.032.

[14] Sabiha M, Saidur R, Mekhilef S, Mahian O. Progress and latest developments of evacuated tube solar collectors. *Renewable and Sustainable Energy Reviews*. 2015;51:1038-1054. doi:10.1016/j.rser.2015.07.016.

[15] Islam MT, Huda N, Abdullah A, Saidur R. A comprehensive review of state-of-the-art concentrating solar power (CSP) technologies: Current status and research trends. *Renewable and Sustainable Energy Reviews*. 2018;91:987-1018. doi:10.1016/j.rser.2018.04.097.

[16] Mohamad A, Orfi J, Alansary H. Heat losses from parabolic trough solar collectors. *International Journal of Energy Research*. 2013;38(1):20-28. doi:10.1002/er.3010.

[17] Sharma A. A comprehensive study of solar power in India and World. *Renewable and Sustainable Energy Reviews*. 2011;15(4):1767-1776. doi:10.1016/j.rser.2010.12.017.

[18] Ummadisingu A, Soni M. Concentrating solar power – Technology, potential and policy in India. *Renewable and Sustainable Energy Reviews*. 2011;15(9):5169-5175. doi:10.1016/j.rser.2011.07.040.

[19] Boukelia TE, Mecibah M-S. Parabolic trough solar thermal power plant: Potential, and projects development in Algeria. *Renewable and Sustainable Energy Reviews*. 2013;21:288-297. doi:10.1016/j.rser.2012.11.074.

[20] Belgasim B, Aldali Y, Abdunnabi MJ, Hashem G, Hossin K. The potential of concentrating solar power (CSP) for electricity generation in Libya. *Renewable and Sustainable Energy Reviews*. 2018;90:1-15. doi:10.1016/j.rser.2018.03.045.

[21] Cavallaro F. Multi-criteria decision aid to assess concentrated solar thermal technologies. *Renewable Energy*. 2009;34(7):1678-1685. doi:10.1016/j.renene.2008.12.034.

[22] Manente G, Rech S, Lazzaretto A. Optimum choice and placement of concentrating solar power technologies in integrated solar combined cycle systems. *Renewable Energy*. 2016;96:172-189. doi:10.1016/j.renene.2016.04.066.

[23] Muller-Steinhagen H, Trieb F, Trieb F. Concentrating solar power: a review of the technology. Stuttgard, Germany: Institute of technical Thermodynamic, German Aerospace Center. https://www.dlr.de/tt/Portaldata/41/Resources/dokumente/institut/system/publications

[24] Gharbi NE, Derbal H, Bouaichaoui S, Said N. A comparative study between parabolic trough collector and linear Fresnel reflector technologies. *Energy Procedia*. 2011;6:565-572. doi:10.1016/j.egypro.2011.05.065.

[25] International Energy Agency. International Energy Agency Technology Roadmap-concentrating solar power. Published 2010

[26] INNOVA ENERGY SOLUTIONS S.P.A. Trinum vers. Turbocaldo Datasheet.

[27] Al-Karaghouli A, Kazmerski LL. Energy consumption and water production cost of conventional and renewable-energy-powered desalination processes. *Renewable and Sustainable Energy Reviews*. 2013;24:343-356. doi:10.1016/j.rser.2012.12.064.

[28] Drioli E, Ali A, Macedonio F. Membrane distillation: Recent developments and perspectives. *Desalination*. 2015;356:56-84. doi:10.1016/j.desal.2014.10.028.

[29] Deshmukh A, Elimelech M. Understanding the impact of membrane properties and transport phenomena on the energetic performance of membrane distillation desalination. *Journal of Membrane Science*. 2017;539:458-474. doi:10.1016/j.memsci.2017.05.017.

[30] Deshmukh A, Boo C, Karanikola V, et al. Membrane distillation at the water-energy nexus: limits, opportunities, and challenges. *Energy & Environmental Science*. 2018;11(5):1177-1196. doi:10.1039/c8ee00291f.

[31] Srisurichan S, Jiraratananon R, Fane A. Mass transfer mechanisms and transport resistances in direct contact membrane distillation process. *Journal of Membrane Science*. 2006;277(1-2):186-194. doi:10.1016/j.memsci.2005.10.028.

[32] Sherwood TK, Pigford RL, Wilke CR. *Mass Transfer*. New York: McGraw-Hill; 1975.

[33] Fane A, Schofield R, Fell C. The efficient use of energy in membrane distillation. *Desalination*. 1987;64:231-243. doi:10.1016/0011-9164(87)90099-3.

[34] Aquastill B.V. Aquastill Lab Unit datasheet.

[35] Sharqawy MH, Lienhard JH, Zubair SM. Thermophysical properties of seawater: a review of existing correlations and data. *Desalination and Water Treatment*. 2010;16(1-3):354-380. doi:10.5004/dwt.2010.1079.

[36] Nayar KG, Sharqawy MH, Banchik LD, V JHL. Thermophysical properties of seawater: A review and new correlations that include pressure dependence. *Desalination*. 2016;390:1-24. doi:10.1016/j.desal.2016.02.024.

[37] Bergman TL, DeWitt DP, Incropera FP, Lavine AS. *Principles of Heat and Mass Transfer*. Hoboken (N.J.): J. Wiley; 2011.

[38] Phattaranawik J. Effect of pore size distribution and air flux on mass transport in direct contact membrane distillation. *Journal of Membrane Science*. 2003;215(1-2):75-85. doi:10.1016/s0376-7388(02)00603-8.

[39] Alkhudhiri A, Darwish N, Hilal N. Membrane distillation: A comprehensive review. *Desalination*. 2012;287:2-18. doi:10.1016/j.desal.2011.08.027.

[40] Alva G, Lin Y, Fang G. An overview of thermal energy storage systems. *Energy*. 2018;144:341-378. doi: 10.1016/j.energy.2017.12.037

[41] Stutz B, Le Pierres N, Kuznik F, Johannes K, Palomo Del Barrio E, Bédécarrats J, Giboute S, Marty P, Zalewski L, Soto J, Mazet N, Olives R, Bezian J, Pham Minh D. Storage of thermal solar energy. *Comptes Rendus Physique*. 2017;18:404-414. doi:10.1016/j.crhy.2017.09.008

[42] Lefebvre D, Tezel FH. A review of energy storage technologies with a focus on adsorption thermal energy storage processes for heating applications. *Renewable and Sustainable Energy Reviews*. 2017;67:116-125. doi:10.1016/j.rser.2016.08.019.

[43] Vaillant GmbH. Vaillant Solar systems: The best solution for the sun. allSTOR Technical Data

[44] Morciano M, Fasano M, Secreto M, Jamolov U, Chiavazzo E, Asinari P. Installation of a Concentrated Solar Power System for the Thermal Needs of Buildings or Industrial Processes. *Energy Procedia*. 2016;101:956-963. doi:10.1016/j.egypro.2016.11.121.

[45] The MathWorks, Inc. Simulink getting started guide. https://it.mathworks.com/help/simulink/getting-started-with-simulink.html Accessed May 25, 2018

[46] European Commission, Joint Research Centre, Energy Efficiency and Renewables Unit. PVGIS. http://re.jrc.ec.europa.eu/pvgis/

[47] Fracastoro GV, Perino M. Slides notes of the "Technology for renewable energy sources" class, Turin, Italy: Politecnico di Torino; 2016.

[48] Eykens L, Sitter KD, Dotremont C, Pinoy L, Bruggen BVD. Characterization and performance evaluation of commercially available hydrophobic membranes for direct contact membrane distillation. *Desalination*. 2016;392:63-73. doi:10.1016/j.desal.2016.04.006.

Acknowledgment

I would like to thank Prof. Chiavazzo, Prof. Tiraferri and Prof. Fasano for the opportunity to work on this actual topic, for their efforts in advising me and for the time granted to me and my work during this thesis course.

I would also like to thank M. Alberghini, M. Morciano and F. Ricceri for their kind willingness, support and advising, this work would have been poorer without them.

Personal thanks go to my family: my mother Alessandra, my father Sergio and my brother Alberto. They gave me the tools to take on this academic course and life in general, and they never made me lack their love and support of every kind along these journeys.

I am grateful for all the friends that still surround me. I have been absent during my study period, nevertheless they never forsaken me.

Finally, I would like to thank from my heart Miriam, my fiancee. We first met in the Polito classrooms and from that moment on, she has given me all the love and support that a man could desire and beyond. In this journey, we traveled together and today we conclude it still together, learning from each other and growing in so many ways. I love you.